https://doi.org/10.1016/j.pmatsci.2022.101054

Templating strategies for 3D-structured thermally conductive composites: Recent advances and thermal energy applications

Jie Yang[1, 3], Xi Shen[2, *], Wei Yang[3, *], Jang-Kyo Kim[1, 4, *]

[1] Department of Mechanical and Aerospace Engineering, The Hong Kong University of Science and Technology, Clear Water Bay, Kowloon, Hong Kong

[2] Department of Aeronautical and Aviation Engineering, The Hong Kong Polytechnic University, Hung Hom, Kowloon, Hong Kong

[3] College of Polymer Science and Engineering, Sichuan University, State Key Laboratory of Polymer Materials Engineering, Chengdu 610065, Sichuan, People's Republic of China

[4] School of Mechanical and Manufacturing Engineering, University of New South Wales, Sydney 2052 NSW Australia

* Corresponding author: xi.shen@polyu.edu.hk (X. Shen); weiyang@scu.edu.cn (W. Yang); mejkkim@ust.hk (J.-K. Kim)

Abstract

Thermally conductive polymer nanocomposites are enticing candidates for not only thermal managements in electronics but also functional components in emerging thermal energy storage and conversion systems and intelligent devices. A high thermal conductivity (k) depends largely on the ordered assembly of high-k fillers in the composites. In the past decades, various templating assembly techniques have been developed to rationally construct nanoscale fillers into three-dimensional (3D) interconnected structures, further improving the k of composites compared to conventional methods. Herein, recent advances are summarized in developing thermally conductive polymer composites based on self-templating, sacrificial templating, foam-templating, ice-templating and template-directed chemical vapor deposition techniques. These unique templating methods to fabricate 3D interconnected fillers in the form of segregated, cellular, lamellar, and radially aligned structures are reviewed, and their correlations to the k of composites are thoroughly probed. Moreover, multiscale structural design strategies combined with different templating methods to further improve the k of composites are highlighted. This review offers a constructive guidance to fabricate next-generation thermally conductive polymer composites for diverse thermal energy applications.

Keywords: Templating strategy, 3D interconnected filler, Multiscale design, Thermally conductive composites, Thermal energy application

Acronyms

0D	Zero-dimensional
1D	One-dimensional
2D	Two-dimensional
3D	Three-dimensional
APTS	*3*-aminopropyltriethoxysilane
BN	Boron nitride
BNNS	Boron nitride nanosheet
CB	Carbon black
CF	Carbon fiber
CMC	Cellulose microcrystal
CNC	Cellulose nanocrystal
CNF	Cellulose nanofiber
CNT	Carbon nanotube
CVD	Chemical vapor deposition
EG	Expanded graphite
EMI	Electromagnetic interference
EMT	Effective medium theory
FEA	Finite element analysis
F-F	Filler-filler
F-M	Filler-matrix
GF	Graphene foam
GNP	Graphite nanoplatelet
GO	Graphene oxide
IoT	Internet of Things
ITR	Interfacial thermal resistance
LBL	Layer-by-layer
LLDPE	Linear low-density polyethylene
MD	Molecular dynamics
MF	Melamine–formaldehyde

MPPW Multilayer plastic packaging waste

NFC Nanofibrillated Cellulose

NR Natural rubber

PA6 Polyamide 6

PBO Polybenzobisoxazole

PBT Poly(butylene terephthalate)

PBz Polybenzoxazine

PCL Polycaprolactone

PCM Phase change material

PDA Polydopamine

PDDA Poly(diallyl dimethyl ammonium chloride)

PDMS Polydimethylsiloxane

PE Polyethylene

PEG Polyethylene glycol

PEG-*g*-PDMS PEG grafted PDMS

PES Polyethersulfone

PI Polyimide

PLA Polylactic acid

PMMA Poly(methyl methacrylate)

PP Polypropylene

PPS Polyphenylene sulfide

PPSU Poly(phenylene sulfone)

PS Polystyrene

PSR Polysulfide rubber

PTM Personal thermal management

PU Polyurethane

PVA Poly(vinyl alcohol)

PVDF Poly(vinylidene fluoride)

rGO Reduced graphene oxide

ROM Rule of mixtures

RPC Reticulated porous structure

SEM Scanning electron microscopy

SR Silicone rubber

TCE Thermal conductivity enhancement

TCEE Thermal conductivity enhancement efficiency

TCAR Thermal conductivity anisotropy ratio

TEM Transmission electron microscopy

TIM Thermal interface material

TPU Thermoplastic polyurethane

T-ZnOw Tetrapod-like zinc oxide whiskers

UHMWPE Ultra-high molecular weight polyethylene

Symbols

β Conductivity exponent depending on the aspect ratio of filler

μ_1 Orientation coefficient of filler struts with a 2D in-plane orientation

μ_2 Orientation coefficient of filler struts with a 3D random orientation

ξ Relative concentration of struts with an in-plane orientation

ψ Sphericity of filler

Φ_m Maximum packing fraction of particle

B A constant related to shape and orientation of particle

C_1 Influence factor of crystallinity and crystal size of polymer after adding fillers

C_2 Difficulty of forming the heat conduction chain

C_v Specific heat capacity per unit volume

h Interfacial thermal conductance

k Thermal conductivity

k_0 Pre-exponential factor from the contribution of 3D network

k_c Thermal conductivity of composite

k_f^{eff} *E*ffective thermal conductivity of filler

k_f Thermal conductivity of filler

k_m Thermal conductivity of matrix

k_s Thermal conductivity of filler strut

l Phonon mean free path

L Size of filler

n Shape parameter of filler

r Radius of spherical filler

R Thermal resistance or Kapitza resistance

t Thickness of filler

T_g Glass transition temperature

v Phonon group velocity

V_c Critical volume fraction

V_f Volume fraction of filler

Table of Contents

1. Introduction

Electronic devices have become an indispensable part of our daily life. With ever-growing realization of miniaturization, integration and multi-functions of electronics, the power density and the heat output per unit volume increase significantly, deleterious to their performance and service life if the heat is not effectively dissipated. The overheating of microelectronic components has become the bottleneck restricting the development and application of high-frequency and high-power devices and systems for advanced communication and information technology.[1-5] In particular, the rapid deployment of 5G technology in consumer electronics poses new challenges to more efficient thermal management solutions because of the exponential surge of heat generated from the high power consumption. To tackle the challenge, myriad thermally conductive polymer composites have been developed over the past decade as thermal interface materials (TIMs), focusing on improving the thermal conductivity of composites without degrading their mechanical properties using small quantities of conductive fillers.[6, 7]

In addition to electronics, thermal energy regulation also plays a crucial role in energy storage and conversion systems such as batteries[8-10] and solar thermal energy storage technology based on photo-driven phase change materials (PCMs).[11]. For example, thermally conductive separators [8, 9] and electrolytes [10] have been developed to facilitate heat dissipation in batteries, mitigating the temperature rise during operation and improving the safety and service life. Most recently, thermally conductive polymer composites with excellent thermoresponsive capacities have been used to meet rapidly increasing demands for fast responses to temperature changes in wearable devices, human-machine interactions and artificially intelligent (AI) technology.[12] The high thermal conductivity not only helps the heat dissipation in wearable fabrics for personal cooling [13-15] and high-current actuators [16], but also contributes to fast responses to heat in shape memory devices [17, 18] and temperature sensors for soft robotics [19]. Despite these promising applications, the vast majority of polymers exhibit intrinsically low thermal conductivities, k, below 0.5 W m^{-1} K^{-1},[20, 21] significantly hampering

their thermal applications. One effective way to ameliorate their *k* is to incorporate thermally conductive fillers in them. Various types of fillers, including electrically conductive metal particles (*e.g.*, silver (Ag),[22, 23] copper (Cu),[24-26] aluminum (Al),[27] and nickel (Ni)[28, 29]), carbon materials (*e.g.*, carbon black (CB),[30] carbon fiber (CF),[31, 32] carbon nanotube (CNT),[33] graphite,[34, 35] and graphene[36-39]), MXene,[40, 41] and electrically insulating ceramics (*e.g.*, alumina (Al_2O_3),[42, 43] silicon nitride (Si_3N_4),[44, 45] silicon carbide (SiC),[46, 47] aluminum nitride (AlN),[48, 49] and boron nitride (BN)[50, 51]) have been introduced into polymer matrices to yield thermally conductive polymer composites. Many of these fillers possess immensely anisotropic *k* arising from their anisotropic structures. For example, the in-plane *k* of two-dimensional (2D) graphene and BN sheets can reach 5300 and 360 W m^{-1} K^{-1},[52, 53] respectively, while their through-plane *k* are two orders of magnitude lower.[54, 55] The anisotropic *k* necessitates the design of aligned structures to fully utilize their high in-plane *k*. Yet, it remains a formidable task to fully translate their excellent *k* to bulk composites. This is because conventional processing routes, such as direct solution mixing and melt compounding, are not conducive to form percolated networks of thermally conductive fillers even with homogeneous dispersion, leading to huge thermal resistance at the filler-matrix (F-M) interfaces and thus unsatisfactory *k* of composites, usually lower than 5 W m^{-1} K^{-1}.[3, 56]

Contrary to uniform dispersion strategies, constructing three-dimensional (3D) conductive networks through various rational assembly techniques allow thermally conductive fillers to aggregate and assemble in an orderly manner.[57] The pre-constructed filler networks ensure inherent percolation of nanofillers when made into composites. The phonons can therefore transport through the interconnected networks without being significantly scattered at the F-M interfaces,[58, 59] maximizing the *k* improvement in composites with a minimal filler loading. Exhaustive efforts have been made to produce thermally conductive composites containing 3D fillers through rational design of building blocks, microstructures, and macro-architectures.[59-62] Among different methods, the templating strategy is an emerging and effective approach to realize ordered and controlled assemblies of low-dimensional nanofillers.

Various 3D interconnected structures, including isotropic segregated, unidirectional cellular, bidirectional lamellar, and radial continuous conductive structures, have been constructed by templating strategies and served as 3D filler networks in polymer matrices to tailor thermally conductive behaviors of the final composites.[19, 63-68] Although general strategies to build 3D thermally conductive structures are discussed in a few review articles,[37, 58, 69] specific discussions on the processes of various templating methods are not available. Moreover, the correlations among different templating methods, the micro- and macrostructures created therefrom, and the resulting *k* of composites have yet to be established. In addition, the existing reviews focus primarily on thermal management of electronics without accounting for other important applications such as thermal energy conversion and smart devices, which are emerging fields for the application of thermally conductive composites.[3, 36]

In this contribution, recent progresses in templating strategies involving self-templating, sacrificial templating, foam-templating, ice-templating and template-directed chemical vapor deposition (CVD) for versatile, thermally conductive composites, including robust,[70] flexible[71] and phase change energy storage[72] composites, are critically summarized. **Fig. 1** schematically illustrates the overall methodology used in this review. The technical characteristics, nanofiller structures, microstructural design, macro-architecture assembly, performance optimization, and application fields of different templating methods are highlighted and holistically compared by probing the process-structure-property-application correlations across multi-length scales. This review provides a meticulous guideline for manufacturing high-performance thermally conductive polymer composites using templating strategies, furthering their application in all heat-related scenarios.

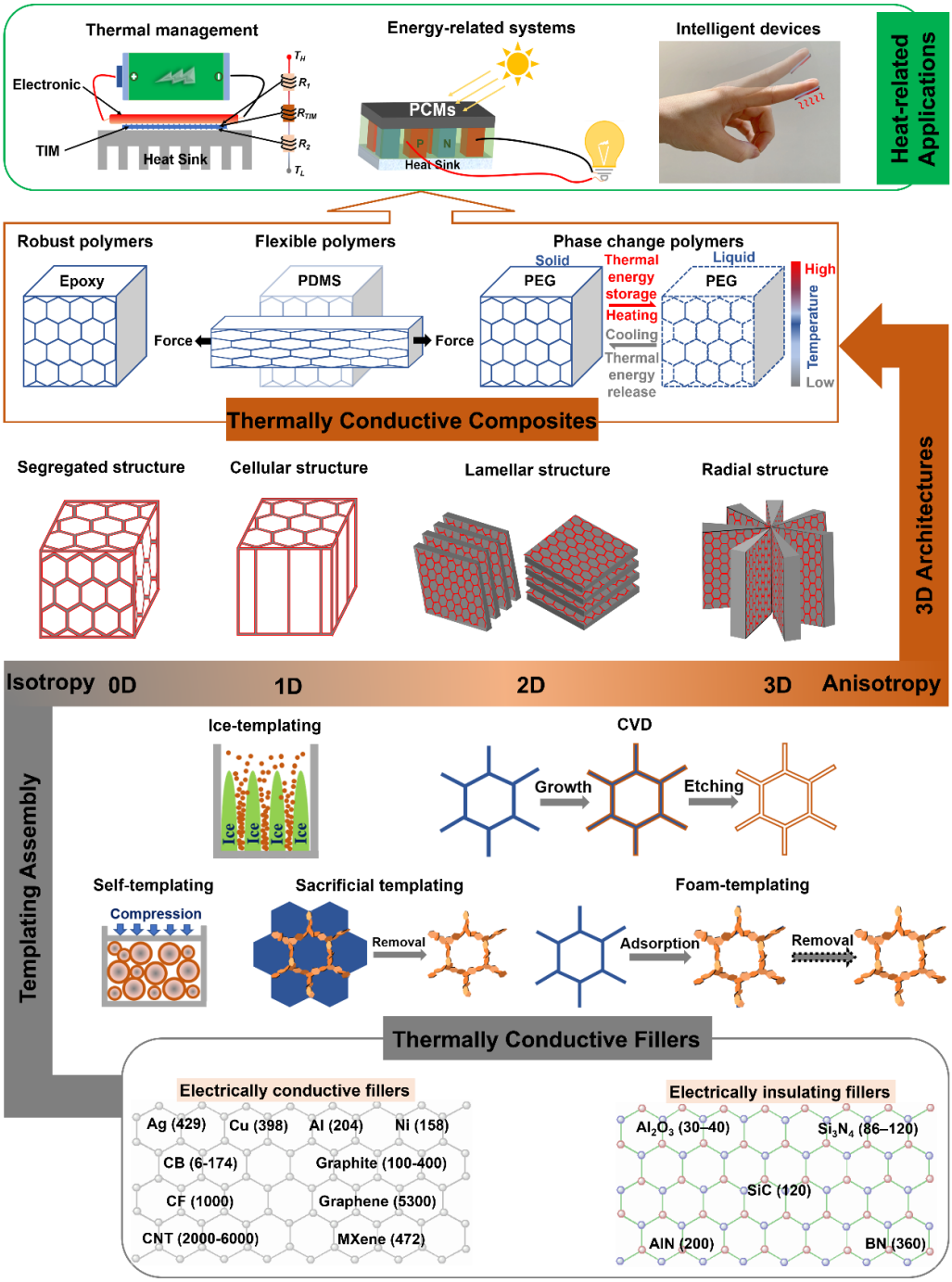

Fig. 1. Overview of templating strategies to produce thermally conductive polymer composites for thermal energy applications. The numbers in the brackets are the *k* values in W m^{-1} K^{-1} of fillers frequently used for thermally conductive polymer composites.

2. Thermal Transport in Polymer Composites

2.1. Thermal conduction mechanisms

It is well-known that heat transfer can be classified into four major mechanisms, namely, thermal radiation, thermal convection, thermal conduction, and transfer of energy by phase changes. In solid materials, the heat is transferred mainly by conduction. The two main heat carriers in solids are electrons capable of free migration and phonons in the form of lattice vibration, while the phonons predominate the heat conduction in polymers.[33] The k of polymers can be determined by the Debye equation:

$$k = \frac{C_v v l}{3} \quad (1)$$

where C_v is the specific heat capacity per unit volume, v and l are the phonon group velocity and phonon mean free path, respectively. For most polymers, phonons travel through amorphous polymer chains with rather short l due to phonon scattering between individual chains or at defects, leading to inherently low k in the range of 0.1 – 0.5 W m^{-1} K^{-1}.[73]

The addition of fillers with orders of magnitude higher k than polymer matrices can improve the k of composites to a different extent depending on filler loading. At low filler loadings, phonons transport through conductive fillers and polymer matrices with high interfacial resistance between them. Therefore, the improvement in k is limited especially for nanofiller/polymer systems where a large volume of interphase exists. When the filler loading increases to form physical contacts between fillers, the thermal conduction pathway theory is the most widely-accepted thermal conduction mechanism. The heat flux preferentially flows along the conductive networks formed by interconnected fillers rather than through the polymer matrix.[20, 74] Similar to electrical percolation,[75, 76] an abrupt change in k with increasing filler loading is observed in several thermally conductive composites.[77-80] The thermal resistance between individual fillers is much lower than that occurring at the filler/polymer interfaces,[81] thus large enhancements in k are expected when interconnected filler networks are formed in the composite. However, for most thermally conductive composites with dispersed fillers, the thermal percolation hardly appears even at very high filler loadings of 17 – 50 vol%,[78, 82, 83] much higher than that required for

electrical percolation which is often less than 1 vol%.[75] The difficulty in forming thermal percolation networks can be understood from the following aspects. First, the k of most thermally conductive fillers is only 10 to 10^3 times higher than the polymer counterpart, in contrast to the over 10 orders of magnitude difference between their electrical conductivities. The matrix is not a thermal insulator, making the thermal percolation phenomenon less prominent than the electrical percolation. Second, unlike electrons, there is no tunneling effect for phonons. This means that physical contacts between fillers are essential for effective phonon transport. Third, phonon scattering is more prominent than electron scattering at interfaces and defects, where electron hopping and tunneling help the formation of electrical percolation. Therefore, dedicated engineering of interfaces between the fillers for matched phonon vibration characteristics is necessary to reduce phonon scattering at the interfaces for thermal percolation. It follows that constructing interconnected filler networks with tailored inter-filler contacts is vital to highly enhanced k of composites.

2.2. Factors affecting *k* of composites containing interconnected fillers

Many theoretical models have so far been developed to predict and analyze k of polymer composites by taking into account various important factors, as summarized in **Table 1**.[6, 61, 84-86] Depending on the explicit parameters studied, these models can be classified into three types, namely, (i) simple models without considering interfacial effects, (ii) F-M interfacial models, and (iii) filler-filler (F-F) interfacial models. These models are discussed in the following, focusing on their applications to identify the important factors affecting the k of composites containing interconnected filler networks.

In the simple models without considering interfacial effects, only the k values of fillers and matrices, k_f and k_m, as well as filler loading, V_f, are specifically included in the mathematical expressions. The simplest forms are the parallel (arithmetic mean), series (harmonic mean), and random models (geometrical mean) based on the rule of mixtures (ROM).[87-89] Typically, the parallel and series models predict the upper and lower limits of k of two-component composites, respectively. Another commonly used

Maxwell–Eucken model presents a good agreement with experimental data for composites containing uniformly distributed fillers at low loadings.[90] For the composites having high filler contents, the Bruggeman model provides a better prediction.[91, 92] In addition to k_f and k_m, other important factors, such as the geometry, shape, aspect ratio, and packing of dispersed fillers, are also explicitly studied in the Hamilton-Grosser model [93] and the Lewis−Nielsen model.[94, 95] For analyzing the k of composites (k_c) containing interconnected fillers, these simple models, especially the ones based on ROM, are normally used to predict their upper and lower bound values.

The F-M interfacial models account for the interfacial thermal resistance (ITR) between fillers and matrices in addition to k_m and k_f. The F-M ITR or Kapitza resistance, R, is an important factor leading to the reduction of k at the F-M interfaces, frequently stemming from the difference in the vibrational modes between them.[96] Specifically, the phonon scattering occurs because of the incompatible phonon vibrational modes or incomplete contacts at the interface, inevitably giving rise to a high F-M ITR.[97] To incorporate the contribution of reduced interfacial thermal conduction, the Hasselman–Johnson model was proposed to predict the k_c by replacing k_f in the Maxwell–Eucken model with the effective value taking into account the adverse effects of F-M interfaces.[98, 99] A more commonly-used theory is the Nan's model based on the effective medium theory (EMT).[100, 101] The ITR at the F-M interface was taken into account in this model, yielding a more accurate prediction of k_c than the simple models without considering the interfacial effects as discussed above. Other factors such as filler alignment [102-105] and hybrid fillers [106] were also studied by modifying the Nan's model. Nevertheless, the theoretical models based on EMT only holds well for filler loadings below thermal percolation.[107] In general, these models tend to underestimate k_c of composites containing interconnected filler networks where the resistance between individual fillers in the percolated network becomes more important.[108]

Table 1
Summary of models for predicting k_c.

Type of model	Model name	Formula	Characteristics	Parameters
Simple models without considering interfacial effect	Parallel	$k_c = (1 - V_f) \cdot k_m + V_f \cdot k_f$	• Fillers with various shapes and sizes • Prediction of maximum value	k_m: Thermal conductivity of polymer matrix k_f: Thermal conductivity of filler V_f: Volume fraction of filler
	Series	$\frac{1}{k_c} = \frac{(1 - V_f)}{k_m} + \frac{V_f}{k_f}$	• Fillers with various shapes and sizes • Prediction of minimum value	
	Random	$k_c = k_m^{(1-V_f)} + k_f^{V_f}$	• Fillers with various shapes and sizes	
	Maxwell–Eucken	$k_c = k_m \left(\frac{2k_m + k_f + 2V_f (k_f - k_m)}{2k_m + k_f - V_f (k_f - k_m)} \right)$	• Uniformly distributed spherical filler • Low loading	
	Bruggeman	$1 - V_f = \frac{k_f - k_c}{k_f - k_m} \left(\frac{k_m}{k_c} \right)^{1/3}$	• Uniformly distributed spherical filler • High loading	
	Hamilton-Grosser	$k_c = k_m \left(\frac{(n-1)k_m + k_f + (n-1)V_f (k_f - k_m)}{(n-1)k_m + k_f - V_f (k_f - k_m)} \right)$ $n = \frac{3}{\psi}$	• Considering the effect of geometry of fillers	n: Shape parameter of filler ψ: Sphericity of filler, which is defined as the ratio of the surface area of a sphere to that of the filler with the same volume
	Lewis–Nielsen	$k_c = k_m \frac{1 + \frac{B(k_f - k_m)}{k_f + Bk_m} V_f}{1 - \frac{k_f - k_m}{k_f + Bk_m} \left[1 + \left(\frac{1 - \emptyset_m}{\emptyset_m^{\,2}} \right) V_f \right] V_f}$	• Considering the effect of shape, aspect ratio and packing factor of fillers	B: A constant related with shape and orientation of particle Φ_m: Maximum packing fraction of particle

(*continued on next page*)

Table 1 (*continued*)

Type of model	Model name	Formula	Characteristics	Parameters
F-M interfacial models	Hasselman–Johnson	$k_c = k_m\left(\frac{2k_m + k_f^{eff} + 2V_f\left(k_f^{eff} - k_m\right)}{2k_m + k_f^{eff} - V_f(k_f^{eff} - k_m)}\right)$ $k_f^{eff} = \frac{k_f}{1 + \frac{k_f}{h \cdot r}}$	• Uniformly distributed spherical filler • Considering the effect of two-phase interface	k_f^{eff}: Effective thermal conductivity of filler h: Interfacial thermal conductance r: Radius of spherical filler
	Nan's	$k_c = k_f\left(\frac{3k_m + 2V_f\left(k_f - k_m\right)}{\left(3 - V_f\right)k_f + k_m V_f + \frac{Rk_m k_f V_f}{t}}\right)$	• Considering the effect of ITR	t: Thickness of filler
	Agari-Uno	$lg\ k_c = \left(1 - V_f\right)\lg\left(C_1 k_m\right) + V_f C_2 lg k_f$	• Fillers with various shapes and sizes • Considering the formation of heat	C_1: Influence factor of the crystallinity and crystal size of the polymer after adding fillers C_2: Difficulty of forming the heat conduction chain
F-F interfacial models	Foygel	$k_c = k_0\left(V_f - V_c\right)^{\beta}$ $R = \frac{1}{k_0 L^{\left(\right)}\left(V_c\right)^{\beta}}$	• 3D thermal percolation threshold	k_0: Pre-exponential factor from the contribution of 3D network V_c: Critical volume fraction L: Size of filler β: Conductivity exponent depending on the aspect ratio of filler
	3D ROM	$k_c = \frac{1}{3}V_f k_s + (1 - V_f)k_m$	• Isotropic 3D structure	k_s: Thermal conductivity of 3D filler strut
	Modified 3D ROM	$k_c = \mu_1 \xi V_f k_s + \mu_2(1 - \xi)V_f k_s + (1 - V_f)k_m$	• Anisotropic 3D structure	μ_1: Orientation coefficient of filler struts with a 2D in-plane orientation μ_2: Orientation coefficient of filler struts with a 3D random orientation

To better predict the k_c of composites containing interconnected fillers, the F-F interfacial models were developed to account for the ITR between individual fillers when percolation networks are formed in the composites. Considering the formation of heat conduction chains between fillers, an empirical Agari model was developed to estimate the k_c of composites at high filler loadings.[109, 110] The model introduced two fitting parameters, C_1 and C_2, to account for the ITR between interconnected fillers, where a higher value of C_2 signifies more conductive chains in the composites. Another nonlinear model for 3D thermal percolation threshold in composites is the Foygel model.[111] Similar to the electrical percolation threshold, a critical volume fraction of fillers required for forming thermal percolation was obtained by fitting the Foygel model with the experimental data.[81, 112] Moreover, the ITR between individual fillers was also estimated from the fitting, which was two orders of magnitudes lower than the counterpart between filler and matrix.[81] This means that the lower ITR between fillers than that at the F-M interface was responsible for the higher k_c of the composites containing interconnected fillers than dispersed fillers.

In addition to the above empirical models, analytical models explicitly involving the ITR between individual fillers were also developed based on the EMT.[113, 114] Compared to the underestimation of k_c by the EMT models with only the F-M ITR, the models taking into account the F-F ITR more accurately fitted the experimental data when percolated networks were formed at high filler loadings. This confirms that the formation of interconnected networks is conducive to a higher k_c because of the lower resistance at the F-F than the F-M interfaces.[108] When continuous conductive networks were formed in isotropic 3D structures of preconstructed fillers, such as graphene foams, the k_c was better predicted using a simple 3D ROM model based on the metal foam theory.[68] The 3D ROM model considered the filler and matrix as two continuous phases and thus only entailed the k values of filler strut and matrix without accounting for their ITR. The agreement between the 3D ROM model and the experimental data substantiated the trivial effect of F-M ITR when interconnected fillers were formed. Further including two parameters, the orientation (μ) and concentration (ξ) parameters, into the above model yielded a modified 3D ROM model

capable of predicting the k_c of composites containing anisotropic 3D filler structures.[115] A higher k_c was achieved in the alignment than transverse directions, signifying the important role of alignment in improving the k_c of composites even when 3D fillers were used.

2.3. Strategies to improve k_c of composites containing interconnected fillers

The foregoing discussion indicates that the k_c of composites with highly thermally conductive fillers are much lower than theoretical predictions from the ROM. This is commonly attributed to various factors at different length scales inducing high ITR at the F-M and F-F interfaces. To further improve the k_c, several strategies have been proposed to mitigate the ITR. Because many common methods for improving k_c of composites containing dispersed fillers have been extensively discussed in previous reviews,[73, 74, 86] we focus mainly on major strategies for high k_c of composites containing interconnected filler networks in the following discussion.

As shown in **Fig. 2**, early efforts have been dedicated to optimizing the dispersion of fillers in the composites for enhanced k_c. However, the resulting composites exhibited only a moderate improvement in k_c because of the large ITR at the F-M and F-F interfaces even at high filler loadings.[63] Moreover, the uniform dispersion became increasingly difficult at high filler loadings owing to the rising viscosities, adding to existing processing difficulties, and thus degrading the mechanical properties. In recent years, many studies have been directed towards exploring 3D interconnected filler networks capable of offering continuous phonon transfer pathways in the matrix, minimizing the unfavorable ITR at the F-M interfaces.[114] Rather than randomly dispersing fillers in the matrix, pre-constructing 3D-conductive filler architectures using various templating strategies followed by polymer infiltration are more effective in ameliorating phonon transfer routes in the composites. The 3D fillers also do not alter the viscosity of polymer matrix, eliminating the processing challenges arising from increased viscosities.

To further improve the heat transfer efficiency of 3D fillers and thus k_c of the final composites, several important parameters need to be optimized through multiscale

structural design, such as filler loading, pore size, secondary network, alignment, filler hybridization, F-M interfacial engineering, and F-F interfacial engineering, as illustrated in **Fig. 2**. Detailed discussion on individual parameters is provided in the following. Apparently, k_c is positively correlated to the filler loading.[63] Among various strategies, 3D structures with high densities made from high-density templates are an ideal approach to achieve a high filler loading.[115] This is because the high-density 3D fillers with interconnected thermal pathways are more efficient in improving k_c than the fillers of the same loading evenly dispersed in the matrix. For a given filler loading, the pore size in the 3D filler structures plays an important role in determining k_c. Generally, the larger is the pore size, the thicker are the cell walls and the smaller are the interfacial contact areas between the 3D filler and matrix, with higher k_c.[116, 117] The term 'secondary network' refers to the additional thermal transfer pathways formed in the matrix other than the primary conductive network of 3D fillers, as shown in **Fig. 2**. Generally, the secondary networks supplement the 3D fillers featuring relatively large primary skeletons or pores, such as those made based on large-size self-templated polymer granules [118] and commercial foam templates [119]. On one hand, the secondary network is beneficial to reducing the thermal resistance from the matrix inside the large pores to the conductive strut walls, furthering the heat transfer capacity for relatively large primary skeletons or pores derived from templating strategies. On the other hand, the construction of secondary networks within the 3D fillers can overcome the limitation of filler loading in the self-templating method and template-directed CVD.

The filler geometries, *e.g.*, shape, size, and aspect ratio, were also optimized to improve k_c.[120] The filler shape directly determines the F-F contact type, such as point, line, and face contacts, in turn affecting the F-F ITRs. Spherical fillers tend to form point contacts, exhibiting isotropic heat transfer behavior. By contrast, fillers with tubular and platelet shapes form line and face contacts, respectively, both showing anisotropic heat transfer characteristics. Amongst fillers with different shapes, anisotropic fillers having face contacts, such as 2D graphene and BN, showed the lowest F-F ITR because of larger contact area,[74, 121] making them the most promising candidates for

improving k_c. Different from segregated structures with isotropic properties, highly oriented structures, including cellular, lamellar and radial structures, were constructed using these 2D fillers by templating strategies to improve k_c along the desired directions.[19, 66, 67, 122] To more effectively exploit the advantages of 2D fillers, hybrid fillers with different geometries have been used to synergistically enhance k_c, where the loading ratio of these hybrid fillers plays a decisive role. For example, large-size fillers formed a network structure, while small-size ones filled the gap between adjacent large-size fillers, achieving more efficient packing along with reduced F-F ITR.[123-125] Moreover, the devise of hetero-structured thermally conductive fillers fabricated by physical interaction or in-situ chemical growth is an enticing solution to reduce F-F ITR in the filler hybridization systems, enlarging the synergistic improvement effect.[126-128]

At atomic or molecular levels, the thermally conductive fillers in the 3D framework are usually in contacts *via* weak physical interactions, such as van der Waals forces, hydrogen bonds, and π-π interaction. Nevertheless, the phonon transport is closely related to the vibrational frequencies of atoms across the interface between different materials, which is directly proportional to the bond strength at the interface.[129] Therefore, non-covalent or covalent modification of the interfaces to enhance the bond strength and afford resonant atomic motions constitutes another effective alternative to improving k_c through reducing the ITR at the F-M and F-F interfaces.[130] Surface functionalization of nanofillers using chemical groups, such as polydopamine (PDA) and silane, and covalent-connecting fillers are common routes to improve the interfacial interactions between physically contacted fillers.[131-133] Although the covalent modification is more beneficial to reducing the ITR than the non-covalent counterpart, the former can deteriorate the intrinsic k of fillers causing the k_c to be worse off. This means that the selection between the covalent and non-covalent modifications should be dependent on whether it would adversely affect the intrinsic k of fillers, such that the overall k_c can be enhanced to the maximum possible extent. Another effective way is to prepare continuous, covalently-bonded 3D monolithic fillers by template-directed CVD.[68] The covalent bonds in the 3D fillers allowed unspoiled phonon transport

along the filler networks with minimum adverse effects from the F-F interfaces.[115] However, k_c is normally limited by the low filler content arising from the large pore size in CVD-grown 3D fillers. Therefore, a useful strategy is to build the aforementioned secondary network within the 3D fillers to enhance the overall filler loading and thus k_c.[80, 134] Overall, the rational design of 3D fillers from atomic/molecular-scale functionalization to nano-micro structural optimization constitutes among the most intriguing means for developing high-performance thermally conductive polymer composites. The design principles of 3D fillers realized by different templating methods are discussed in the next Section.

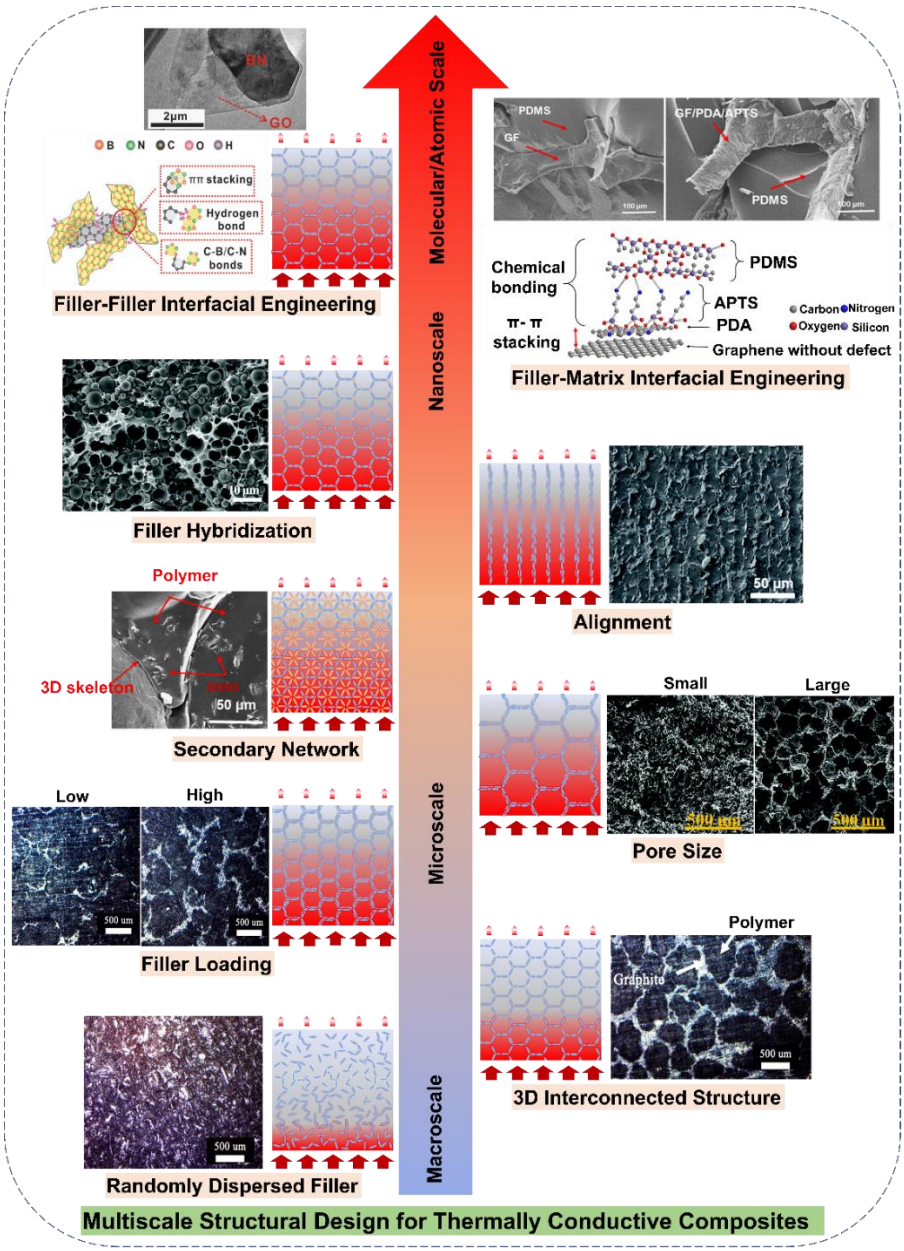

Fig. 2. Schematics and optical/scanning electron microscopy (SEM)/transmission electron microscopy (TEM) images showing the morphologies and heat transfer in thermally conductive composites filled with randomly-dispersed fillers or 3D interconnected filler networks, and the strategies to optimize the 3D filler networks by tuning various factors, including filler loading, pore size, alignment, filler hybridization, secondary network, and filler/matrix or filler/filler interfaces. Optical images of randomly-dispersed fillers, 3D interconnected filler networks, and filler loading are reproduced with permission from ref. [63]. Copyright 2016, American Chemical Society. SEM images for pore size are reproduced with permission from ref. [116]. Copyright 2016, Royal Society of Chemistry. SEM image for secondary networks is reproduced with permission from ref. [134]. Copyright 2017, Elsevier Ltd. SEM image for alignment is reproduced with permission from ref. [122]. Copyright 2016, Royal Society of Chemistry. SEM image for filler hybridization is reproduced with permission from ref. [125]. Copyright 2018, Royal Society of Chemistry. Schematic illustration and SEM images for F-M interface are reproduced with permission from ref. [132]. Copyright 2017, American Chemical Society. Schematic illustration and SEM image for F-F interface are reproduced with permission from ref. [133]. Copyright 2018, WILEY-VCH.

3. Templating Strategies to Produce 3D Interconnected Fillers

Templating strategies exploit templates in various forms to direct the assembly of thermally conductive fillers into 3D interconnected architectures having continuous heat transport networks. The orderly stacking of functional components in the composites can be attained through controlling various materials and processing parameters. Depending on the types of templates used in the assembly processes, the templating methods can be categorized into self-templating, sacrificial templating, foam-templating, ice-templating, and template-directed CVD, which are discussed in the following parts. The correlation among processing methods, material compositions, structural characteristics, and thermal conductivities for each of templating strategies is highlighted. In addition, we emphasize the benefits of multiscale design to further

improve the heat transfer performance using the isotropic and anisotropic structures built by various templating strategies.

3.1. Self-templating

Self-templating refers to the construction of segregated structures of fillers by directly using the interfaces among polymer particles as templates without introducing a third phase during the templating process.[135, 136] In the final composites, the segregated fillers are located primarily at these polymer particle interfaces to achieve a locally high filler loading and full contacts between individual fillers, allowing the formation of 3D percolated networks at an overall low filler loading compared to the counterparts comprising dispersed fillers. In a typical process, two steps, namely, mixing and compaction are carried out in sequence. Polymer granules coated with conductive fillers are dry- or solution-blended, followed by hot pressing to construct the segregated conductive networks in bulk composites by means of interconnection of polymer granules. Worthy of note is that the polymers should possess relatively high melt viscosities to maintain the segregated networks while a low filler concentration is preferred to ensure good adhesion between fillers and polymer granules while alleviating the processing difficulties during hot press.

In the thermally conductive composites, the segregated fillers form continuous conductive pathways, significantly mitigating the phonon scattering at the F-M interfaces. Different thermally conductive filler materials, including metal particles, carbon materials, and ceramics, were incorporated into polymer matrices to form segregated networks by self-templating.[63, 114, 137-140] Depending on the size of polymer granules, filler geometries, applied pressure and temperature during compaction, 3D interconnected fillers with either isotropic or anisotropic segregated structures were constructed. Isotropic segregated structures were formed when zero-dimensional (0D) particles, such as Cu or Ag nanoparticles [137, 138], or 2D platelets [139], were blended with matrix. For example, graphite flakes were coated on polypropylene (PP) particles with a diameter of hundreds of microns followed by hot pressing to form graphite/PP composites (**Fig. 3**a). [63] Percolated networks of

segregated graphite flakes at the interfaces were formed in the PP matrix (**Fig. 3**b), giving rise to a significant enhancement in k_c. Compared to the composites with randomly distributed graphite flakes fabricated by conventional melt compounding, the segregated graphite/PP composite exhibited a much superior k_c of 5.4 W m^{-1} K^{-1} at a graphite loading of 21.2 vol%, 227 % higher than that of its random counterpart at the same filler loading. (**Fig. 3**c).

When the granule size was reduced to only a few microns, 2D nanofillers with high flexibility were ideal to allow conformable assembly on the polymer surfaces for controllable filler orientation owing to the large deformation of micro-sized granules. For example, a high-performance thermally conductive composite was developed based on 2D BN nanosheets (BNNSs) and polystyrene (PS) microspheres of ~1.4 μm in diameter using self-templating (**Fig. 3**d).[141] The core-shell shaped microspheres fabricated by self-assembling BNNSs on PS microspheres *via* electrostatic interactions were hot-pressed at the glass transition temperature (T_g) of PS to selectively distribute BNNSs along the boundaries of the deformed polymer particles. The compressive load applied during molding induced in-plane orientation of BNNSs, causing an anisotropic k_c owing to the anisotropic structure of the resulting BNNS/PS composites, with a high in-plane k_c of 8.0 W m^{-1} K^{-1} at a BNNS loading of 13.4 vol%. Similarly, self-assembled BNNS/polyimide (PI) microspheres of ~3.0 μm in diameter were also compressed to form a composite. The in-plane k_c of the resultant composite with 12.4 vol% oriented BNNSs was enhanced to 4.25 W m^{-1} K^{-1}, which is 400 % and 227 % higher than the PI matrix and the random-structured composite with the same BNNS loading, respectively.[142] The self-templating strategy is suitable for thermally conductive composites with most thermoplastic matrices, such as polyethylene (PE), linear low-density PE (LLDPE), poly(vinyl alcohol) (PVA), poly(methyl methacrylate) (PMMA), poly(vinylidene fluoride) (PVDF), ultra-high molecular weight PE (UHMWPE), polyphenylene sulfide (PPS), polylactic acid (PLA), and multilayer plastic packaging waste (MPPW).[112, 140, 143-147]

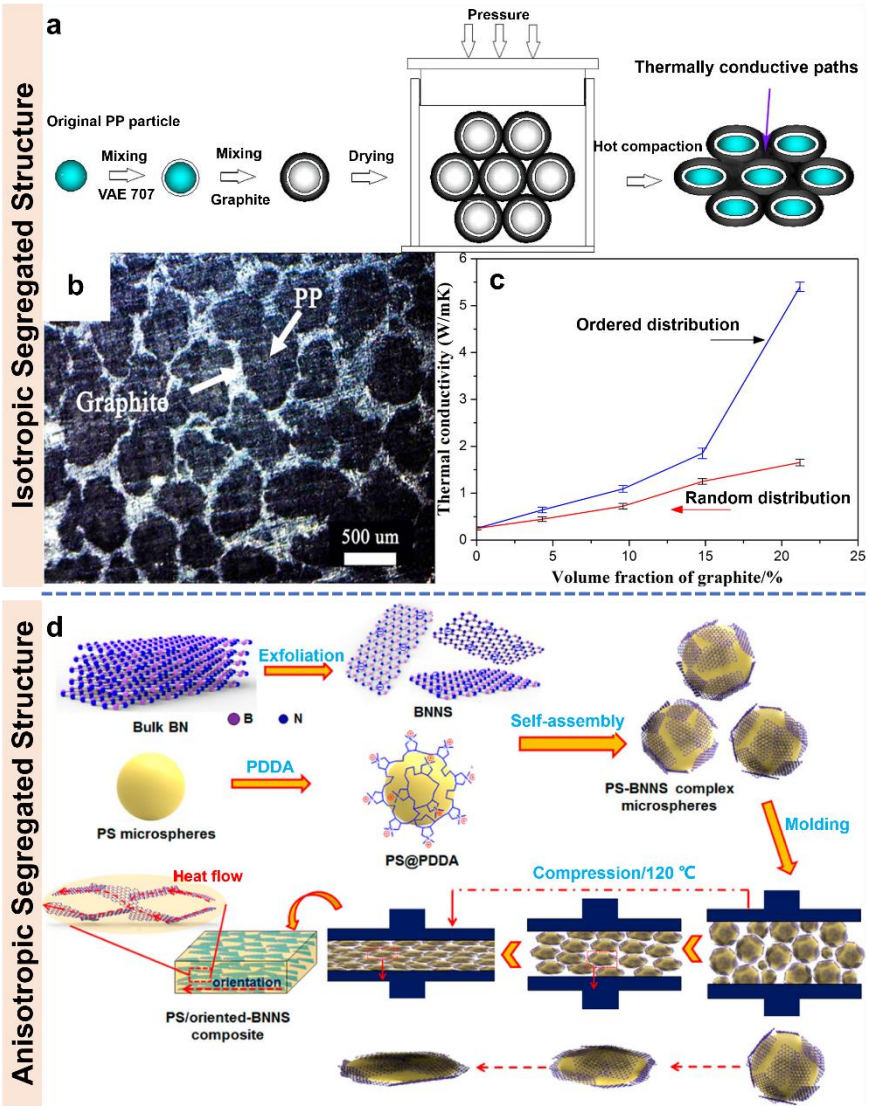

Fig. 3. Self-templating strategy to fabricate thermally conductive composites with (a-c) isotropic and (d) anisotropic segregated structures. (a) Processing route, (b) optical image and (c) k_c of graphite/PP composites. Reproduced with permission from ref. [63]. Copyright 2016, American Chemical Society. (d) Schematic of the preparation of PS-BNNS hybrid microspheres and the resulting oriented BNNS/PS composites. Reproduced with permission from ref. [141]. Copyright 2017, American Chemical Society.

The k_c of composites containing segregated fillers is controlled mainly by thermal transport in the 3D conductive pathway. In an effort to enhance the thermal transport by reducing the ITR, three major strategies, including interfacial engineering, filler hybridization, and secondary networks, have been extensively studied, as shown in **Fig.**

4. The interfacial modification aims to reduce the ITR between segregated fillers and at the F-M interfaces through chemically or physically altering the structures of matrices and fillers. The matrix modification and filler functionalization have been adopted to enhance the interfacial interaction between polymers and fillers. Inspired by the chemical structure of mussels, a matrix modification was carried out by coating PDA on PP granules (**Fig. 4**a).[131] After pressing, the adhesion between the PP matrix and graphene was improved because of the hydrogen bonds and π-π interactions created between PDA and graphene, significantly reducing the F-M ITR. To simultaneously reduce the ITR at the F-M and F-F interfaces, filler functionalization is necessary. Expanded graphite (EG) was functionalized with epoxy groups using a commercial modifier (Elvaloy) before mixing with poly(butylene terephthalate) (PBT) particles (**Fig. 4**b).[148] The interactions between fillers and at the F-M interfaces were improved because of good compatibility between Elvaloy and PBT, giving rise to reduced ITR. A combination of non-covalent and covalent modifications with PDA and silane was also adopted to improve the interfacial interactions between bare BN and silicone rubber (SR) matrix, in which non-covalent functionalization of PDA on BN surfaces facilitated further grafting silane by covalent modification for improved interfacial adhesion.[149] In addition to interfacial engineering, segregated structures assembled from hybrid fillers of different geometries were found to synergistically improve the k_c. Large-size 2D fillers such as graphene and BNNS were the main constituents in the segregated structures because of their large face-to-face overlapping areas. After incorporating secondary fillers, such as 0D Cu particles, polyhedral AlN, and one-dimensional (1D) CNTs, the gaps between the adjacent 2D fillers were effectively bridged, facilitating phonon transport along the segregated channels formed between templating granules (**Fig. 4**c and d).[114, 150, 151] It is worth noting that for composites made by self-templating, the large-size polymer particles of hundreds of micrometers in diameter resulted in a large thermal resistance when the heat transferred through these polymers, limiting the overall k_c. To address this issue, synergistic double networks consisting of primary segregated networks between polymer particles and secondary embedded networks within the polymer particles (**Fig. 4**e and f) were

constructed using hybrid fillers with different dimensions and sizes including CNTs, graphite nanoplatelets (GNPs) and BN flakes.[118, 152-154] In this strategy, composite particles containing high-*k* fillers instead of neat polymer particles were used as the templating units to construct the segregated networks of two different routes by forming additional conductive pathways within the polymer particles that ameliorated the heat conduction within the matrix. The assembly of double conductive networks was also widely used to improve the k_c of composites with electrically insulating primary segregated networks. The addition of high-*k* but electrically conductive fillers such as graphene in the secondary networks compensated the relatively low *k* of the electrically insulating fillers without impairing the overall electrically insulating nature of the composites.[118, 154, 155]

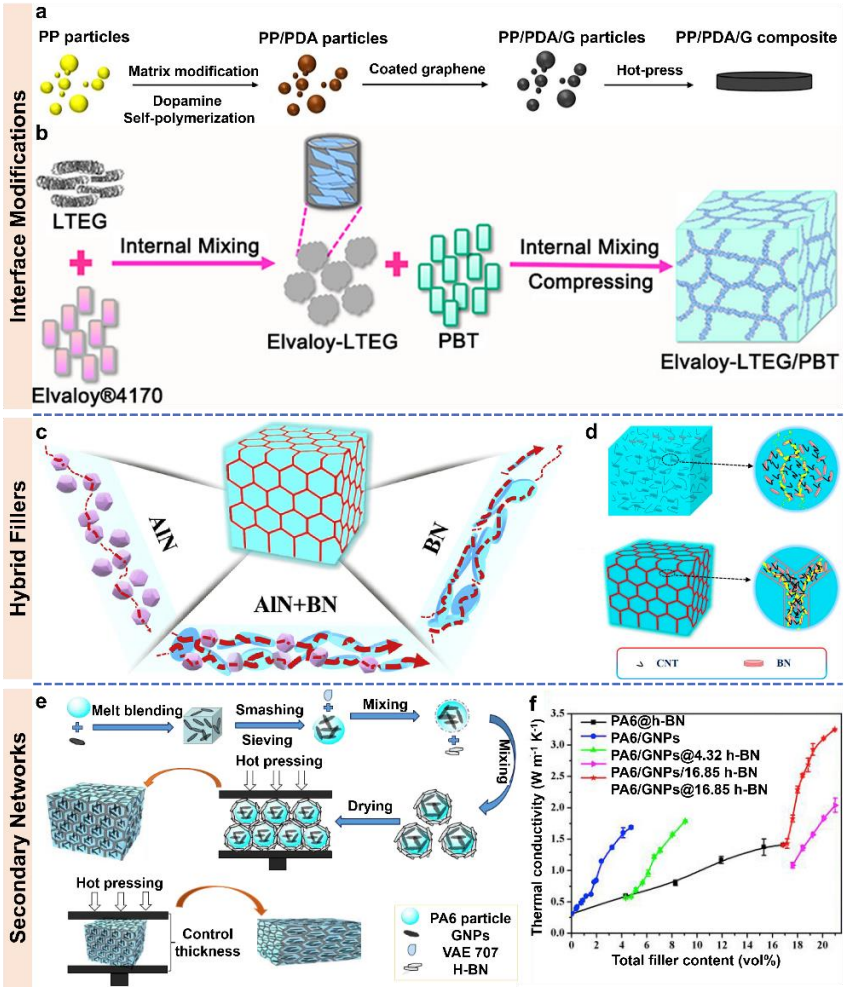

Fig. 4. Strategies to improve the *k* of composites containing segregated structures. (a) Schematic illustration of the preparation of graphene/PDA@PP composites through

matrix modification. Reproduced with permission from ref. [131]. Copyright 2020, Elsevier Ltd. (b) Schematic illustration of the preparation of Elvaloy@EG/PBT composites through filler modification. Reproduced with permission from ref. [148]. Copyright 2017, American Chemical Society. (c) Schematic illustration of the heat transport pathways in UHMWPE composites containing hybrid fillers of BN and AlN. Reproduced with permission from ref. [114]. Copyright 2018, Elsevier Ltd. (d) Schematic illustration of the filler networks in BN-CNT/PVDF composites. Reproduced with permission from ref. [151]. Copyright 2018, American Chemical Society. (e) Schematic illustration of the preparation and (f) k of polyamide 6 (PA6) composites containing secondary GNP networks within the primary segregated h-BN networks. Reproduced with permission from ref. [118]. Copyright 2019, Elsevier Ltd.

Despite the above impressive k_c values achieved using the self-templating strategy, it is highly desirable yet challenging to produce composites with a high through-plane k_c due to the in-plane orientation of fillers. The resulting thermally conductive composites or films typically showed highly anisotropic k_c values in two orthogonal directions, with much higher in-plane values than the through-plane ones. To tackle the challenge of low through-plane k_c, thermally conductive fillers of spherical shapes, instead of polymer granules, were used as templates to form interlocked networks in the thickness direction by the spherical fillers in direct contact.[156-159] A pea-pod-like binary alumina-graphene architecture was constructed in an epoxy composite using alumina particles as templates, as shown in **Fig. 5**a. The in-plane and through-plane k_c values of the resulting composites containing 12.1 wt% graphene and 42.4 wt% alumina were 33.4 and 13.3 W m^{-1} K^{-1}, respectively (**Fig. 5**b).[156] The particularly impressive through-plane k_c was made possible by forming the thermally conductive networks with interconnected graphene and alumina in the thickness direction, as shown in **Fig. 5**c.[157] The individual alumina particles were fully wrapped by graphene sheets to form effective conductive pathways in the through-plane direction, giving rise to a through-plane k_c over three times higher than those containing either filler alone (**Fig. 5**d). It thus can be said that spherical fillers are conducive to the construction of heat

conduction pathways along the thickness direction.

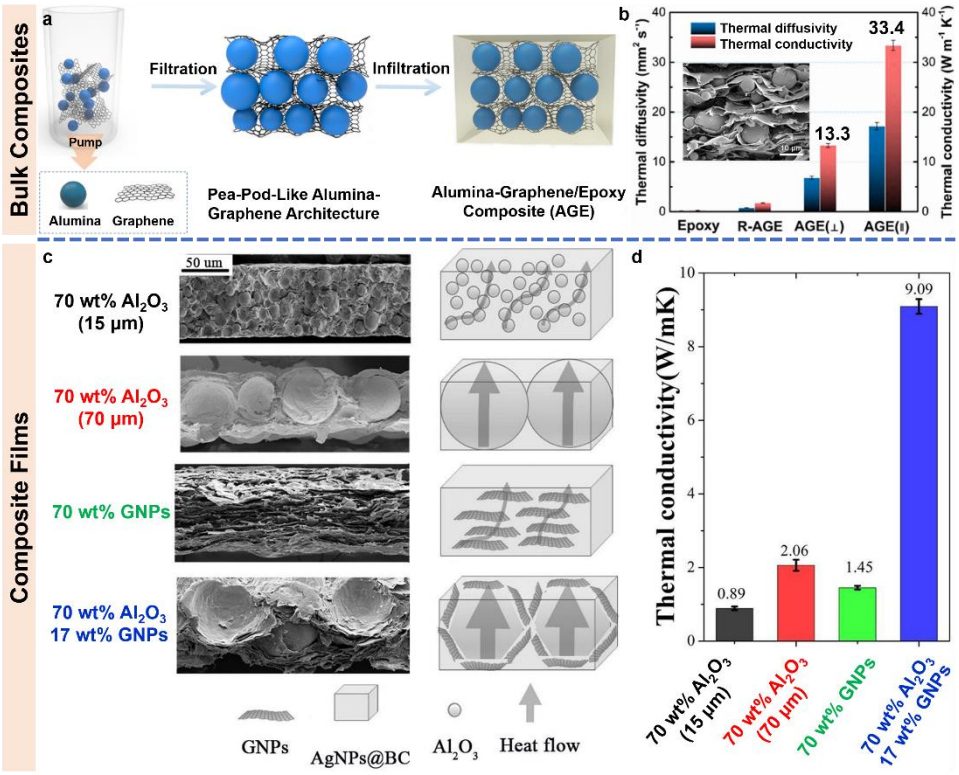

Fig. 5. Self-templating using spherical fillers as templates for composites with enhanced through-plane k_c. (a) Schematic illustration of the fabrication and (b) k_c of a pea-pod-like Al_2O_3-graphene/epoxy bulk composite. Reproduced with permission from ref. [156]. Copyright 2019, Elsevier Ltd. (c) Morphologies and (b) through-plane k_c of Al_2O_3-GNPs/bacterial cellulose composite films with different thermally conductive networks. Reproduced with permission from ref. [157]. Copyright 2019, Elsevier Ltd.

Although segregated fillers forming interconnected networks can significantly improve k_c, the mechanical properties of these composites are generally poor because of the discontinuous polymer matrix and the voids generated in the filler networks. To address the issue of poor mechanical properties, a segregated structure reinforced by BN wrapped PP fibers was developed.[160] The tensile strength and elongation at break of BN/PP composites containing such PP fibers were improved by 225% and 267%, respectively, against those without PP fibers while maintaining an excellent k_c. In addition to the fiber-reinforcement strategy, other modifications involving crosslinking treatment [161] and interfacial crystallization [162] were also proposed to achieve

improved mechanical properties. Directly using commercial nylon gauze fabrics as templates was another attractive approach to yield satisfactory mechanical properties owing to the continuous polymer matrix phase.[163] Therefore, enhancing the interfacial interaction between the matrix and filler skeleton and maintaining the continuity of the matrix while constructing ordered heat conduction filler networks are the key to the preparation of thermally conductive composites with excellent mechanical properties in the self-templating strategy. Another limitation of self-assembling strategy is its restricted application to thermoplastic matrices with high melting viscosities. Recently, a dynamic cross-link reshuffling strategy was employed to engineer segregated structures in thermosets,[164] further extending the suitability of self-templating to broadly-based polymer matrices. In addition to the commonly-used melt compounding, a gelation approach was also developed to guide the assembly of graphene oxide (GO) into a 3D segregated network using natural rubber (NR) particles as templates.[165]

3.2. Sacrificial templating

The thermosetting polymers are also commonly used for thermal management applications because of their excellent mechanical properties and high heat resistance. Although the above thermoplastic composites with segregated structures made by self-templating can be used as scaffolds after sintering for infiltrating thermosetting resins, the process is rather complicated for practical applications.[166] Instead, sacrificial templates have been widely employed to guide the assembly of fillers to form 3D filler networks. The resulting scaffolds after removing the initial templates are infiltrated with thermoset resins to yield thermally conductive composites containing 3D interconnected fillers. Salts are widely used as sacrificial templates to fabricate sensors,[167] energy harvesters,[168] adsorbents,[169] and bio-scaffolds[170] because they can be easily removed by washing with water or high-temperature treatments. Thermally conductive scaffolds have been prepared using the salt-templating method. For example, water-soluble NaCl particles were used as sacrificial templates to produce BN-PVDF scaffolds with pore sizes of 400−500 μm (**Fig. 6**a).[64] Upon solvent

evaporation, the majorities of 2D BN platelets with a high aspect ratio gathered around the salt particles owing to the volume repulsion effect of the salt template, creating an isotropic cellular structure after salt removal (**Fig. 6**b). The resulting BN-PVDF/epoxy composite with a BN loading of 21 wt% exhibited a k_c of 1.227 W m^{-1} K^{-1}, which was further improved to 1.466 W m^{-1} K^{-1} through converting PVDF adhesive into carbon with reduced phonon scattering at the interfaces. In addition to water-soluble NaCl, NH_4HCO_3 capable of decomposition at high temperatures were also used as templates for the assembly of BN networks.[171] The through-plane k_c of 3D-BN/epoxy composites was as high as 6.11 W m^{-1} K^{-1} at a BN loading of 59.43 vol%. Apart from 3D porous scaffolds, the salt-templating method was also applied to prepare hollow microbeads which were dispersed in the matrix for simultaneously enhancing the in-plane and through-plane k_c after compression and infiltration.[172]

In addition to salts, water-soluble sugars were also employed as sacrificial templates for constructing 3D fillers for thermally conductive composites. An eco-friendly cotton candy-templating was developed to create 3D porous channels in epoxy-based composites (**Fig. 6**c).[173] The continuous sucrose fibers embedded in the epoxy resin were dissolved in water, leaving behind interconnected hollow channels in the matrix after washing. These hollow channels were subsequently infiltrated with Al_2O_3 particles by vacuum-assisted impregnation followed by refilling the interparticle space with epoxy resin, yielding 3D thermally conductive pathways formed by interconnected Al_2O_3 particles in the epoxy composites (**Fig. 6**d). Compared with the randomly-dispersed fillers prepared by a conventional mixing method, the sugar-templated composites exhibited consistently higher k_c at equivalent filler loadings (**Fig. 6**d). The differences in k_c became increasingly prominent with increasing filler loading, which is attributed to the much-enhanced thermal percolation and multiple thermal pathways in the composites containing interconnected Al_2O_3 beads. This facile strategy has also been successfully adopted to fabricate electrical conductors,[174] sensors,[175] electromagnetic interference (EMI) shielding devices,[176] and oil adsorbents.[177]

The bubble template is another promising candidate complementing the solid-based salt or sugar templates. Specifically, the foaming technique – a universal process capable

of generating lightweight porous materials – has been used to produce thermally conductive porous [178] and solid [179, 180] composites. In this technique, the gas bubbles serve as the templates to direct the assembly of fillers at their interfaces. For example, BN platelets were expelled into the narrow walls surrounding the air bubbles created by the foaming agent, producing a 3D interconnected BN aerogel for effective heat transfer (**Fig. 6**e). The vacuum infiltration of polydimethylsiloxane (PDMS) into the porous scaffold yielded 3D BN/PDMS composites (**Fig. 6**f).[179] The 3D interconnected networks led to much enhanced heat dissipation than the randomly dispersed BN fillers, as confirmed by finite element analysis (FEA), as shown in **Fig. 6**g. A large heat flux with a low thermal resistance was possible through the well-defined BN skeletons in the 3D cellular composite. Conversely, the heat flux was much lower in the composite containing randomly-dispersed BN fillers without clear conductive pathways because of the high thermal resistance between the isolated BN fillers, significantly impeding heat conduction.

Other commonly used media for sacrificial templating include surfactant solution and emulsion. It is worth mentioning that amphiphilic GO sheets can be assembled at liquid–air and liquid–liquid interfaces in surfactant solution [181] and water-oil[182]/water-organic[183] emulsion, respectively, leading to 3D graphene architectures with spherical pores duplicating the shape of air bubbles or oil/organic droplets. In addition, a particle-stabilized emulsion method was used to produce porous titanium dioxide (TiO_2) and Al_2O_3@graphite foams for improving the k of low-molecular-weight organic PCMs.[184, 185]

At present, the sacrificial templating method has been chiefly employed to construct isotropic segregated structures with relatively large-size pores. Therefore, multiscale structural designs, such as aligned structures and hybrid fillers, can be introduced in the sacrificial templating method to enhance k_c of composites. Similar to the self-templating, developing paper-like thermally conductive products using sacrificial templating is possible by optimizing the processing parameters.

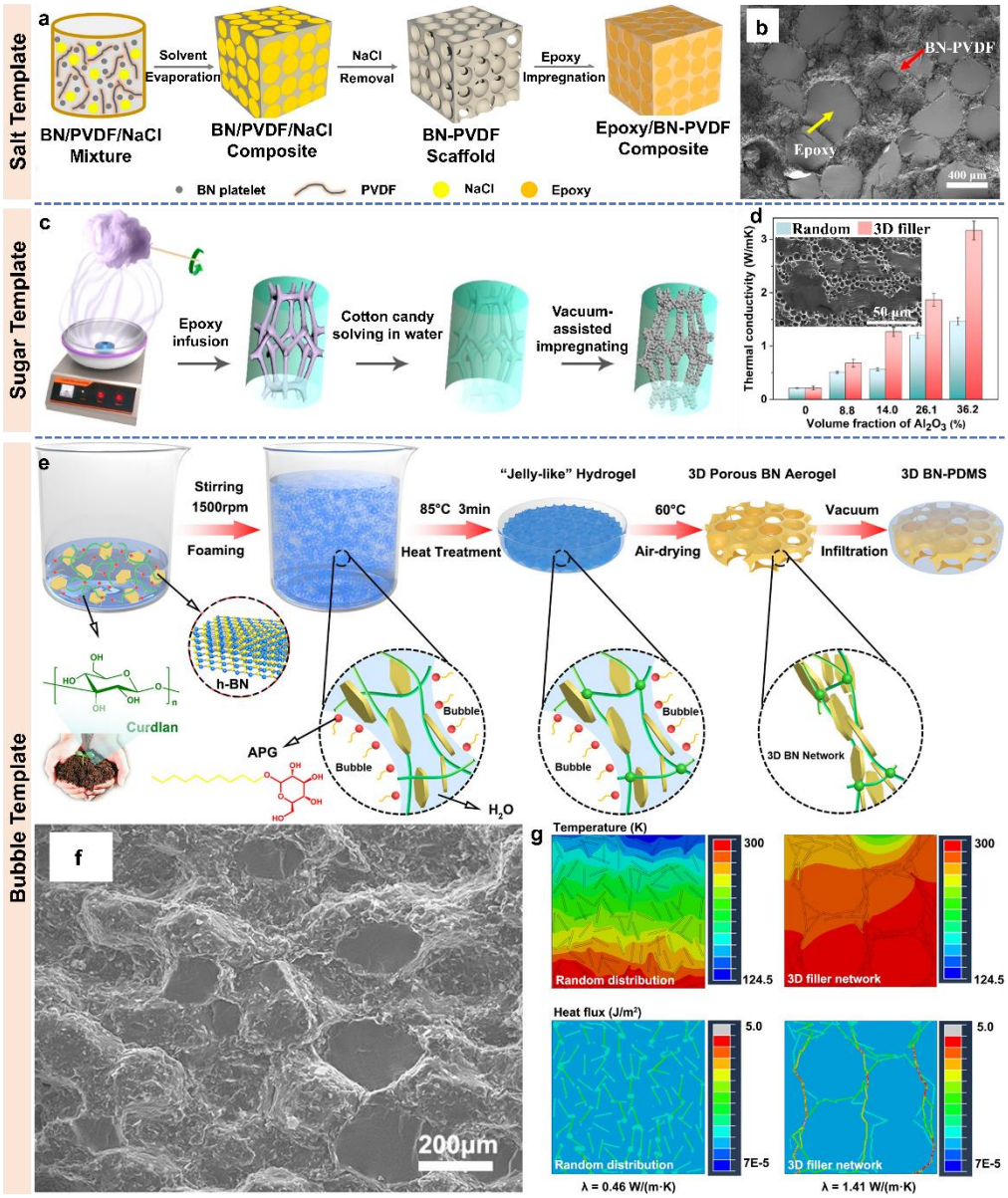

Fig. 6. Sacrificial templating method to fabricate thermally conductive composites using salt, sugar, and air bubble as templates. (a) Schematics showing the fabrication of 3D BN/PVDF scaffolds followed by epoxy infiltration using salt as the template. (b) SEM image showing the microstructure of BN-PVDF/epoxy composites. Reproduced with permission from ref. [64]. Copyright 2016, American Chemical Society. (c) Schematics showing the fabrication of Al_2O_3/epoxy composites using the sugar templating method. (d) Comparison of k_c for composites made by sugar templating and powder mixing methods. The inset shows SEM image of the fracture surface of Al_2O_3/epoxy composites. Reproduced with permission from ref. [173]. Copyright 2019, American Chemical Society. (e) Schematics showing the fabrication of 3D BN/PDMS

composites using air bubbles as template. (f) SEM image showing the microstructure of BN/PDMS composites. (g) Simulated temperature and heat flux distributions of randomly-dispersed BN/PDMS and 3D BN/PDMS composites by FEA. Reproduced with permission from ref. [179]. Copyright 2020, American Chemical Society.

3.3. Foam-templating

Commercial polymer foams have been used as facile templates to directly deposit functional materials onto the 3D skeleton to form interconnected fillers. The foam-templating technique has been widely applied to produce high-performance polymer composites for multifunctional applications, such as sensors,[186] shape memory devices,[187] EMI shielding,[188] and energy-related applications.[189] Templates based on commercial melamine-formaldehyde (MF) foam [19, 190, 191] and polyurethane (PU) foam [119, 192, 193] were most widely used for high-k polymer composites. Other foams, including metal foams,[194] ceramic foams,[195] and carbon foams,[196] were either directly employed as conductive skeletons or as templates for the assembly of additional fillers to further improve the k_c. In view of the same assembly process involved, we focus mainly on the polymer foam templates in the following discussion.

3D graphene foams (GFs) were fabricated using commercial foams as templates and GO sheets as precursors by dip-coating.[192] The commercial MF was dip-coated in GO solution followed by the reduction of GO and impregnation of liquid PDMS to yield a hyperelastic, double-continuous network of graphene and MF in the PDMS matrix (**Fig. 7**a).[19] The simple dip-coating process was easily scaled up for roll-to-roll fabrication using roller equipment (**Fig. 7**b). The 3D structure was effectively tailored by compressing the MF template in one or multiple directions, as shown in **Fig. 7**c. The unidirectional compression in the thickness direction resulted in the orientation of struts in the horizontal plane, showing an enhanced in-plane k_c with increasing the compression ratio (**Fig. 7**d). Tri-axial compression gave rise to a compact network and thus a higher filler loading, isotropically improving the k_c. Therefore, the densification and orientation of thermally conductive networks by mechanical compression are

effective methods to improve the in-plane and isotropic k_c of composites made from polymer foam templates.

A dual-assembly strategy with a multiscale structural optimization was used to construct vertically-oriented graphene frameworks for an augmented through-plane k_c (**Fig. 7**e).[197] After stretching and rolling, the quasi-isotropic graphene skeleton with loosely stacked graphene sheets was transformed into a highly ordered structure with fairly dense graphene stacking because of the circumferential stresses generated from the natural contraction of porous PU film (**Fig. 7**f). As a result, the dense graphene skeleton with intimate contacts and large overlapping areas among the adjacent graphene sheets endowed the composites with an exceptionally high through-plane k_c of 62.4 W m^{-1} K^{-1}. The F-F interfacial thermal conductance of adjacent graphene sheets from the Foygel model and the nonequilibrium molecular dynamics (MD) simulation confirmed the importance of overlapping area among the adjacent graphene sheets (**Fig. 7**g).

The continuous filler networks established by foam templating depends on uniform deposition of fillers on the templates. Unlike GO with good dispersion for facile coating, specific treatments and additives are required for metals, GNPs and BNNSs to uniformly deposit on the foam skeleton. An electroless plating method was used to prepare Cu-coated MF for electro-driven polyethylene glycol (PEG)-based composites.[190] Cellulose nanofibers (CNFs) and GO were employed to facilitate the dispersion of GNPs and BNNSs, improving their uniformity on MF templates for thermally conductive phase change composites.[191, 198] Another issue arising from retaining the polymer templates in the final product may affect the properties of composites if the polymer constituting the template is not the same as the matrix. In this case, the polymer templates can be removed by high-temperature treatments before impregnating the matrix. For example, the pyrolysis treatment was used to remove the PU foam template after coating with GNPs, resulting in a freestanding GF as the 3D filler for thermally conductive polymer composites with an exceptionally high k_c of 8.04 W m^{-1} K^{-1} at a relatively low graphene loading of 6.8 wt%.[199, 200]

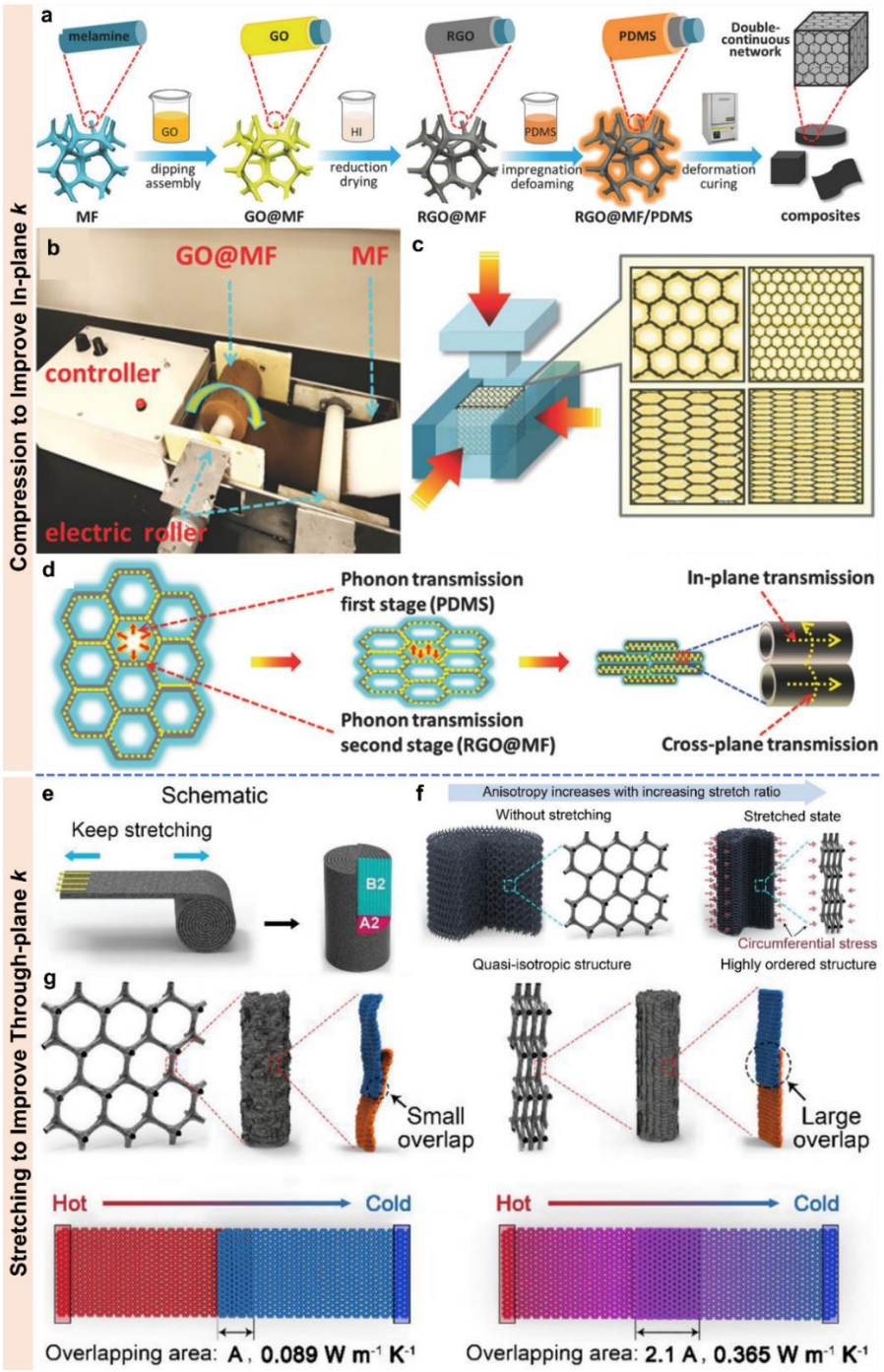

Fig. 7. Foam-templating methods to prepare thermally conductive composites. (a) Schematics showing the preparation of reduced GO (rGO)@MF/PDMS composites. (b) The roller impregnating apparatus for continuous fabrication of GO@MF. (c) Schematics of tuning the density and orientation of the networks through directional compression. (d) Schematics of phonon transport in rGO@MF/PDMS composites. Reproduced with permission from ref. [19]. Copyright 2018, WILEY-VCH. Schematics of (e) graphene framework prepared through stretching and (f) the conversion of

graphene framework from a quasi-isotropic to highly ordered state by stretching. (g) The junction thermal conductance among the adjacent graphene sheets having small and large overlapping areas in quasi-isotropic and highly-ordered composites, respectively, as calculated from the nonequilibrium MD simulations. Reproduced with permission from ref. [197]. Copyright 2021, WILEY-VCH.

In addition to the aforementioned alignment designs through compression and stretching, the foam-templating method was modified by means of interfacial engineering, incorporating hybrid fillers and constructing secondary networks to further augment the k_c. The PU foam surface was treated with PDA to improve the interfacial adhesion between BN and PU for enhanced k of the resultant PEG composite (**Fig. 8**a).[201] The PDA modification effectively reduced the ITR between PU and BN, giving rise to an increase in k_c from 2.2 to 2.4 W m^{-1} K^{-1} (**Fig. 8**b). Hybrid fillers of different sizes were also used to construct effective conductive networks. For example, Al_2O_3 particles of micron and submicron sizes were infiltrated into the porous PVA foam using a vacuum-assisted infiltration method (**Fig. 8**c).[125] The submicron-size particles filled the gap between micron-size particles, forming direct contacts among adjacent fillers and thus creating thermally conductive strings of Al_2O_3 particles for effective thermal transport (**Fig. 8**d). Similar to segregated structures, constructing a secondary filler network within the pores of foam templates is another effective way to boost k_c. Very recently, a ceramic foam with a reticulated porous structure (RPC) was fabricated by depositing Al_2O_3 on a PU foam template. After sintering at a high temperature of 1500 °C, the PU foam template was removed and the RPC consisting of continuous millimeter-sized cell pores and hollow ceramic struts was obtained (**Fig. 8**e).[119] After infiltrating epoxy resin containing tetrapod-like zinc oxide whiskers (T-ZnOw) into the ceramic foam, the resulting ternary composites exhibited a k_c of 1.968 W m^{-1} K^{-1} at a RPC loading of 11.7 vol% and T-ZnOw loading of 6 vol%. The dual thermal conduction channels constructed by RPCs and T-ZnOw synergistically improved the k_c.

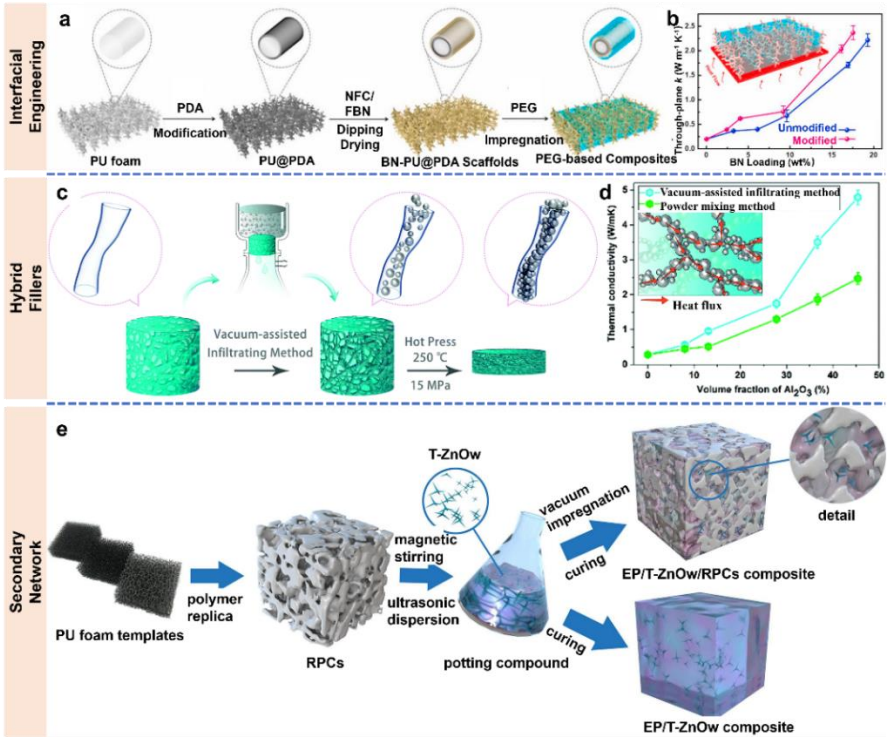

Fig. 8. Modified foam-templating methods through interfacial engineering, incorporating hybrid fillers and constructing secondary networks for enhanced k_c. (a) Schematic illustration of interfacial engineering using PDA in the BN-PU@PDA scaffold/PEG composite. (b) Through-plane k_c of unmodified and modified composites with PDA. Reproduced with permission from ref. [201]. Copyright 2021, Elsevier Ltd. (c) Schematic illustration of the preparation and microstructures of Al_2O_3/PVA composites. (d) Comparison of k_c of Al_2O_3/PVA composites prepared by vacuum-assisted infiltration and powder mixing methods. The inset is a schematic illustration of the thermal transport pathways in the vacuum-assisted infiltrating composites. Reproduced with permission from ref. [125]. Copyright 2018, Royal Society of Chemistry. (e) Schematic illustration of the fabrication of RPC/T-ZnOw/epoxy composites. Reproduced with permission from ref. [119]. Copyright 2020, Elsevier Ltd.

For the foam-templating, a proper selection of foam templates is also critical, especially when aligned fillers are desired. Aligned skeletons are realized through stretching and compression, thus foam templates with good mechanical flexibility and compressibility are preferred.[19, 197] Another crucial parameter is the interaction between fillers and skeletons, which determines the uniformity and integrity of filler dispersion on the

skeleton. In addition to stretching and compression, customized assembly approaches to thermally conductive networks through rolling and folding are also an attractive solution to realizing layered filler structures.[202]

3.4. Ice-templating

Ice-templating or freeze-casting [203-205] is a facile yet powerful processing technique to produced 3D interconnected filler networks with controlled morphologies. A typical ice-templating process is divided into four steps, namely, (i) preparation of precursor suspensions, (ii) solidification, (iii) sublimation, and (iv) post-fabrication involving sintering, densification, and surface modification, as shown in **Fig. 9**a.[206-209] The freezing step plays a significant role in controlling the morphologies of the 3D networks by tuning the nucleation and growth of ice crystals, which are the two individual yet consecutive stages during ice solidification.[210] Additionally, the ice-templating technique is applicable to a wide range of fillers from inorganics to organics with diverse dimensionalities from 0D nanoparticles to 2D nanosheets of metals,[211] ceramics,[212] carbon materials,[213, 214] polymers,[215] and their hybrids[216-218](**Fig. 9**b).[209, 219] These fillers were assembled into multifarious architectures in the form of beads or microspheres,[220-222] fibers,[223] films or membranes,[224-226] and scaffolds [122, 227, 228] with controlled microstructures, such as isotropic, honeycomb-like/cellular, lamellar and radial structures (**Fig. 9**c), further manipulating the performance of the final materials and devices. A representative freezing apparatus and process is presented in **Fig. 9**d.[229-231] Briefly, the solid components in the freezing suspension are expelled by the growing ice crystals and then gathered at the interfaces between the ice crystals once fully frozen. After sublimation of ice by freeze-drying, a porous scaffold with solid walls replicating the morphology of ice crystals is obtained. Some solid particles may be entrapped between the adjacent ice dendrites and within the ice crystals to create characteristic roughness on the walls and bridges between neighboring walls. The morphologies of the porous structure can be tailored by controlling the freezing conditions and parameters, such as the distribution of cold source,[232] the shape of mold,[233] the freezing substrate,[234, 235] the concentration

of precursor suspensions,[236] the freezing temperature/rate,[210, 237] and the additives.[238, 239] Moreover, the directions of ice crystal growth can be modified using the random freezing, unidirectional freezing, bidirectional freezing, or radial freezing methods, generating a range of different microstructures including isotropic,[240, 241] honeycomb,[75, 227, 242, 243] long-range lamellar,[244-250] and radially aligned structures.[251-254] (**Fig. 9**e).[255] The integration of ice-templating strategy with various external fields such as electric,[256] magnetic,[257] and acoustic fields[258] provides ample possibilities for producing more effective and complex microstructures (**Fig. 9**e).[259] These tailored structures endow materials made by ice-templating with desired multifunctional properties.[260, 261]

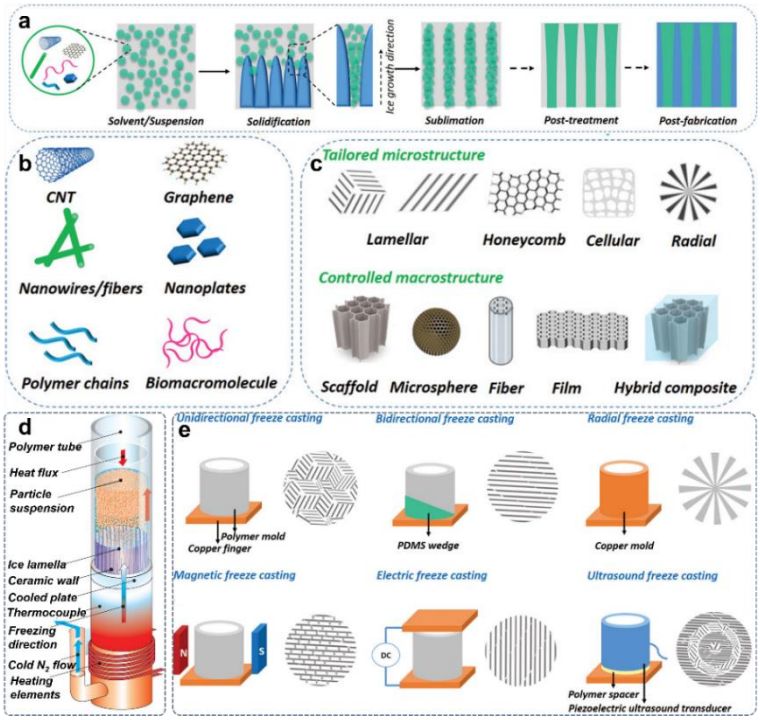

Fig. 9. (a) Schematics of the ice-templating process. Schematics of (b) building blocks, (c) tailored microstructures, and macrostructures. Reproduced with permission from ref. [209]. Copyright 2020, Wiley-VCH. (d) Typical setup for ice-templating. Reproduced with permission from ref. [230]. Copyright 2014, Springer Nature. (e) Modified ice-templating setups for controlling the microstructures. Reproduced with permission from ref. [209]. Copyright 2020, Wiley-VCH.

The ice-templating method has been successfully adopted to produce high-*k* composites after infiltrating polymer resins into the 3D thermally conductive fillers. Both electrically conductive (*e.g.*, CF,[262-264] CNT,[265] graphene,[265-269] Cu nanowire,[270] Ag nanowire,[271-273] and MXene[264, 274, 275]) and insulating (*e.g.*, BN platelets,[67, 116, 117, 122, 133, 276-285] BNNS,[65, 66, 81, 250, 272, 273, 286-288] AlN,[289] and SiC micro-[290]/nanowires [283, 291, 292]) low-dimensional fillers are assembled into 3D architectures for enhanced *k* of robust (*e.g.*, epoxy[66, 81, 133, 262, 264-270, 273, 275, 278, 282, 286-290, 292] and PA6[284]), flexible (*e.g.*, PI[250, 272], PDMS[65, 122, 263, 274, 283, 291] and NR[276, 277]), biodegradable (*e.g.*, polycaprolactone (PCL)),[281] and phase change (*e.g.*, PEG)[67, 116, 117, 279, 280, 285] polymers. Compared with other techniques, the ice-templating strategy is capable of controlling the spatial arrangement and orientation of thermally conductive fillers, leading to rich microstructures encompassing isotropic,[116, 117] cellular,[65, 81, 122, 133, 262-267, 270, 273-283, 286, 289-292] lamellar,[66, 250, 268, 269, 272] and radial structures[67, 271, 287, 288] for the rational design of heat conduction pathways according to different application scenarios (**Fig. 10**). A nondirectional ice templating without temperature gradient was adopted to fabricate a 3D isotropic BN architecture (**Fig. 10**a), whose composite showed a higher k_c than the randomly-dispersed BN counterpart made by melt blending. It is worthy of note that the composite made from a higher freezing temperature or at a slower freezing rate generally exhibited superior k_c because of the thicker BN walls with fewer defects and thermal contact interfaces (**Fig. 10**b).[117] To make full use of anisotropic *k* of low-dimensional fillers, highly-aligned cellular and lamellar structures were constructed using the unidirectional and bidirectional ice templating methods, respectively (**Fig. 10**c-g).[65, 66] The highly-aligned structure not only imparted a high k_c in the alignment direction,[269] but also endowed the composites with improved mechanical properties such as fracture toughness.[293, 294] Nonetheless, both uni- and bidirectional freezing routes can only provide a high k_c in the aligned direction with a much lower k_c transverse to it. Recently, a radial ice templating route was developed to construct a radially-aligned centrosymmetric structure for PEG-based phase change composites

with simultaneously enhanced in-plane and through-plane k_c (**Fig. 10**h and i).[67] The radially-oriented filler composites offered rapid and uniform heat dissipation in all directions with a relatively uniform temperature distribution across the whole body compared to the vertically-aligned composites in which the heat flow was restricted in a local region (**Fig. 10**j and k). These representative cases demonstrate that the ice-templating approach is an ideal solution to building 3D conductive networks using low-dimensional fillers with desired alignments for various application scenarios by tuning the freezing dynamics.

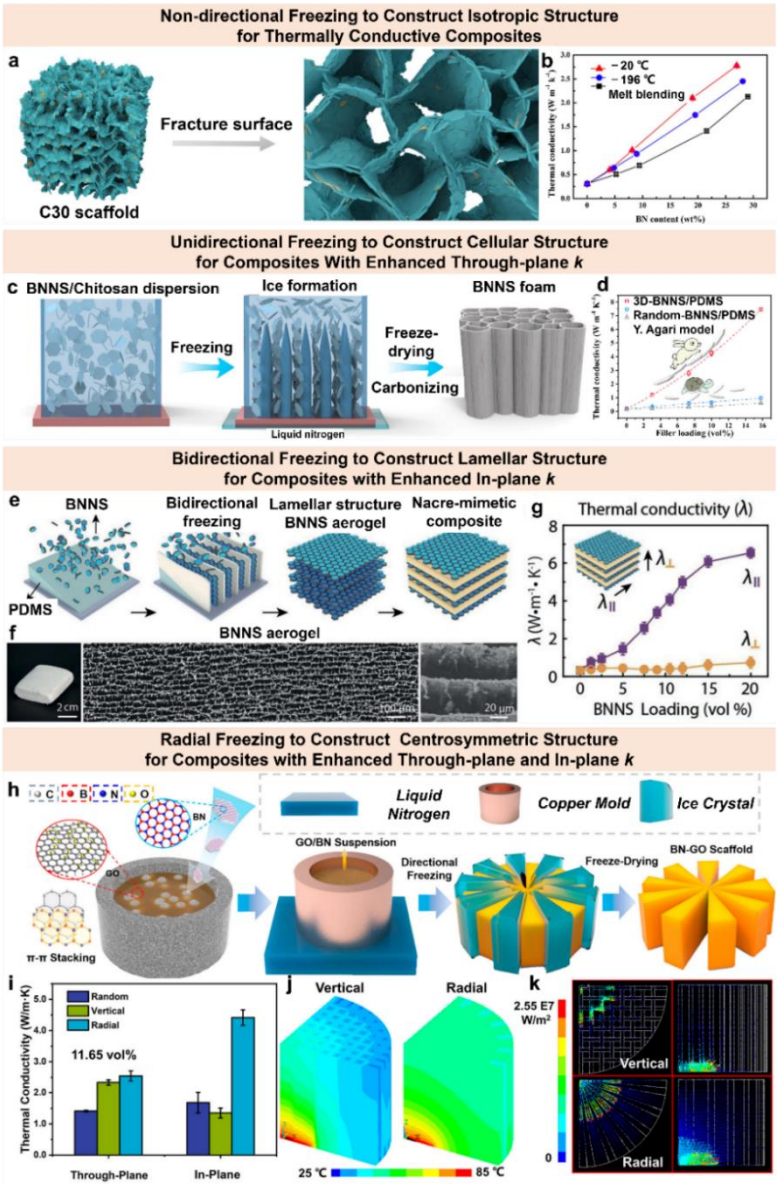

Fig. 10. Ice-templating strategy to prepare thermally conductive composites. (a) Schematic illustration indicating the microstructure and (b) k_c of BN@chitosan/PEG

composites made by non-directional freezing. Reproduced with permission from ref. [117]. Copyright 2019, Elsevier Ltd. (c) Schematics of the fabrication of vertically-aligned BNNS foam using unidirectional freezing and (d) the corresponding k_c of BNNS/PDMS composites. Reproduced with permission from ref. [65]. Copyright 2019, American Chemical Society. (e) Schematics of the fabrication of nacre-mimetic BNNS aerogel and corresponding epoxy composites using bidirectional freezing. (f) SEM images showing long-range aligned lamellar structures of BNNS aerogel. (g) k of BNNS/epoxy composites in the parallel and perpendicular to aligned lamellar layers. Reproduced with permission from ref. [66]. Copyright 2019, WILEY-VCH. (h) Schematics of the fabrication of a centrosymmetric GO-BN scaffold using radial freezing. (i) Through-plane and in-plane k_c of GO-BN/PEG composites. (j) Temperature distribution and (k) heat flux vector (heated for 1 s) of a quarter model of the GO-BN/PEG composite with vertical and radial alignments by FEA. Reproduced with permission from ref. [67]. Copyright 2020, American Chemical Society.

In addition to controlling the filler alignment by varying the freezing directions, cell wall compositions and structures have been modified through F-M/F-F interfacial engineering and the use of hybrid fillers to further improve the k_c. For example, the PEG grafted PDMS (PEG-*g*-PDMS) was used to modify the interface between the SR matrix and rGO fillers for enhanced interfacial interactions by hydrogen bonds (**Fig. 11a**).[291]. One-dimensional SiC nanowires were also added to assist the formation of synergistic filler networks with 2D rGO sheets, reducing the ITR between rGO. The vertically-aligned 3D fillers containing 1D SiC nanowires and 2D rGO sheets were obtained by unidirectional freeze-casting (**Fig. 11**b-c), which were infiltrated with a SR matrix to form thermally conductive composites. The collective effects of interfacial engineering, hybrid fillers, and aligned structures endowed the composites with a high k_c of 2.74 W m^{-1} K^{-1}, 683 % higher than that without interfacial modification and filler alignment (**Fig. 11**d).

Unlike freestanding graphene monoliths made from GO precursors, most other nanofillers are unable to form freestanding 3D architectures without the assistance of

supporting materials or binders because of their smaller aspect ratios and fewer functional groups than GO. Therefore, graphene and water-based polymers, such as PVA, cellulose, and chitosan, are commonly used as binders to improve the mechanical integrity of 3D structures made from fillers like BNNS.[81, 117, 133, 295, 296] To improve the interaction between fillers and binders, C-N covalent bonds were created between BN and GO originating from the reaction between the amino and carboxyl groups during high-energy ball milling (**Fig. 11**e).[133, 277] The resulting fillers were unidirectionally freeze-cast to construct a covalently bonded, highly aligned 3D rGO-BN network for polymer composites (**Fig. 11**f-g). The combination of covalent bond modification and ice templating generated 3D rGO-BN networks having a much higher k_c than those with electrostatic interactions (**Fig. 11**h) or randomly mixed rGO-BN fillers (**Fig. 11**i), thanks to the greatly reduced ITR between the two fillers which was facilitated by covalent bonds as well as the alignment via ice templating (**Fig. 11**j). Similarly, covalent bonds between BN and SiC were introduced by high-temperature sintering after a BN-SiC scaffold was obtained by unidirectional freeze-casting, lowering the ITR between BN and SiC for enhanced k_c.[283]

The above discussions indicate that ice-templating is a convenient strategy to specifically improve the isotropic, through-plane or in-plane k_c by controlling the freezing direction and F-F interactions. A relatively high freezing temperature is instrumental to an isotropic conduction network with fewer thermal contact interfaces, leading to a highly isotropic k_c. Cellular and lamellar structures with highly aligned cell walls constructed by unidirectional and bidirectional freezing routes are preferable for the fabrication of thermally conductive composites with enhanced in-plane or through-plane k_c. Radially frozen composites with centrosymmetric structures exhibited simultaneously improved k_c in the two orthogonal directions. Nevertheless, it is still challenging to obtain large-size products with long-range alignment using directional freezing strategies because of the limitation of temperature increase at the freezing front when it moves far away from the cold source.[297, 298] In addition to bulk composites by infiltrating liquid resins into the porous scaffolds, a combination of directional freezing methods and hot press was used to fabricate laminate thin films with improved

in-plane k.[250, 272]

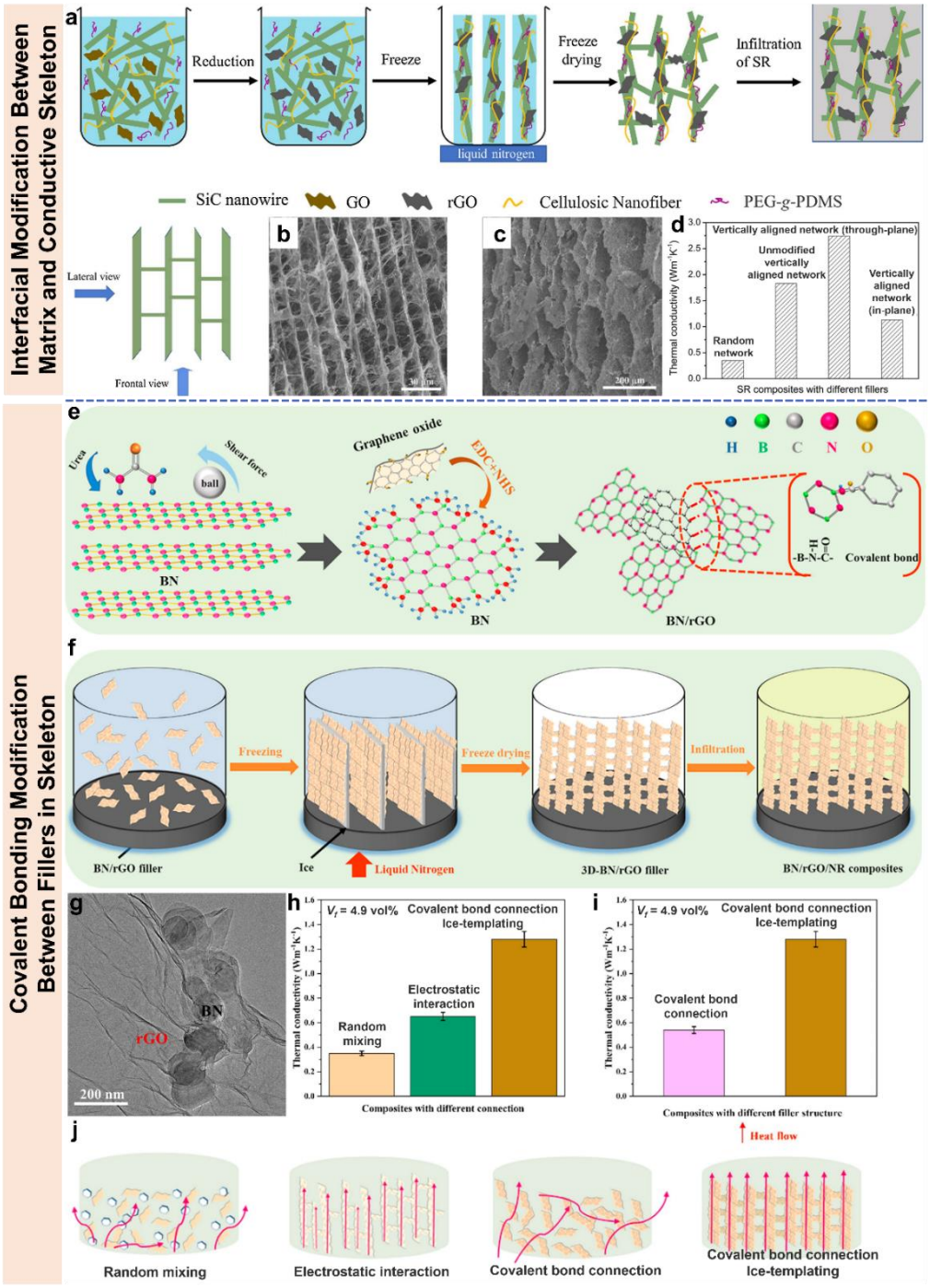

Fig. 11. Modified ice-templating methods through interfacial engineering and the use of hybrid fillers for enhanced k_c. (a) Schematics of the fabrication of vertically-aligned SiC nanowires/rGO networks and corresponding PEG-*g*-PDMS-based composites. SEM images taken from the (b) front and (c) side showing vertically-aligned SiC nanowires/rGO networks. (d) Through-plane k_c of the composites with random

networks, unmodified vertically-aligned networks and vertically-aligned networks with interfacial modification as well as the in-plane k_c of vertically-aligned composites. Reproduced with permission from ref. [291]. Copyright 2020, Elsevier Ltd. Schematic illustrations of the fabrication of (e) BN-rGO hybrids with covalent bonds and (f) 3D BN-rGO/NR composites using a unidirectional freezing method. (g) TEM image of the BN-rGO hybrids. The effects of (h) covalent bonds and (i) filler structures on k_c. (j) Schematic illustrations of thermal transport in four composites with different microstructures and bonding types between fillers. Reproduced with permission from ref. [277]. Copyright 2019, Elsevier Ltd.

3.5. Template-directed CVD

The 3D fillers prepared by the aforementioned templating methods are assembled from nanoscale building blocks with physical interactions, *e.g.*, van der Waals forces, hydrogen bonds and π–π interactions, between individual fillers, resulting in significant phonon scattering at the F-F interfaces. Although covalent bonds can be achieved between adjacent fillers by interfacial engineering, the scattering of phonons is still significant because of the discontinuity at the interfaces. Seamlessly continuous 3D structures, such as graphite or graphene foams, are constructed by template-directed CVD to provide uninterrupted phonon transfer channels. Moreover, CVD-grown graphene possesses a better crystalline structure with fewer defects than rGO. Therefore, the high-quality conductive structures fabricated by template-directed CVD give rise to highly improved k_c.

In a typical template-directed CVD process, monolayer to few-layer graphene sheets are grown on the surface of 3D templates, such as Cu and Ni foams, to realize 3D graphene architectures. 3D GFs were first fabricated on Ni foams using methane and ethanol as carbon sources in 2011.[299, 300] The decomposed carbon atoms were deposited on the surface of Ni foam at a high temperature of over 1000 °C, prompting the nucleation and growth of graphene when the temperature was quickly reduced to room temperature. The metal templates were then removed by acid etching to yield a freestanding 3D GFs. Of note, a thin polymer layer such as PMMA is usually deposited

to support the original morphologies and protect them from collapsing during etching. In addition to metal templates, porous Al_2O_3 [301] and SiO_2 [302, 303] were also utilized as templates to prepare 3D graphene architectures.

The 3D GFs prepared by CVD on commercial metal foam templates usually contain large open pores. Therefore, the porous structure can be designed or filled with polymers to make composites with unique properties for diverse applications, including electrically conductive composites,[304] thermally conductive composites,[68] electrodes for supercapacitors [300, 305] and rechargeable batteries,[306] solar steam generation,[307] strain sensors,[308] and EMI shielding [309, 310]. For thermally conductive polymer composites, several modified CVD methods have been developed to improve the *k* of composites, including interfacial engineering (**Fig. 12**a and b),[132] construction of secondary networks (**Fig. 12**c-e),[80, 134, 311-313] mechanical densification (**Fig. 12**f-h),[115] the use of ice-templating scaffolds as growth templates (**Fig. 12**i-k),[314, 315] and the direct growth of hierarchical structures (**Fig. 12**l-n).[316, 317] Given that the CVD-grown graphene contains little or no functional groups, the interfacial interaction between graphene and matrix is predominantly by weak van der Waals forces, resulting in additional phonon scattering at the interface. A versatile noncovalent functionalization based on mussel-inspired PDA coatings and silane coupling agents (*e.g.*, *3*-aminopropyltriethoxysilane (APTS)) was developed to improve the interfacial interaction between the graphene networks and the PDMS matrix (**Fig. 12**a and b).[132] The improved interfacial adhesion gave rise to a substantially improved k_c. Instead of infiltrating neat polymers into the porous scaffolds, fillers/polymer mixtures have also been employed as masterbatches in which the functional fillers dispersed in the polymer form secondary conductive networks in addition to the primary conductive scaffolds. Several secondary fillers including CB,[313] multilayer graphene flakes,[312] graphene nanosheets,[80] and BN[311] were incorporated into the common matrix to create synergistic multi-level networks with foam structs as the primary conducting network. For example, a continuous GF filled with aligned graphene sheets endowed thermally conductive NR composites with an unexpectedly high in-plane k_c of 10.64 W m^{-1} K^{-1} at a graphene loading of 6.2 vol%

and a record-high thermal conductivity enhancement (TCE) of 1300% per 1 vol% filler (**Fig. 12**c-e).[80] Similarly, a BN foam containing BNNS secondary networks was used to fabricate electrically insulating composites with enhanced thermal conduction performance.[134] Although the k_c can be substantially improved using CVD-templating foams, it is nontrivial to achieve a high filler loading because of the large open pores in the metal templates, limiting the absolute value of k_c. To tackle this issue, a high-density and in-plane oriented 3D multilayer graphene web was grown on a highly compressed Ni foam, imparting an exceptional k_c of 8.8 W m^{-1} K^{-1} when made into epoxy composites at a high graphene loading of 8.3 wt% (**Fig. 12**f-h). Notably, the obtained thermally conductive nanocomposite did not sacrifice its mechanical properties despite the high filler loading, exhibiting an excellent fracture resistance thanks to the graphene network uniformly-constructed over the entire composite.[115] Moreover, the integration of ice-templating method with CVD provides extra benefits for the fabrication of thermally conductive composites with tailored structures, expanding from an isotropic structure duplicated from the metal foam template to an oriented structure resembling the ice-templated scaffold. An ice-templated anisotropic graphene scaffold was employed as the template for growing SiC sheets by CVD (**Fig. 12**i-k). The 3D covalently interconnected SiC sheets with vertically aligned structures led to a high through-plane k_c of 14.32 W m^{-1} K^{-1} for the epoxy-based composite at a SiC loading of 3.71 vol%.[314] Similar to the secondary network, secondary structures such as CNT forests were grown directly on the graphene struts to form multiscale, hierarchical structures for more effective, thermally conductive networks (**Fig. 12**l-n).[316, 317] Although the template-directed CVD method can produce high-quality 3D networks for thermally conductive composites with continuous phonon transfer pathways, it is of relatively high-cost and time-consuming, limiting its practical applications.

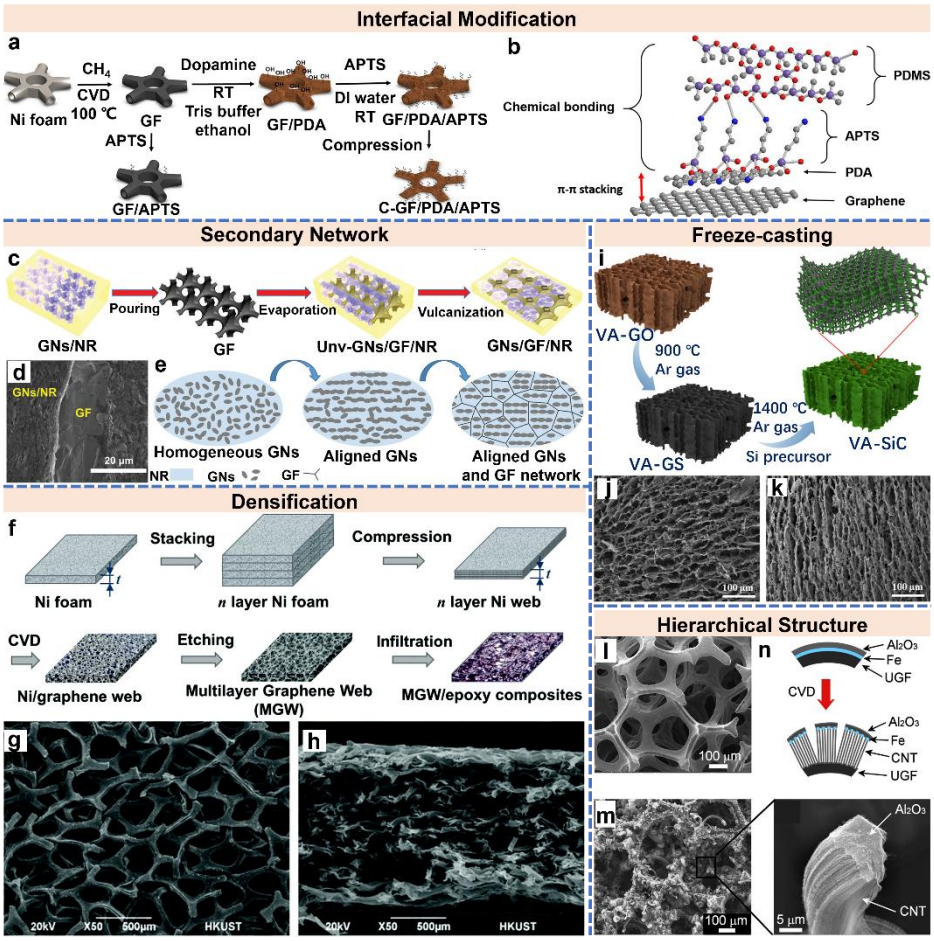

Fig. 12. Modified template-directed CVD methods for thermally conductive composites. (a) Schematic illustration of the preparation of compressed GF coated with PDA and APTS. (b) Molecular models showing the interactions between PDMS, APTS, PDA and graphene. Reproduced with permission from ref. [132]. Copyright 2017, American Chemical Society. (c) Schematic illustration of the preparation and (d-e) microstructures of GF-graphene nanosheets/NR composites. Reproduced with permission from ref. [80]. Copyright 2019, WILEY-VCH. (f) Schematic illustration of the fabrication of multilayer graphene web and the corresponding epoxy composites. SEM images of (g) top surface and (h) cross-section of multilayer graphene web. Reproduced with permission from ref. [115]. Copyright 2018, Royal Society of Chemistry. (i) Schematic illustration of the fabrication of vertically aligned SiC scaffold using ice-templated vertically aligned graphene scaffold as the CVD template. (j) Top- and (k) side-view SEM images of vertically aligned SiC scaffolds. Reproduced with permission from ref. [314]. Copyright 2020, American Chemical Society. SEM images

showing microstructures of GFs (l) without and (m) with CNT networks. (n) Schematic illustration of CNT growth on GF. Reproduced with permission from ref. [316]. Copyright 2015, American Chemical Society.

Different from other templating strategies, the CVD method features covalently bonded porous skeletons, which form continuous heat transfer pathways in the thermally conductive composites with small ITR. Owing to the limitations of large-size pores and low filler loadings, the absolute thermal conductivity of the composites is low. A principal reason behind these modified strategies is to reduce the effect of pore size or increase the filler content. Because the heat transfer network constructed by the CVD method replicates the structure of templates, those with oriented structures are ideal candidates for achieving high thermal conductivities at low filler contents. Given the composites prepared by CVD are usually in the form of bulk blocks, it is also important to prepare thin film products with covalently bonded filler heat conduction networks.

4. Comparison of Various Templating Strategies

To establish the structure-property relationship and the advantages of different templating strategies, a comprehensive comparison and systematic analysis of material systems and structural characteristics resulting from different templating methods and their effects on thermal conduction performance of composites are carried out as follows.

4.1. Comparison of k_c and thermal conductivity enhancement efficiency (TCEE)

The thermal conduction performance is measured by both the absolute k_c values and TCEE. Taking into account the effect of filler loading, TCEE, defined as the enhancement in thermal conductivity per volume fraction of fillers, is calculated by:

$$TCEE = \frac{k_c - k_m}{100 V_f k_m} \times 100\% \quad (2)$$

where k_c and k_m are the thermal conductivities of composite and matrix, respectively. A high TCEE value signifies that an effective conductive network is constructed in the matrix and thus a high k_c is expected at a low filler loading. Depending on the

applications, the k_c and TCEE values are evaluated along either in-plane or through-plane directions. When thermally conductive materials are used as state-of-the-art TIMs, a high through-plane k_c is highly desired to dissipate the heat generated from the electronics to heat sink in the thickness direction. **Table 2** compares the through-plane k_c and TCEE of composites made by different templating methods. In fact, enormous efforts have been made to improve the through-plane k_c by vertically aligning the fillers through various approaches, such as electric [318-320] or magnetic field [321-323] assisted alignments, hydrothermal self-assembly[295, 324], film rolling[325], mechanical rotating and cutting,[326-329] and 3D printing[330, 331]. Nevertheless, forming interconnected filler networks using these methods is found highly challenging. In comparison, the templating strategies are the preferred choice of fabricating 3D fillers with interconnected networks to greatly enhance the through-plane k_c, as shown in **Fig. 13**a. Amongst different templating strategies, the foam-templating, ice-templating and template-directed CVD methods are more effective than the others in improving the through-plane k_c. The template-directed CVD is more efficient than the others when the k_c values are low at relatively low filler loadings because it could yield nanofillers with higher qualities, thus requiring a lower filler loading to deliver a similar k_c. Nevertheless, the foam-templating and ice-templating methods can give rise to even higher absolute through-plane k_c values and high TCEEs. This is because the alignment of fillers can be controlled by manipulating the structure of templates, realizing highly aligned fillers in the thickness direction of composites. For example, by mechanically stretching the PU foam templates to align the struts followed by dip-coating in a graphene solution and rolling up, graphene/PU foam composites with highly aligned graphene-coated struts in the thickness direction were obtained. After infiltrating epoxy into the porous structure, an exceptionally high through-plane k_c of 62.4 W m^{-1} K^{-1} was reported.[197] In addition to using a single templating strategy, modifying the aligned filler networks through hybrid fillers or interfacial engineering [265] and combining different templating strategies together, such as ice-templating and template-directed CVD,[314] resulted in excellent through-plane k_c and TCEE values of over 10 W m^{-1} K^{-1} and 1000%, respectively.

Table 2

Through-plane k_c and TCEE values of thermally conductive polymer composites produced by templating strategies.

Methods	Materials	Characteristics	Filler loading* (vol%)	Through-plane k_c (W m^{-1} K^{-1})	TCEE (%)	*Ref.*
Self-templating	Cu-plated PS beads	Segregated structure	23.0	26.14	627	2013[137]
	Ag/Thermoplastic PU (TPU)	Segregated structure	15	4.45	117	2021[138]
	Graphite flake/PP	Segregated structure	21.2	5.4	97	2016[63]
	GNP/PP	Segregated structure	4.5	1.53	132.2	2017[143]
	GNP/PE	Segregated structure	4.5	1.84	101.6	2017[143]
	GNP/PVA	Segregated structure	6.2	1.43	93.5	2017[143]
	BN//PMMA	Segregated structure	50	6.34	88.6	2020[112]
	GNP/PVDF	Segregated structure	8.2	1.47	82.1	2017[143]
	BN/UHMWPE	Segregated structure	25.93	5.7	49.8	2017[140]
	BN/PPS	Segregated structure	40	4.15	39	2017[144]
	BN/PS/PP	Segregated structure	29	5.57	97.6	2020[145]
	EG/LLDPE	Segregated structure	~32	4.5	36	2018[147]
	EG/MPPW	Segregated structure	~32	9.7	77	2018[147]
	BN@cellulose/PLA	Interface modification	15.7	1.09	22,6	2020[146]
	BN/PS	Interface polymerization	19	0.94	27.7	2019[139]
	Graphene/ PP-PDA	Interface modification	27	10.93	198.7	2020[131]
	Elvaloy-EG/ PBT	Interface modification	30	17.8	225	2017[148]
	BN/SR	Interface modification	30	2.24	34	2021[149]
	BN@Cu/ Polybenzoxazine (PBz)	Hybrid fillers	14.9	1.049	24.2	2020[150]
	BN/AlN/UHMWPE	Hybrid fillers	28.4	7.1	60.6	2018[114]
	CNT/BN/PVDF	Hybrid fillers	25	1.8	~ 28.7	2018[151]
	GNP/PS-CNT	Segregated double network	5	1.02		2017[152]
	GNP/BN/PA6	Segregated double network	20.97	3.25	48.7	2019[118]
	BN/PVDF-CNT	Segregated double network	39.09	0.83		2019[154]
	BN/PEG-GNP	Segregated double network	15.625	3.63	64	2021[155]
	Al_2O_3-graphene/Epoxy	Pea-pod-like structure	30.4	13.3	215.5	2020[156]
	Al_2O_3/GNP/Cellulose	Film	74	9.09	80.5	2020[157]
	BN/AlN/CNF	Film	32	5.93	34	2020[158]
	Al_2O_3@BNNS/Epoxy	Film	65	2.43		2019[159]
	PP/PP fiber@BN	Fiber-enhanced segregated structure	21.6	3.85	69.6	2020[160]
Salt-templating	BN-C/Epoxy	Isotropic structure	11.96	1.466	63.7	2020[64]
	BN/Epoxy	Isotropic structure	59.43	6.11	55.4	2020[171]

Sugar-templating	Al_2O_3/Epoxy	Isotropic structure	36.2	3.17	38.9	2019[173]
Bubble-templating	Al_2O_3/Epoxy	Isotropic structure	23.32	2.58	42	2019[180]
	BN/PDMS	Isotropic structure	14.82	1.58	50.5	2020[179]
Foam-templating	rGO@MF/PDMS	Compression & Orientation	2.58	2.19	460.5	2018[19]
	rGO-BN/PEG	Isotropic structure	4.17	0.79	39	2019[198]
	BN/PEG	Interfacial modification	10.08	2.4	109	2021[201]
	Al_2O_3/PVA	Hybrid fillers	45.4	4.79	35.5	2018[125]
	GF/Epoxy	Isotropic structure	2.68	1.52	277.6	2016[199]
	GF/Epoxy	Isotropic structure	3.67	8.04	1189.9	2019[200]
	rGO/Polysulfide rubber (PSR)	Isotropic structure	0.31	~0.578	458	2021[192]
	Al_2O_3/Epoxy-T-ZnOw	Bi-network	17.7	1.968	23.9	2020[119]
	Al_2O_3/Epoxy	Isotropic structure	13.8	2.54	32.3	2020[193]
	Graphene/Epoxy	Stretching orientation	13.3	62.4	2436	2021[197]
Ice-templating	BN@chitosan/PEG	Isotropic structure	16.35	2.78	48.7	2019[117]
	BN@GO/PEG	Isotropic structure	11.16	1.84	42.9	2016[116]
	Graphene/Epoxy	Vertically aligned structure	0.92	2.13	1338	2016[266]
	Graphene/Epoxy	Vertically aligned structure & Graphitization at 2800 °C	0.75	6.57	5020	2018[267]
	BN/Epoxy	Vertically aligned structure	34	4.42	65.5	2017[278]
	BNNS/Epoxy	Vertically aligned structure	9.29	2.85	181	2015[81]
	BNNS/Epoxy	Vertically aligned structure	4.4	1.56	167	2019[286]
	SiC microwires/Epoxy	Vertically aligned structure	1.32	0.62	218	2019[290]
	SiC nanowires/Epoxy	Vertically aligned structure	2.17	1.67	381	2018[292]
	CF/Epoxy	Vertically aligned structure	13.0	2.84	107	2020[262]
	Cu nanowires/Epoxy	Vertically aligned structure	1.12	0.79	326	2020[270]
	AlN/Epoxy	Vertically aligned structure	47.26	9.48	72	2020[289]
	CF/PDMS	Vertically aligned structure	12.8	6.04	252.9	2019[263]
	BN/PDMS	Vertically aligned structure	11.2	1.4	74.4	2016[122]

BNNS/PDMS	Vertically aligned structure	15.8	7.46	248.9	2019[65]
MXene/PDMS	Vertically aligned structure	2.5	0.576	88	2020[274]
BN/PCL	Vertically aligned structure	13.41	1.42	45.5	2020[281]
BN@GO/PEG	Vertically aligned structure	13.64	2.36	45.1	2017[279]
BN@GO/PEG	Vertically aligned structure	17.54	3.18	49.3	2018[280]
BN/PEG	Vertically aligned structure	8.1	1.3	67.9	2021[285]
MXene/Epoxy-Ag	Vertically aligned structure & Hybrid fillers	15.1	2.65	81	2020[275]
CF/MXene/Epoxy	Vertically aligned structure & Hybrid fillers	16.6	9.68	271.7	2020[264]
BN platelet/BN particle/Epoxy	Vertically aligned structure & Hybrid fillers	32	3.6	59.4	2020[282]
BNNS/Ag nanowire/Epoxy	Vertically aligned structure & Hybrid fillers	5	1.1	117.5	2021[273]
BN/GNP/PA6	Vertically aligned structure & Hybrid fillers	15	2.80	55.6	2021[284]
BN/NR	Vertical alignment & Covalent bond connection	12.68	0.79	26.7	2020[276]
BN-SiC Nanowire/PDMS	Vertical alignment & Sintering-introduced bonding	8.35	3.87	219.8	2020[283]
rGO-BN/NR	Vertical alignment & Covalent bond connection	4.9	1.28	124.7	2019[277]
rGO-BN/Epoxy	Vertical alignment & Covalent bond connection	13.16	5.05	205.6	2018[133]
rGO@SiC Nanowire/PDMS	Vertical alignment & Interfacial modification & Hybrid fillers	1.84	2.74	876.4	2020[291]
Graphene/CNT/Epoxy	Vertical alignment & Interfacial modification	9	30.09	1661	2021[265]

		& Hybrid fillers				
	Graphene/Epoxy	Lamellar structure & High-temperature annealing	2.3	20	4310	2020[269]
	BNNS/Epoxy	Radially aligned structure	15	4.02	142	2020[287]
	BNNS/Epoxy	Radially aligned structure	11	2.53	106	2021[288]
	GO-BN/PEG	Radially aligned structure	11.65	2.94	75.5	2020[67]
Template-directed CVD	GF/PDMS	Isotropic structure	0.37	0.56	527	2015[332]
	GF/PDMS	Isotropic structure	0.21	0.62	1164	2017[132]
	GF/PDMS-CB	Bi-network	5.84	0.686	38	2016[313]
	GF/PDMS-graphene flake	Bi-network	2.9	1.08	151.7	2016[312]
	BN foam/PDMS	Isotropic structure	0.2	0.36	357	2017[134]
	BN foam/PDMS-BNNS	Bi-network	5.6	0.56	29.8	2017[134]
	SiC sheet/Epoxy	Vertical alignment & Ice-templating scaffold	3.71	14.32	1651	2020[314]
	SiC/Epoxy	Isotropic structure & Ice-templating scaffold	6.52	10.26	859	2020[315]

*Volume fraction of partial systems is converted by mass fraction using the related information in Materials Handbook.[333]

Table 3

Comparison of in-plane k_c and TCARs of thermally conductive composites fabricated by templating strategies and other methods.

Methods	Materials	Filler loading (vol%)	In-plane k (W m^{-1} K^{-1})	Through-plane k_c (W m^{-1} K^{-1})	Anisotropy (TCAR)	*Ref.*
Self-templating	EG/MPPW	~32	10.1	9.7	1.04	2018[147]
	BNNS/PS microsphere	13.4	8.0	~0.3	27	2017[141]
	BNNS/PI	12.4	4.25	0.4	11	2020[142]
	GNP/Nylon	~6.5	15.8	0.66	24	2021[163]
	rGO@Al_2O_3/NR	33.9	3.233			2020[165]
	Al_2O_3-graphene/Epoxy	30.4	33.4	13.3	2.5	2020[156]
	Al_2O_3/GNP/Cellulose	74	27.78	9.09	3.0	2020[157]
	BN/AlN/CNF	32	~ 13.4	5.93	2.3	2020[158]
Salt-templating	BN/Epoxy	65.6	17.61	5.08	3.5	2019[172]
Foam-templating	Graphene/Epoxy	13.3	24.8	62.4	0.4	2021[197]
Ice-templating	BN/PCL	13.41	1.01	1.42	0.7	2020[281]
	Janus GO/Epoxy	0.49	~5.6	~0.35	16	2020[268]
	BNNS/Epoxy	15	6.07	~0.5	12	2019[66]

	BNNS-Ag nanowire/PI	11.7	4.75	0.55	8.6	2020[272]
	BNNS/Epoxy	15	3.83	4.02	0.95	2020[287]
	BNNS/Epoxy	11	2.40	2.53	0.95	2021[288]
	GO-BN/PEG	11.65	4.41	2.55	1.7	2020[67]
	BNNS/PI	1.3	0.84	0.13	6.5	2019[250]
	graphene/CNT/Epoxy	9	8.77	30.09	0.29	2021[265]
Template-directed CVD	GF/PDMS	6.43	28.77	1.62	18	2017[132]
	GF/NR	0.42	1.07	0.21	5.1	2019[80]
	GF/NR-graphene nanosheet	6.2	10.64	3.0	3.5	2019[80]
	GF/PDMS-BN	20.7	23.45	2.11	11	2017[311]
	Graphene web/Epoxy	4.5	8.8	~2.0	4.4	2018[115]
LBL	rGO/CNF	37	7.3	0.13	56	2017[334]
	rGO/Nanofibrillated Cellulose (NFC)	0.6	12.6	0.042	300	2017[335]
	BNNS/NFC	36.6	145.7			2014[77]
	Ag nanoparticle/NFC	2.0	6.0	0.8	7.5	2018[336]
	Fluorinated CNT/NFC	24	14.1	0.83	17	2018[337]
	BN nanotube/CNF	16	21.39	~1.8	12	2017[338]
	BNNS/CNF	57	30.25			2017[339]
	BNNS/CNF	16	22.67	1.08	21	2018[340]
	MoS_2-SiC nanowire/CNF	22.5	19.76	0.68	29	2020[46]
	BN@PDA/Cellulose nanocrystal (CNC)	90	40	4.8	8.3	2018[341]
	SiC nanowire-Ag/Cellulose microcrystal (CMC)	50	33.97	~0.6	57	2016[47]
	BNNS/PVA	84	120.7	1.1	110	2018[342]
	Fluorinated graphene/PVA	89	61.3	~0.4	153	2019[343]
	BNNS/Poly(diallyl dimethyl ammonium chloride) (PDDA)	83	212.8	1.0	213	2017[344]
	BNNS/Aramid nanofiber	21.37	46.7	~0.16	292	2020[345]
	BNNS@PDA/Aramid nanofiber	39	3.94	0.62	6.4	2020[346]
Electrospinning	BNNS/PVDF	28	10.4	~0.5	21	2019[347]
	BNNS/PVA	22.2	21.4	~0.66	32	2019[348]
	BNNS/PVA	27.8	19.99			2021[349]
	GNP/PS	20.6	4.72	0.32	15	2019[350]
	Al_2O_3@BNNS/PBz	6.9	3.24	~0.5	6.5	2021[351]
Hot-pressing	BN/TPU	90.7	50.3	6.9	7.3	2018[352]
	Polyethersulfone (PES)@BN/PVDF	42	20.56	2.82	7.3	2021[353]
Blading	BN@PDA/PVA	30	8.8			2015[354]

Tape-casting	BN/PI	13.6	14.7	~0.45	33	2020[355]
Casting	rGO/NR	38.53	20.84	0.56	37	2019[356]
	GO/PVA	~3	~25			2021[357]
	PEG@graphene/PA6	2.6	9.710	0.376	26	2015[358]
Solution blending	GNP-PDA@CNT/Poly(phenylene sulfone) (PPSU)	17.6	5.4	3.8	1.4	2021[359]

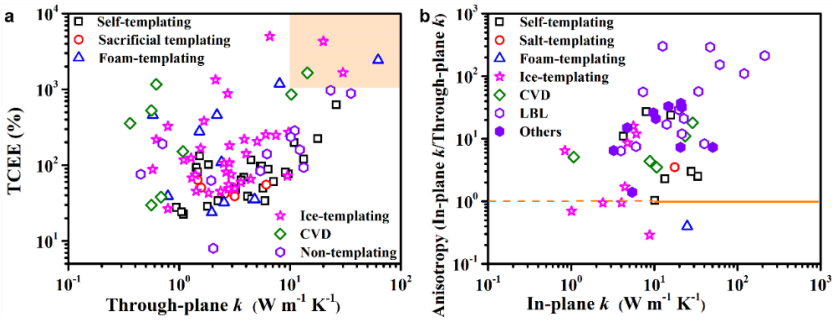

Fig. 13. (a) Relationship of TCEE *versus* through-plane k of composites made by different templating strategies. (b) Comparison of thermal conductivity anisotropy ratio (TCAR = in-plane k over through-plane k) *versus* in-plane k among composites made by different templating strategies, LBL assembly and other methods.

A high in-plane k_c is more desirable than a high through-plane k_c, when it comes to the application requiring efficient dissipation of concentrated heat in the lateral directions.[360] Thermally conductive composites with high in-plane k_c have been developed by aligning the fillers horizontally using various techniques, such as layer-by-layer (LBL) assembly, spinning, and solution casting.[77, 347, 356] As shown in **Table 3** and **Fig. 13**b, the composite films prepared by LBL assembly exhibited an excellent in-plane k_c of over 100 W m^{-1} K^{-1}, making them a good candidate as lateral heat spreader. However, these composites tended to be highly anisotropic in terms of both structure and k_c value, with their through-plane k_c normally 2 to 3 orders magnitude lower than the in-plane k_c counterparts. The poor k_c in the thickness direction limited the overall heat dissipation from the hot spot to the heat sink despite the excellent in-plane heat spreading. As such, composites with simultaneously high through-plane and in-plane k_c values are preferred to afford more uniform heat transfer in all directions.[67] To quantify the anisotropic effect, the thermal conductivity anisotropy ratio

(TCAR),[361] an in-plane k_c to through-plane k_c ratio, is introduced here. The closer the TCAR is to 1, the more uniform is the heat dissipation along the in-plane and out-of-plane directions. For the composites prepared by the LBL methods, the TCARs varied from 10^2 to 10^3 (**Fig. 13**b), indicating a highly anisotropic thermal conduction behavior. By contrast, the composites made by various templating strategies, such as self-templating,[156, 157] salt-templating,[172] foam-templating[197], ice-templating,[67] and template-directed CVD,[80, 115] exhibited a unique advantage of simultaneously improved through-plane and in-plane k_c with TCARs much closer to 1 (orange lines in **Fig.13**b: dash line for k below 10 W m^{-1} K^{-1} and solid line for k above 10 W m^{-1} K^{-1}), although the in-plane k_c values were not as high as those made by the LBL assembly. Among different templating strategies, the self-templating and ice-templating methods seem to be more effective than the others for simultaneously augmenting both k_c values. When spherical fillers were used as templates, the self-templating method was preferred as it could not only construct the in-plane oriented structure similar to the LBL method, but also retain the transversely oriented structure due to the shaping effect of the spherical filler template (**Fig. 5**).[156, 157] A radially oriented structure formed in the ice-templating method highlighted an exclusive advantage of simultaneously improving both in-plane and through-plane k_c (**Fig. 10**h).[67]

4.2. Comparison of other factors for practical applications

In addition to the thermal conduction performance compared above, a few other factors are also an important consideration for practical applications of different templating methods. To more critically assess the advantages and disadvantages of different templating strategies in fabricating high-performance thermally conductive composites, several key factors, including structural tunability, diversity of raw materials, scalability, and cost, are plotted along with thermal conduction performance in a radar chart, as shown in **Fig. 14**. From the perspective of structure tunability, the ice-templating strategy can generate both isotropic and anisotropic 3D filler structures with pore sizes

ranging from a few to hundreds of micrometers by tuning the freezing parameters.[210, 362] This unique capability of the ice-templating strategy makes the composites made therefrom outperform the products from other templating methods that generally contain isotropic 3D fillers. To achieve anisotropic fillers in the other templating methods, additional treatment of the templates is necessary, *e.g.*, stretching or compressing the templates to form oriented structures and using monoliths with oriented structures as CVD-grown templates.[115, 197, 314]

Suitable matrix and filler materials are other important criteria for selecting templating strategies. Thermoplastics suitable for hot pressing are the main matrix materials for self-templating. Meanwhile, thermosets prepared from cured monomers and low-viscosity polymers are suitable for the other four templating methods as they can be easily infiltrated into the pore space of the 3D filler skeletons to produce composites. Therefore, it can be said that the matrix materials suitable for self-templating are more diverse than the other four methods, while less efforts are needed in dispersing the nanofillers and assembling them into 3D structures in self templating. Regarding the suitable filler materials, the template-directed CVD approach has relatively fewer choices than others with successful synthesis of graphene, BN, or SiC foams. It is worth mentioning that the maximum loading of fillers attainable in polymer composites using the template-directed CVD method is low because of the difficulty in growing thick layers and the intrinsically large pore volumes in the metal templates. Although CVD-grown 3D fillers can enhance the TCEE, the absolute k_c values are not high because of the low filler loadings, requiring additional fillers to form a secondary network. For the templating methods other than CVD, excessive peeling and surface modification of nanofillers are often undesired owing to the destruction of their crystal structures, which in turn necessitates extra time and cost for subsequent reduction treatment and high-temperature annealing.[19, 267, 269] This means that micron-size GNPs, EG and BN microplates having highly crystalline structures with few defects may be more useful for high k_c. In addition, such high-quality micron-size fillers are conducive to low-cost production of thermally conductive composites using the templating methods.

In terms of scalability, the foam-templating and self-templating methods are the most

promising for large-scale production. The self-templating method mainly involves hot-pressing operation and the dimensions of final products depend on the size of the hot-pressing mold, making it easy to scale up. An injection molding method was developed for industrial-scale production of segregated composites.[363] The foam-templating, especially when using polymer foams as templates, is another promising templating strategy for large-scale production. The simple dip-coating process can be easily scaled up using a roll-to-roll apparatus capable of immersing the foam into a coating bath and collecting the coated foam on a roller in a continuous process. [19, 197] Unlike the foam-templating unnecessary to remove the templates, the sacrificial templating requires the complete etching of templates which would be difficult if the sample size is too large. For the ice-templating method, the lateral dimensions of final products are limited by the size of freeze-drier when non-directional or unidirectional freezing is done in the thickness direction. Recently, a simple approach involving an ambient drying instead of freeze drying has been developed, making the ice-templating more amenable to scalability.[364] The template-directed CVD is a time-consuming method involving growth, transfer and two-step etching, placing it among the least favorable for scalable manufacturing. A cost-effective roll-to-roll process is currently under development toward continuous and mass production of high-quality CVD graphene products.[365]

The last consideration, but of foremost importance, is the cost. The overall cost usually depends on the costs of templating materials and the manufacturing costs. For self-templating without additional templating materials, the cost mainly includes the fabrication of granules or microspheres, surface treatments and hot pressing. The use of waste plastics can further reduce the cost of self-templating method.[147] The templating materials required for sacrificial templating and foam-templating are normally cheap commercial products. The washing and impregnation processes involved are also relatively simple, making the cost comparable to that of self-templating. The ice-templating technique is yet to be commercialized with multiple processing steps. However, the processes are simple without the need of a complex setup and the freeze-drying technique has long been widely used in the food industry.

Therefore, the cost can be greatly reduced if the freeze-casting setup is scaled up for large-scale production.[59] Among different techniques, the cost of template-directed CVD is the highest owing to the expensive equipment, harsh processing conditions, *e.g.*, high temperature, high vacuum, and continuous gas flow, and post-treatments like the removal of template.[366]

To summarize, the self-templating, foam-templating, and ice-templating techniques cover relatively large areas in the radar plots (**Fig. 14**) when considering all the five important aspects, making them most viable for fabricating 3D fillers of thermally conductive composites. Specifically, the advantages, disadvantages and development trends of various templating strategies are listed in **Table 4**. Although each method has its own merits and weaknesses relative to others, special emphasis is placed on examining several important features for futuristic development of templating strategies, such as thermally conductive film products with a vertically aligned structure, mechanical performance of thermally conductive composites, employment of waste or biodegradable materials, continuous covalently-bonded filler heat transfer network structures, and scalable manufacturing. In addition, combining templating strategies with other techniques, such as self-templating LBL assembly and electric field-assisted CVD, is an effective way to further unlock the potential of templating strategies.[157, 367]

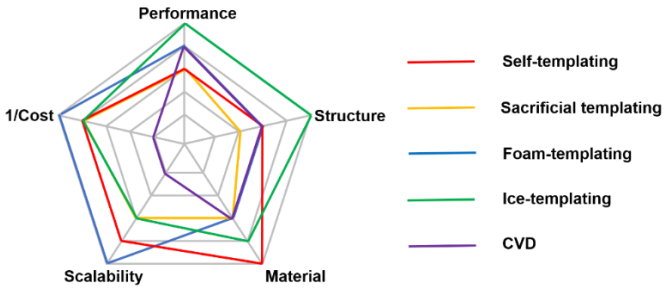

Fig. 14. Radar plots comparing different templating methods in respect of their relative performance, structure, material, scalability, and cost.

Table 4 Comparison of different templating strategies from the perspectives of advantages, disadvantages, and development trends.

Methods	Advantages	Disadvantages	Development trends
Self-templating	• Thermoplastics • Less efforts required in dispersing nanofillers • Easy processing	• Unsatisfactory mechanical properties • Limited structures	• Hybrid granules as templates • Film products with a vertically alignment structure • Mechanical properties • Use of waste or biodegradable plastics
Sacrificial templating	• Thermosets and low-viscosity polymers • Cheap commercial templates	• Difficulty in removing templates • Limited structures	• Air templating • Interfacial design
Foam-templating	• Thermosets and low-viscosity polymers • Easy processing • Cheap commercial templates	• Large pores • Limited selection of template materials	• Continuous production • Alignment through stretching and compression
Ice-templating	• Thermosets and low-viscosity polymers • Tunable structures	• Limited lateral dimensions of final products • Multiple processing steps	• Scalable manufacturing • Ambient drying
Template-directed CVD	• Thermosets and low-viscosity polymers • Covalent bonding between fillers	• Limited filler types • Low filler loading • Time-consuming • Expensive equipment • Harsh processing conditions	• Continuous production • New nanomaterials

5. Applications of Thermally Conductive Polymer Composites Made by Templating Strategies

The thermally conductive polymer composites fabricated by templating strategies have found a wide range of applications in thermal management, energy-related systems and smart devices as discussed in the below.

5.1. Thermal management

With the miniaturization, integration, and multi-functional operation of electronic products, the need for controlling the generated heat has become increasingly important as excessive heat can seriously degrade their operation and service life. In order to realize efficient heat dissipation and maintain normal operating temperature, high-performance polymeric TIMs and PCMs containing thermally conductive fillers are widely used. In practical applications, TIMs are sandwiched between the active electronic components and heat sinks to reduce their contact thermal resistance (**Fig. 15**a).[3] Generally, the *k* of TIMs made by conventional mixing methods increases with increasing filler loading, which comes at the expense of higher costs, difficulty in processing and deteriorated mechanical properties. A major benefit of using templating methods against conventional methods is the much lower filler loadings required for the same *k*, making them ideal for fabricating TIMs. Furthermore, a high *k* in the thickness direction is essential for TIMs to maximize the heat dissipation from the heat source to the sink. The vertical alignment of 3D fillers can be more readily achieved using templating methods than conventional dispersing strategies. A homemade device with TIMs sandwiched between a CPU and a heat sink (**Fig. 15**b) was used to highlight the better thermal management capability of the thermally conductive composite made by the templating method for TIM applications.[157] Owing to the 2D planar nature of GNPs and their anisotropic conductivities, it is rather difficult to improve the through-plane *k* of GNP/cellulose composites using the LBL assembly technique. After introducing spherical Al_2O_3 particles as templates, a segregated GNP network was formed, leading to a high through-plane *k* of Al_2O_3/GNP/cellulose composite films. Unlike the neat cellulose and GNP/cellulose films, the hybrid-filler cellulose film was

capable of dissipating the heat vertically from the heat source (**Fig. 15**c), which was also proven by the finite volume simulations (**Fig. 15**d).

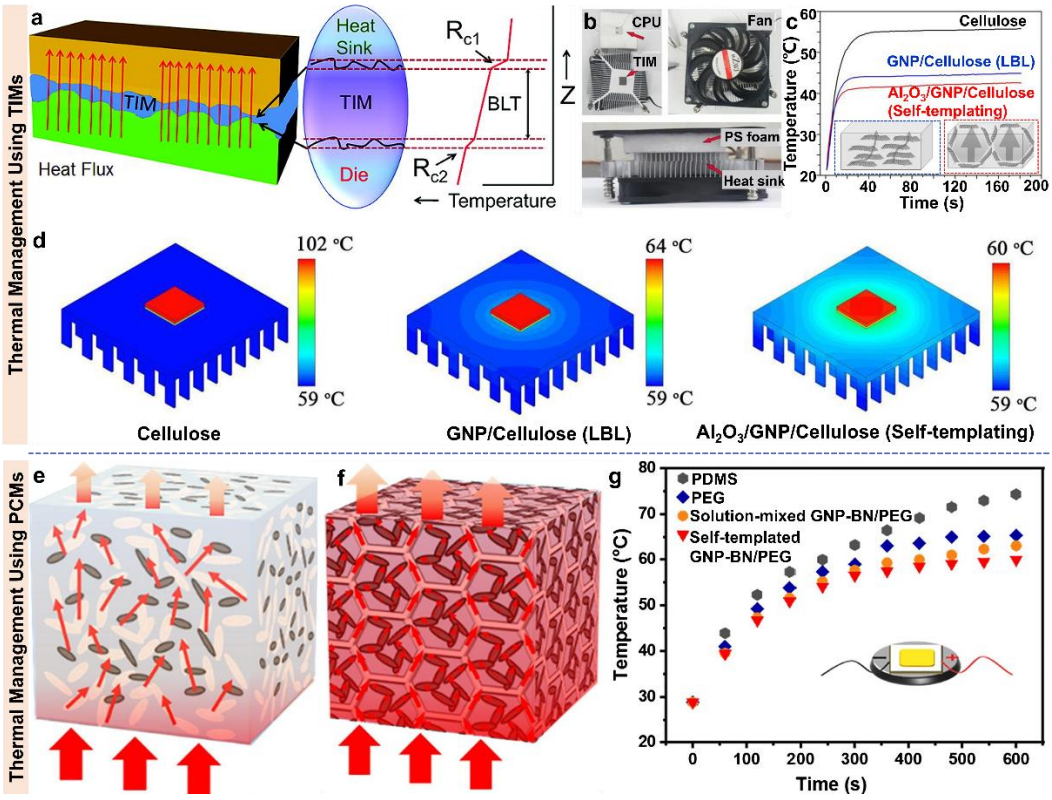

Fig. 15. Thermally conductive TIMs and PCMs for thermal management. (a) Schematic illustration of the working principle of TIMs filling the gap between heat source and sink. Reproduced with permission from ref. [368]. Copyright 2012, American Chemical Society. (b) Photographs of Al_2O_3/GNP/cellulose composite films made by self-templating as TIMs for CPU thermal management. (c) Temperatures of CPU *versus* working time for three different TIMs made from neat cellulose, GNP/cellulose, and Al_2O_3/GNP/cellulose. The insets are schematics of the microstructures of GNP/cellulose and Al_2O_3/GNP/cellulose TIMs. (d) Simulated temperature profiles of three TIMs obtained from finite volume simulations. Reproduced with permission from ref. [157]. Copyright 2019, Elsevier Ltd. Schematics of heat transfer in GNP-BN/PEG composites with (e) randomly distributed fillers and (f) a segregated double-network structure. (g) Temperature changes of LED chips with TIMs made from neat PDMS, neat PEG, solution-mixed GNP-BN/PEG, and self-templated GNP-BN/PEG composites. Reproduced with permission from ref. [155]. Copyright 2021, Elsevier Ltd.

Different from TIMs which only transfer the heat, PCM is another promising candidate for thermal management as it can absorb or release thermal energy in the form of latent heat during phase transition, maintaining the working temperature of electronics close to the phase change temperature.[369] Thanks to their excellent *k* and thermal energy storage capability, thermally conductive PCMs have been widely used for transient cooling of electronics.[155] Composites containing 3D fillers made by templating methods prevail over those with randomly dispersed fillers for PCM applications because the former composites not only exhibit a higher *k* than the latter counterpart but also contain the molten PCM within the 3D structure during phase change to avoid leakage (**Fig. 15**e and f). For example, a GNP-BN/PEG ternary phase change composite with a segregated double-network structure was fabricated using a self-templating method. The self-templated composite maintained consistently lower working temperatures for a LED chip than TIMs prepared with other materials, such as neat PDMS without a phase change capacity, neat PEG, and GNP-BN/PEG composites prepared by direct solution mixing (**Fig. 15**g). When a PCM with a lower phase change temperature was used, the working temperature of electronics was further reduced.[370] In addition to keeping the electronics cool, an electro-driven phase change composite was applied to raise the working temperature of electronic devices in a cold environment.[190] Besides, composites with highly anisotropic structures made by ice-templating can work as thermal protection components in electronics to effectively avoid the catastrophic damages caused by localized heat accumulation.[66] At present, the thermally conductive composites are mainly used for heat dissipation in electronic devices and systems. Other emerging thermal management applications such as thermal regulation of human body and buildings are also potential areas to explore.[371, 372]

5.2. Energy-related applications

Solar energy, a green and sustainable energy source, has attracted great interest in solving the energy crisis, mitigating global warming and narrowing the mismatch between the energy supply and demand. However, the intermittent nature of solar energy requires the conversion of solar energy to other forms for practical applications.

Thermal energy generated from the solar-thermal conversion can be either used directly or converted to electricity. Polymer PCMs are ideal for thermal energy storage and conversion applications by utilizing the phase change behaviors of PCMs, but they cannot effectively convert solar energy to thermal energy through photothermal conversion. Therefore, composite PCMs have been fabricated by introducing photothermal materials, such as carbon materials,[373] MXene,[374] and PDA,[375] in the PCM matrices. The stored heat can be converted to electricity by thermoelectric devices.[376] A more creative solar-heat-electricity conversion route has been established by integrating photodriven PCMs with commercial thermoelectric modules.[116] Nevertheless, the low *k* of PCMs hampers the fast heat transfer within the PCM, leading to slow thermal charging and discharging and limiting their photothermal conversion for electricity generation. 3D thermally conductive structures made by templating methods served as ideal scaffolds for enhanced *k* of PCMs. For example, a radial ice-templating method was used to obtain a biomimetic PEG-based phase change composite with centrosymmetric and vertically aligned GO-BN hybrid networks for an efficient solar-heat-electricity conversion with the help of a thermoelectric module (**Fig. 16**a).[67] Compared to the composites with randomly distributed and vertically aligned structures, the composite with a radially arranged structure exhibited a superior energy conversion ability thanks to the quick and uniform heat transfer stemming from the 3D centrosymmetric BN network (**Fig. 16**b). The phase change composite was capable of uninterrupted electricity generation with an output voltage of 251 mV and a current of 64.2 mA when it was exposed to sunlight with the assistance of a convex lens (**Fig. 16**c). Moreover, a solar cell and a thermoelectric module were integrated into an energy conversion system containing a thermally conductive MF@GO-BN/PEG composites made by foam-templating (**Fig. 16**d). Given that the output power of the solar cell was inversely proportional to the operating temperature, the assembly of the MF@GO-BN/PEG composite with a solar cell greatly improved its output power by reducing the surface temperature *via* fast thermal absorption and dissipation of the composite PCM (**Fig. 16**e). A continuous electricity output was realized even after the light source was removed from the system because

the thermoelectric module incessantly functioned when the heat was released from the composite PCM (**Fig. 16**f).

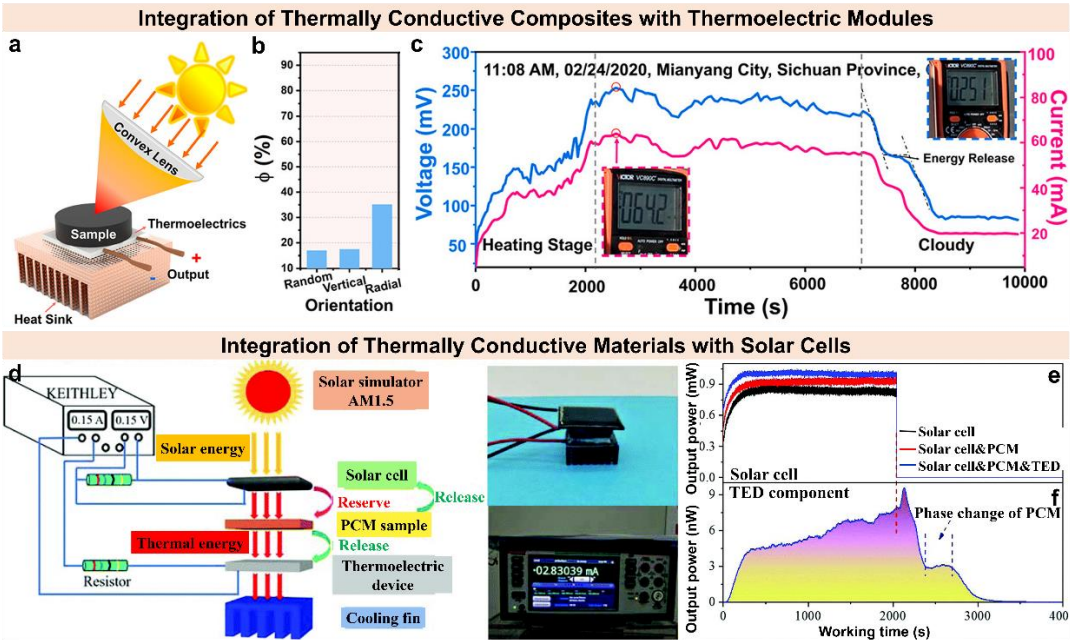

Fig. 16. Integrating thermally conductive phase change composites with energy harvesting and conversion devices. (a) Schematic illustration of the solar-heat-electric conversion system based on thermally conductive PCMs and thermoelectric module. (b) Effect of structure on photothermal energy conversion efficiency. (c) Real-time output voltage and current of the solar-heat-electric conversion system. Reproduced with permission from ref. [67]. Copyright 2020, American Chemical Society. (d) Schematic illustration showing the design of an integrated device comprising a solar cell, a thermally conductive phase change composite, a thermoelectric module, and a cooling fin. (e) Real-time output power of solar cells. (f) Change in output power of thermoelectric module. Reproduced with permission from ref. [198]. Copyright 2019, Royal Society of Chemistry.

5.3. Smart devices

As the world is marching into the era of Internet of Things (IoT), the innovations in wearable devices and portable electronics have emerged as mainstream technologies that require high-*k* materials for efficient heat transfers in various responsive systems.[377] For thermally responsive systems, shape-adaptable PEG-based phase

change composites containing CNF/MF@GNP and MF@Cu fillers were developed by foam-templating.[190, 191] The thermally-induced shape memory behaviors and the corresponding shape recovery ratio curve of the shape memory composites are presented in **Fig. 17**a and b. All the samples recovered from the U-shape to a flat state triggered by heating at 80 °C, and the shape recovery time was greatly shortened after adding GNPs. A high *k* reduced the time required for reaching a phase change temperature (**Fig. 17**c), accelerating the thermal response and shape transition. For intelligent temperature sensing systems, a high *k* is essential to a fast response.[378] For example, flexible rGO/PDMS composites with high *k* were packaged into an artificial robotic hand with temperature sensors to directly feel the temperatures of grabbed objects (**Fig. 17**d).[19] It is of interest to note that the temperature rose quickly to 59.5 °C when the hand grabbed a hot bottle, while it dropped sharply to 2.0 °C when changing to a cold bottle (**Fig. 17**e-g). Nonetheless, the application of thermally conductive composites in intelligent devices remains in its infancy. More diverse applications of the thermally conductive composites in this field, such as artificial skins for robotic hands and heat spreaders for actuators, need to be explored in the future.[16]

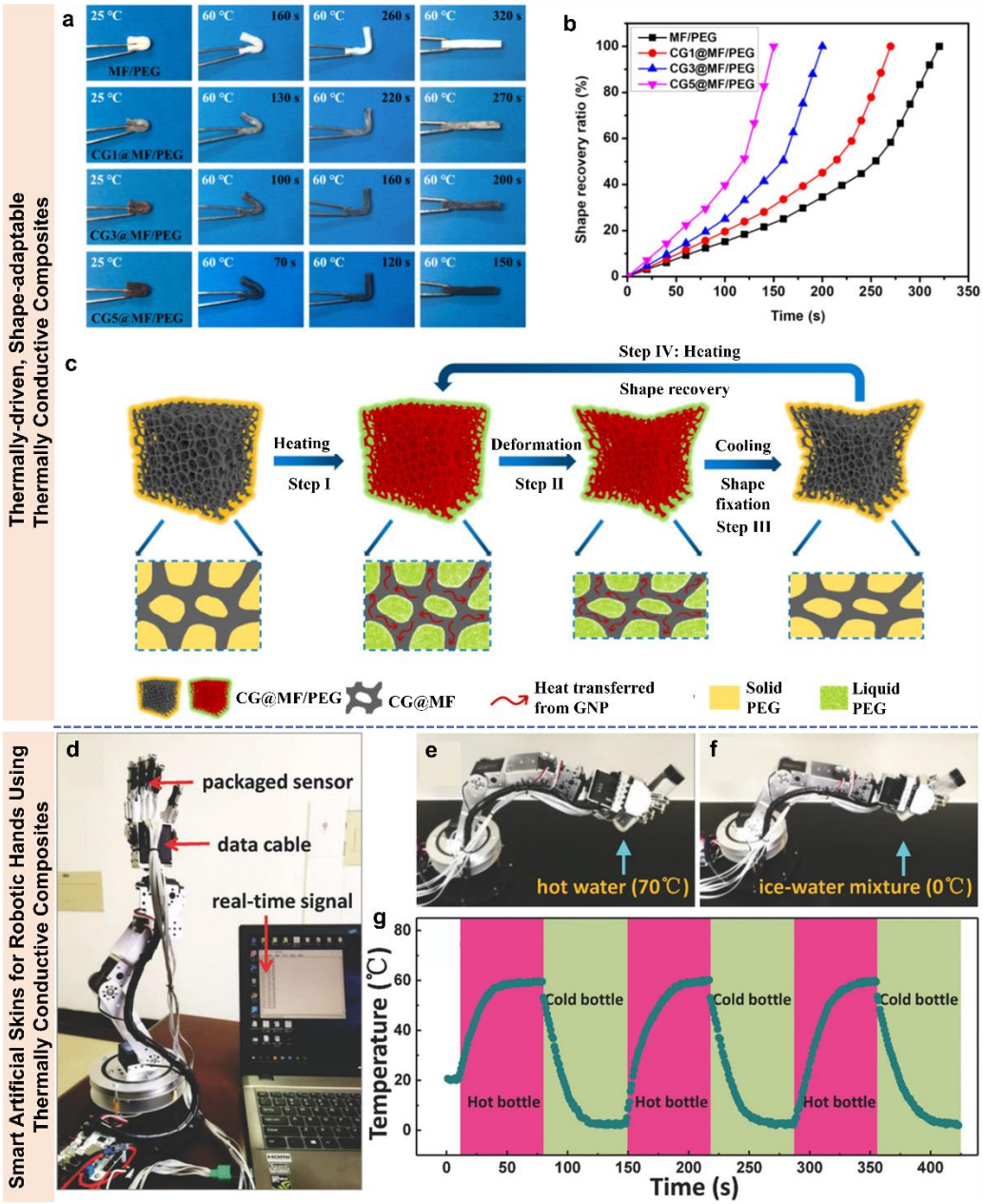

Fig. 17. Thermally conductive composites for smart devices. (a) Photographs showing the thermally-driven shape memory behaviors of PEG-based composite PCMs and (b) their shape recovery ratios with respect to heating time. (c) Thermally-induced shape memory mechanism of PEG-based composite PCMs. Reproduced with permission from ref. [191]. Copyright 2019, American Chemical Society. (d) Setup for robotic hand with artificial skin for temperature detection. Robotic hand grabbing (e) hot and (f) cold bottles. (g) Temperature response to the periodic handling of hot and cold bottles. Reproduced with permission from ref. [19]. Copyright 2018, WILEY-VCH.

6. Conclusion and Outlook

In summary, after the decade-long development, the templating strategy has become one of most promising approaches to fabricate thermally conductive composites. The assembly of thermally conductive fillers into 3D network structures facilitates the thermal percolation of composites at much lower filler loadings than conventional composites made from dispersed fillers, translating the excellent *k* of fillers into the composites to the maximum extent. The microstructures of 3D fillers depend largely on the morphologies of templates and thus can be readily tailored by controlling the various processing parameters of different templating methods. Specifically, isotropic, cellular, lamellar, and radial structures have been constructed for improved *k* of composites isotopically or along specific directions requiring heat dissipation. Furthermore, the pore morphologies and cell wall dimensions of the templated 3D filler structures are tailored at micro- and nanometer scales by optimizing the filler loading, pore size, secondary network, alignment, filler hybridization, and F-M or F-F interfaces. Such a multiscale design strategy is a plausible approach for the preparation of thermally conductive composites. These high-performance thermally conductive composites present great potentials in the fields of thermal management, thermal energy storage and conversion, and smart devices. Despite the tremendous efforts made in developing novel templating strategies, many challenges still remain while numerous opportunities exist in realizing further enhancement of *k* together with other intriguing functional properties. With the abovementioned backdrop, future directions and potential solutions to existing challenges for advancement in templating technology are proposed, as outlined below.

(1) Highly aligned thermally conductive fillers either in the plane or thickness directions can be readily achievable by templating methods such as ice-templating, but they are only suitable for either spreading localized heat (*i.e.*, spot heat source) or dissipating uniform heat (*i.e.*, plane heat source).[356, 360] However, the heat sources in practical devices are normally combined, requiring simultaneously high in-plane and through-plane *k* for more efficient heat dissipation. Although some efforts have been

made using self-templating,[156, 157] foam-templating,[197] and radial freezing approaches,[67, 287] there is still room for improvements in their optimal design and the mass production of these composites. In addition to using isotropic 3D fillers such as spherical and polyhedral BN assembly,[379, 380] the mixed granules or fillers with different geometries can be used in the self-templating method in their optimal proportions. Besides, the unique architecture fabricated by radial freezing can be employed as a template for the CVD growth to realize aligned structures in both the horizontal and vertical directions with high-quality fillers.

(2) To date, fabricating composites with a k value above 10 W m^{-1} K^{-1} and a TCEE exceeding 1000% at filler loadings lower than 10 vol% remains challenging, especially for thermally conductive yet electrically insulating composites. Although the k can be greatly improved by introducing large amounts of fillers, the high filler loading inevitably increases the cost, makes the fabrication process difficult, and even degrades the mechanical properties of composites. In view of this, the development of high-quality fillers with large aspect ratios, such as non-oxidized graphene,[381-383] graphite sheets[384] and BNNSs,[385] is necessary to maintain a high k at a low filler loading. In addition, refining the alignment of high-aspect-ratio fillers is another efficient approach. It is worth noting that in the foam-templating method, a commercial polymer foam with an isotropic structure was stretched or compressed to induce highly oriented polymer struts for more effective alignment of 2D fillers.[19, 197] Currently, the mainstream method is to employ nanoscale carbon materials and ceramics as heat transfer fillers in templating strategies, which inevitably cause phonon scattering at the interface owing to their huge specific surface area and the mismatched phonon vibrational modes between the matrix and functional fillers. To reduce ITR at the interface, polymer fibers with an intrinsically high k, such as highly aligned UHMWPE fibers[386] and actinomorphic[387] or hierarchical spiral[388] arrangement of polybenzobisoxazole (PBO) fibers, have emerged as an alternative to thermally conductive composites. In addition to tailoring the properties and alignments of fillers, infiltrating polymer matrices with a high k into the 3D fillers constructed by templating strategies is also a good choice, for which thermally conductive epoxy and PI are typical

matrices.[389-393]

(3) In terms of practical requirements of thermally conductive materials, other factors such as electrical insulation, thermal expansion coefficient, thermal stability, fire resistance, and long-term service performance also need to be taken into account in addition to k values. Moreover, as thermally conductive composites with multifunctional capabilities may provide additional appealing benefits, they should be actively explored for use in complex application scenarios. Imparting multifunctionalities, such as EMI shielding,[394-396] Joule heating,[397, 398] self-healing function,[399-401] and high temperature resistance,[402, 403] to thermally conductive composites will contribute to their readiness for implementation in broader areas.

(4) The thermal transport in the 3D structured network is limited by the F-F interfacial resistance. The understanding of coupling of fillers with various phonon vibrational characteristics and non-covalent interactions or covalent bonds at the interfaces can facilitate the design of interfacial structures at nanoscale for more efficient interfacial heat transfer. In addition, most of the existing theoretical models based on simple assumptions, such as isotropic structure, spherical fillers, and binary components, cannot fully reflect the actual microstructure of the composites. Thus, improved models need to be formulated for practical composites with sophisticated microstructures by taking into account a few important factors, such as the ITR between fillers and the alignment of fillers. The success of the models in predicting real behaviors of composites depends on the development of a holistic approach encompassing multiscale modeling techniques, including density functional theories, MD simulations, and micromechanics models. Based on the many 3D heat transfer structures constructed by templating methods, the exploration and application of multiscale analysis models and machine learning algorithms will help understand the constitutive structure-property relations and reveal the design principles of composites with high thermal conductivities.[404] This would eventually reduce the labor and material costs as well as shorten the development cycles.

(5) The templating methods are mainly used to prepare 3D fillers for bulk composites.

Other forms of composites, such as 1D fibers and 2D films, fabricated based on templating strategies also need to be developed to meet the diverse requirements for emerging thermal regulating applications in flexible electronics, human body and energy-efficient buildings. Owing to the excellent mechanical flexibility and conformability, 1D fibers and 2D films have shown great potential in wearable electronics and personal thermal management (PTM).[13, 15, 405] A "freeze-spinning" technique combining directional freezing with solution spinning has been proposed to fabricate textile fibers with highly aligned pores, which are useful for thermally conductive fibers with aligned structures.[223] Two-dimensional flexible films with high through-plane *k* are difficult to fabricate but are highly desired to serve as TIMs to efficiently dissipate the heat generated in flexible electronics.[3, 406] Employing an electric field in CVD provides possibility to align the fillers in the fabrication of 2D films with high through-plane *k*.[367]

(6) The composites produced by templating techniques at the current stage are mostly at the laboratory-scale. The lack of scale-up production is among the main factors limiting their practical applications. A creative attempt was made to continuously produce graphene aerogels by a hydroplastic foaming method, providing some insights in scaling up the production.[407] In addition, injection molding for self-templating,[363] bubble-templating without post treatment,[179] ambient drying for ice-templating,[364] and roll-to-roll techniques for foam-templating[19] and template-directed CVD[365] are promising strategies to produce high-performance, large-scale thermally conductive composites. It is highly anticipated that the multifunctionalities and commercialization of high-performance thermally conductive composites will contribute to more diverse applications in thermal management and regulation for electronics, batteries, human body and energy-efficient buildings.

Declaration of Competing Interest

The authors declare that they have no known competing financial interests or personal relationships that could have appeared to influence the work reported in this paper.

Acknowledgements

This project was financially supported by the Research Grants Council (GRF Projects: 16205517, 16209917 and 16200720) and Innovation and Technology Commission (ITS/012/19) of Hong Kong SAR. Dr. Wei Yang acknowledges the financial support of National Natural Science Foundation of China (No 52125301). Dr. Jie Yang acknowledges the financial support of the Fundamental Research Funds for the Central Universities.

References

[1] Pettes MT, Ji H, Ruoff RS, Shi L. Thermal transport in three-dimensional foam architectures of few-layer graphene and ultrathin graphite. Nano Lett 2012;12:2959-64. https://doi.org/10.1021/nl300662q.

[2] Jiang H, Wang Z, Geng H, Song X, Zeng H, Zhi C. Highly flexible and self-healable thermal interface material based on boron nitride nanosheets and a dual cross-linked hydrogel. ACS Appl Mater Interfaces 2017;9:10078-84. https://doi.org/10.1021/acsami.6b16195.

[3] Feng C-P, Yang L-Y, Yang J, Bai L, Bao R-Y, Liu Z-Y, et al. Recent advances in polymer-based thermal interface materials for thermal management: A mini-review. Compos Commun 2020;22:100528. https://doi.org/10.1016/j.coco.2020.100528.

[4] Song H, Liu J, Liu B, Wu J, Cheng H-M, Kang F. Two-dimensional materials for thermal management applications. Joule 2018;2:442-63. https://doi.org/10.1016/j.joule.2018.01.006.

[5] Zhang Y, Ma J, Wei N, Yang J, Pei QX. Recent progress in the development of thermal interface materials: A review. Phys Chem Chem Phys 2021;23:753-76. https://doi.org/10.1039/d0cp05514j.

[6] Zhang H, Zhang X, Fang Z, Huang Y, Xu H, Liu Y, et al. Recent advances in preparation, mechanisms, and applications of thermally conductive polymer

composites: A review. J Compos Sci 2020;4:180. https://doi.org/10.3390/jcs4040180.
[7] Niu H, Ren Y, Guo H, Małycha K, Orzechowski K, Bai S-L. Recent progress on thermally conductive and electrical insulating rubber composites: Design, processing and applications. Compos Commun 2020;22:100430. https://doi.org/10.1016/j.coco.2020.100430.
[8] Yang Y, Huang X, Cao Z, Chen G. Thermally conductive separator with hierarchical nano/microstructures for improving thermal management of batteries. Nano Energy 2016;22:301-9. https://doi.org/10.1016/j.nanoen.2016.01.026.
[9] Luo W, Zhou L, Fu K, Yang Z, Wan J, Manno M, et al. A thermally conductive separator for stable Li metal anodes. Nano Lett 2015;15:6149-54. https://doi.org/10.1021/acs.nanolett.5b02432.
[10] Cheng M, Ramasubramanian A, Rasul MG, Jiang Y, Yuan Y, Foroozan T, et al. Direct ink writing of polymer composite electrolytes with enhanced thermal conductivities. Adv Funct Mater 2020;31:2006683. https://doi.org/10.1002/adfm.202006683.
[11] Tahan Latibari S, Sadrameli SM. Carbon based material included-shaped stabilized phase change materials for sunlight-driven energy conversion and storage: An extensive review. Sol Energy 2018;170:1130-61. https://doi.org/10.1016/j.solener.2018.05.007.
[12] Leung SN. Thermally conductive polymer composites and nanocomposites: Processing-structure-property relationships. Compos Part B Eng 2018;150:78-92. https://doi.org/10.1016/j.compositesb.2018.05.056.
[13] Gao T, Yang Z, Chen C, Li Y, Fu K, Dai J, et al. Three-dimensional printed thermal regulation textiles. ACS Nano 2017;11:11513-20. https://doi.org/10.1021/acsnano.7b06295.
[14] Wu K, Yu L, Lei C, Huang J, Liu D, Liu Y, et al. Green production of regenerated cellulose/boron nitride nanosheet textiles for static and dynamic personal cooling. ACS Appl Mater Interfaces 2019;11:40685-93. https://doi.org/10.1021/acsami.9b15612.
[15] Yu X, Li Y, Wang X, Si Y, Yu J, Ding B. Thermoconductive, moisture-permeable, and superhydrophobic nanofibrous membranes with interpenetrated boron nitride network for personal cooling fabrics. ACS Appl Mater Interfaces 2020;12:32078-89.

https://doi.org/10.1021/acsami.0c04486.

[16] Do TN, Phan H, Nguyen T-Q, Visell Y. Miniature soft electromagnetic actuators for robotic applications. Adv Funct Mater 2018;28:1800244. https://doi.org/10.1002/adfm.201800244.

[17] Jiang F, Cui S, Rungnim C, Song N, Shi L, Ding P. Control of a dual-cross-linked boron nitride framework and the optimized design of the thermal conductive network for its thermoresponsive polymeric composites. Chem Mater 2019;31:7686-95. https://doi.org/10.1021/acs.chemmater.9b02551.

[18] Cui S, Jiang F, Song N, Shi L, Ding P. Flexible films for smart thermal management: Influence of structure construction of a two-dimensional graphene network on active heat dissipation response behavior. ACS Appl Mater Interfaces 2019;11:30352-9. https://doi.org/10.1021/acsami.9b10538.

[19] Qin M, Xu Y, Cao R, Feng W, Chen L. Efficiently controlling the 3D thermal conductivity of a polymer nanocomposite via a hyperelastic double-continuous network of graphene and sponge. Adv Funct Mater 2018;28:1805053. https://doi.org/10.1002/adfm.201805053.

[20] Li A, Zhang C, Zhang Y-F. Thermal conductivity of graphene-polymer composites: Mechanisms, Properties, and applications. Polymers 2017;9:437. https://doi.org/10.3390/polym9090437.

[21] Huang C, Qian X, Yang R. Thermal conductivity of polymers and polymer nanocomposites. Mater Sci Eng R Rep 2018;132:1-22. https://doi.org/10.1016/j.mser.2018.06.002.

[22] Qian T, Li J, Min X, Guan W, Deng Y, Ning L. Enhanced thermal conductivity of PEG/diatomite shape-stabilized phase change materials with Ag nanoparticles for thermal energy storage. J Mater Chem A 2015;3:8526-36. https://doi.org/10.1039/c5ta00309a.

[23] Bai L, Zhang Z-M, Pu J-H, Feng C-P, Zhao X, Bao R-Y, et al. Highly thermally conductive electrospun stereocomplex polylactide fibrous film dip-coated with silver nanowires. Polymer 2020;194:122390. https://doi.org/10.1016/j.polymer.2020.122390.

[24] Tekce HS, Kumlutas D, Tavman IH. Effect of particle shape on thermal conductivity of copper reinforced polymer composites. J Reinforc Plast Compos 2007;26:113-21. https://doi.org/10.1177/0731684407072522.

[25] Rai A, Moore AL. Enhanced thermal conduction and influence of interfacial resistance within flexible high aspect ratio copper nanowire/polymer composites. Compos Sci Technol 2017;144:70-8. https://doi.org/10.1016/j.compscitech.2017.03.020.

[26] Yuan H, Wang Y, Li T, Ma P, Zhang S, Du M, et al. Highly thermal conductive and electrically insulating polymer composites based on polydopamine-coated copper nanowire. Compos Sci Technol 2018;164:153-9. https://doi.org/10.1016/j.compscitech.2018.05.046.

[27] Tavman IH. Thermal and mechanical properties of aluminum powder-filled high-density polyethylene composites. J Appl Polym Sci 1996;62:2161-7. https://doi.org/10.1002/(SICI)1097-4628(19961219)62:12<2161::AID-APP19>3.0.CO;2-8.

[28] Krupa I, Cecen V, Boudenne A, Prokeš J, Novák I. The mechanical and adhesive properties of electrically and thermally conductive polymeric composites based on high density polyethylene filled with nickel powder. Mater Des 2013;51:620-8. https://doi.org/10.1016/j.matdes.2013.03.067.

[29] Zhou W, Gong Y, Tu L, Xu L, Zhao W, Cai J, et al. Dielectric properties and thermal conductivity of core-shell structured Ni@NiO/poly(vinylidene fluoride) composites. J Alloys Compd 2017;693:1-8. https://doi.org/10.1016/j.jallcom.2016.09.178.

[30] Azizi S, David E, Fréchette MF, Nguyen-Tri P, Ouellet-Plamondon CM. Electrical and thermal phenomena in low-density polyethylene/carbon black composites near the percolation threshold. J Appl Polym Sci 2019;136:47043. https://doi.org/10.1002/app.47043.

[31] Hong J-H, Park D-W, Shim S-E. A review on thermal conductivity of polymer composites using carbon-based fillers: carbon nanotubes and carbon fibers. Carbon Lett 2010;11:347-56. https://doi.org/10.5714/CL.2010.11.4.347.

[32] Agari Y, Ueda A, Nagai S. Thermal conductivity of a polyethylene filled with

disoriented short-cut carbon fibers. J Appl Polym Sci 1991;43:1117-24. https://doi.org/10.1002/app.1991.070430612.

[33] Han Z, Fina A. Thermal conductivity of carbon nanotubes and their polymer nanocomposites: A review. Prog Polym Sci 2011;36:914-44. https://doi.org/10.1016/j.progpolymsci.2010.11.004.

[34] Ganguli S, Roy AK, Anderson DP. Improved thermal conductivity for chemically functionalized exfoliated graphite/epoxy composites. Carbon 2008;46:806-17. https://doi.org/10.1016/j.carbon.2008.02.008.

[35] Kim HS, Kim JH, Kim WY, Lee HS, Kim SY, Khil M-S. Volume control of expanded graphite based on inductively coupled plasma and enhanced thermal conductivity of epoxy composite by formation of the filler network. Carbon 2017;119:40-6. https://doi.org/10.1016/j.carbon.2017.04.013.

[36] Huang X, Zhi C, Lin Y, Bao H, Wu G, Jiang P, et al. Thermal conductivity of graphene-based polymer nanocomposites. Mater Sci Eng R Rep 2020;142:100577. https://doi.org/10.1016/j.mser.2020.100577.

[37] Shen X, Kim J-K. 3D graphene and boron nitride structures for nanocomposites with tailored thermal conductivities: Recent advances and perspectives. Funct Compos Struct 2020;2:022001. https://doi.org/10.1088/2631-6331/ab953a.

[38] Fang H, Bai S-L, Wong CP. Microstructure engineering of graphene towards highly thermal conductive composites. Compos Part A Appl Sci Manuf 2018;112:216-38. https://doi.org/10.1016/j.compositesa.2018.06.010.

[39] Zhang Z, Qu J, Feng Y, Feng W. Assembly of graphene-aligned polymer composites for thermal conductive applications. Compos Commun 2018;9:33-41. https://doi.org/10.1016/j.coco.2018.04.009.

[40] Rajavel K, Luo S, Wan Y, Yu X, Hu Y, Zhu P, et al. 2D $Ti_3C_2T_x$ MXene/polyvinylidene fluoride (PVDF) nanocomposites for attenuation of electromagnetic radiation with excellent heat dissipation. Compos Part A Appl Sci Manuf 2020;129:105693. https://doi.org/10.1016/j.compositesa.2019.105693.

[41] Jin X, Wang J, Dai L, Liu X, Li L, Yang Y, et al. Flame-retardant poly(vinyl

alcohol)/MXene multilayered films with outstanding electromagnetic interference shielding and thermal conductive performances. Chem Eng J 2020;380:122475. https://doi.org/10.1016/j.cej.2019.122475.

[42] Gao BZ, Xu JZ, Peng JJ, Kang FY, Du HD, Li J, et al. Experimental and theoretical studies of effective thermal conductivity of composites made of silicone rubber and Al_2O_3 particles. Thermochim Acta 2015;614:1-8. https://doi.org/10.1016/j.tca.2015.06.005.

[43] Yang D, Wei Q, Li B, Yu L, Ni Y, Zhang L. High thermal conductive silicone rubber composites constructed by strawberry-structured Al_2O_3-PCPA-Ag hybrids. Compos Part A Appl Sci Manuf 2021;142:106260. https://doi.org/10.1016/j.compositesa.2020.106260.

[44] Zhou W, Wang C, Ai T, Wu K, Zhao F, Gu H. A novel fiber-reinforced polyethylene composite with added silicon nitride particles for enhanced thermal conductivity. Compos Part A Appl Sci Manuf 2009;40:830-6. https://doi.org/10.1016/j.compositesa.2009.04.005.

[45] Yuan Y, Li Z, Cao L, Tang B, Zhang S. Modification of Si_3N_4 ceramic powders and fabrication of Si_3N_4/PTFE composite substrate with high thermal conductivity. Ceram Int 2019;45:16569-76. https://doi.org/10.1016/j.ceramint.2019.05.194.

[46] Xue B, Yang S, Sun X, Xie L, Qin S, Zheng Q. From tanghulu-like to cattail-like SiC nanowire architectures: Interfacial design of nanocellulose composites toward high thermal conductivity. J Mater Chem A 2020;8:14506-18. https://doi.org/10.1039/d0ta04674d.

[47] Yao Y, Zeng X, Pan G, Sun J, Hu J, Huang Y, et al. Interfacial engineering of silicon carbide nanowire/cellulose microcrystal paper toward high thermal conductivity. ACS Appl Mater Interfaces 2016;8:31248-55. https://doi.org/10.1021/acsami.6b10935.

[48] Yu S, Hing P, Hu X. Thermal conductivity of polystyrene–aluminum nitride composite. Compos Part A Appl Sci Manuf 2002;33:289-92. https://doi.org/10.1016/S1359-835X(01)00107-5.

[49] Zhang K, Tao P, Zhang Y, Liao X, Nie S. Highly thermal conductivity of CNF/AlN hybrid films for thermal management of flexible energy storage devices. Carbohydr

polym 2019;213:228-35. https://doi.org/10.1016/j.carbpol.2019.02.087.

[50] Yu C, Zhang J, Tian W, Fan X, Yao Y. Polymer composites based on hexagonal boron nitride and their application in thermally conductive composites. RSC Adv 2018;8:21948-67. https://doi.org/10.1039/c8ra02685h.

[51] Khalaj M, Zarabi Golkhatmi S, Alem SAA, Baghchesaraee K, Hasanzadeh Azar M, Angizi S. Recent progress in the study of thermal properties and tribological behaviors of hexagonal boron nitride-reinforced composites. J Compos Sci 2020;4:116. https://doi.org/10.3390/jcs4030116.

[52] Balandin AA, Ghosh S, Bao W, Calizo I, Teweldebrhan D, Miao F, et al. Superior thermal conductivity of single-layer graphene. Nano Lett 2008;8:902-7. https://doi.org/10.1021/nl0731872.

[53] Jo I, Pettes MT, Kim J, Watanabe K, Taniguchi T, Yao Z, et al. Thermal conductivity and phonon transport in suspended few-layer hexagonal boron nitride. Nano Lett 2013;13:550-4. https://doi.org/10.1021/nl304060g.

[54] Balandin AA. Thermal properties of graphene and nanostructured carbon materials. Nat Mater 2011;10:569-81. https://doi.org/10.1038/nmat3064.

[55] Tanimoto M, Yamagata T, Miyata K, Ando S. Anisotropic thermal diffusivity of hexagonal boron nitride-filled polyimide films: Effects of filler particle size, aggregation, orientation, and polymer chain rigidity. ACS Appl Mater Interfaces 2013;5:4374-82. https://doi.org/10.1021/am400615z.

[56] Ma P-C, Siddiqui NA, Marom G, Kim J-K. Dispersion and functionalization of carbon nanotubes for polymer-based nanocomposites: A review. Compos Part A Appl Sci Manuf 2010;41:1345-67. https://doi.org/10.1016/j.compositesa.2010.07.003.

[57] Guo Y, Ruan K, Gu J. Controllable thermal conductivity in composites by constructing thermal conduction networks. Mater Today Phys 2021;20:100449. https://doi.org/10.1016/j.mtphys.2021.100449.

[58] Zhang F, Feng Y, Feng W. Three-dimensional interconnected networks for thermally conductive polymer composites: Design, preparation, properties, and mechanisms. Mater Sci Eng R Rep 2020;142:100580.

https://doi.org/10.1016/j.mser.2020.100580.

[59] Shen X, Zheng Q, Kim J-K. Rational design of two-dimensional nanofillers for polymer nanocomposites toward multifunctional applications. Prog Mater Sci 2021;115:100708. https://doi.org/10.1016/j.pmatsci.2020.100708.

[60] Hu D, Ma W. Nanocellulose as a sustainable building block to construct eco-friendly thermally conductive composites. Ind Eng Chem Res 2020;59:19465-84. https://doi.org/10.1021/acs.iecr.0c04319.

[61] He X, Wang Y. Recent advances in the rational design of thermal conductive polymer composites. Ind Eng Chem Res 2021;60:1137-54. https://doi.org/10.1021/acs.iecr.0c05509.

[62] Zhang Y, Heo Y-J, Son Y-R, In I, An K-H, Kim B-J, et al. Recent advanced thermal interfacial materials: A review of conducting mechanisms and parameters of carbon materials. Carbon 2019;142:445-60. https://doi.org/10.1016/j.carbon.2018.10.077.

[63] Feng C, Ni H, Chen J, Yang W. Facile method to fabricate highly thermally conductive graphite/PP composite with network structures. ACS Appl Mater Interfaces 2016;8:19732-8. https://doi.org/10.1021/acsami.6b03723.

[64] Chen X, Lim JSK, Yan W, Guo F, Liang YN, Chen H, et al. Salt template assisted BN scaffold fabrication toward highly thermally conductive epoxy composites. ACS Appl Mater Interfaces 2020;12:16987-96. https://doi.org/10.1021/acsami.0c04882.

[65] Hou X, Chen Y, Lv L, Dai W, Zhao S, Wang Z, et al. High-thermal-transport-channel construction within flexible composites via the welding of boron nitride nanosheets. ACS Appl Nano Mater 2019;2:360-8. https://doi.org/10.1021/acsanm.8b01939.

[66] Han J, Du G, Gao W, Bai H. An anisotropically high thermal conductive boron nitride/epoxy composite based on nacre‐mimetic 3D network. Adv Funct Mater 2019;29:1900412. https://doi.org/10.1002/adfm.201900412.

[67] Liu D, Lei C, Wu K, Fu Q. A multidirectionally thermoconductive phase change material enables high and durable electricity via real-environment solar–thermal–electric conversion. ACS Nano 2020;14:15738-47.

https://doi.org/10.1021/acsnano.0c06680.

[68] Ji H, Sellan DP, Pettes MT, Kong X, Ji J, Shi L, et al. Enhanced thermal conductivity of phase change materials with ultrathin-graphite foams for thermal energy storage. Energy Environ Sci 2014;7:1185-92. https://doi.org/10.1039/c3ee42573h.

[69] Yu S, Shen X, Kim J-K. Beyond homogeneous dispersion: Oriented conductive fillers for high κ nanocomposites. Mater Horiz 2021;8:3009-42. https://doi.org/10.1039/D1MH00907A.

[70] Mu M, Wan C, McNally T. Thermal conductivity of 2D nano-structured graphitic materials and their composites with epoxy resins. 2D Mater 2017;4:042001. https://doi.org/10.1088/2053-1583/aa7cd1.

[71] Ngo I-L, Jeon S, Byon C. Thermal conductivity of transparent and flexible polymers containing fillers: A literature review. Int J Heat Mass Transfer 2016;98:219-26. https://doi.org/10.1016/j.ijheatmasstransfer.2016.02.082.

[72] Wu S, Yan T, Kuai Z, Pan W. Thermal conductivity enhancement on phase change materials for thermal energy storage: A review. Energy Storage Mater 2020;25:251-95. https://doi.org/10.1016/j.ensm.2019.10.010.

[73] Chen H, Ginzburg VV, Yang J, Yang Y, Liu W, Huang Y, et al. Thermal conductivity of polymer-based composites: Fundamentals and applications. Prog Polym Sci 2016;59:41-85. https://doi.org/10.1016/j.progpolymsci.2016.03.001.

[74] Guo Y, Ruan K, Shi X, Yang X, Gu J. Factors affecting thermal conductivities of the polymers and polymer composites: A review. Compos Sci Technol 2020;193:108134. https://doi.org/10.1016/j.compscitech.2020.108134.

[75] Wang Z, Shen X, Han NM, Liu X, Wu Y, Ye W, et al. Ultralow electrical percolation in graphene aerogel/epoxy composites. Chem Mater 2016;28:6731-41. https://doi.org/10.1021/acs.chemmater.6b03206.

[76] Gong T, Liu M-Q, Liu H, Peng S-P, Li T, Bao R-Y, et al. Selective distribution and migration of carbon nanotubes enhanced electrical and mechanical performances in polyolefin elastomers. Polymer 2017;110:1-11. https://doi.org/10.1016/j.polymer.2016.12.056.

[77] Zhu H, Li Y, Fang Z, Xu J, Cao F, Wan J, et al. Highly thermally conductive papers with percolative layered boron nitride nanosheets. ACS Nano 2014;8:3606-13. https://doi.org/10.1021/nn500134m.

[78] Shtein M, Nadiv R, Buzaglo M, Kahil K, Regev O. Thermally conductive graphene-polymer composites: Size, percolation, and synergy effects. Chem Mater 2015;27:2100-6. https://doi.org/10.1021/cm504550e.

[79] Oluwalowo A, Nguyen N, Zhang S, Park JG, Liang R. Electrical and thermal conductivity improvement of carbon nanotube and silver composites. Carbon 2019;146:224-31. https://doi.org/10.1016/j.carbon.2019.01.073.

[80] Wu Z, Xu C, Ma C, Liu Z, Cheng HM, Ren W. Synergistic effect of aligned graphene nanosheets in graphene foam for high-performance thermally conductive composites. Adv Mater 2019;31:e1900199. https://doi.org/10.1002/adma.201900199.

[81] Zeng X, Yao Y, Gong Z, Wang F, Sun R, Xu J, et al. Ice-templated assembly strategy to construct 3D boron nitride nanosheet networks in polymer composites for thermal conductivity improvement. Small 2015;11:6205-13. https://doi.org/10.1002/smll.201502173.

[82] Huang X, Zhi C, Jiang P. Toward effective synergetic effects from graphene nanoplatelets and carbon nanotubes on thermal conductivity of ultrahigh volume fraction nanocarbon epoxy composites. J Phys Chem C 2012;116:23812-20. https://doi.org/10.1021/jp308556r.

[83] Kargar F, Barani Z, Salgado R, Debnath B, Lewis JS, Aytan E, et al. Thermal percolation threshold and thermal properties of composites with high loading of graphene and boron nitride fillers. ACS Appl Mater Interfaces 2018;10:37555-65. https://doi.org/10.1021/acsami.8b16616.

[84] Pietrak K, Wiśniewski TS. A review of models for effective thermal conductivity of composite materials. J Power Technol 2014;95:14-24. https://papers.itc.pw.edu.pl/index.php/JPT/article/view/463.

[85] Dai S, Li J, Lu N. Research progress of diamond/copper composites with high thermal conductivity. Diam Relat Mater 2020;108:107993. https://doi.org/10.1016/j.diamond.2020.107993.

[86] Mehra N, Mu L, Ji T, Yang X, Kong J, Gu J, et al. Thermal transport in polymeric materials and across composite interfaces. Appl Mater Today 2018;12:92-130. https://doi.org/10.1016/j.apmt.2018.04.004.

[87] Kochetov R, Andritsch T, Lafont U, Morshuis P, Picken S, Smit J. Thermal behaviour of epoxy resin filled with high thermal conductivity nanopowders. 2009 IEEE Electr Ins Conf 2009;pp:524-8. https://doi.org/10.1109/EIC.2009.5166402.

[88] Progelhof RC, Throne JL, Ruetsch RR. Methods for predicting the thermal conductivity of composite systems: A review. Polym Eng Sci 1976;16:615-25. https://doi.org/10.1002/pen.760160905.

[89] Woodside W, Messmer JH. Thermal conductivity of porous media. I. unconsolidated sands. J Appl Phys 1961;32:1688-99. https://doi.org/10.1063/1.1728419.

[90] Levy FL. A modified Maxwell-Eucken equation for calculating the thermal conductivity of two-component solutions or mixtures. Int J Refrigeration 1981;4:223-5. https://doi.org/10.1016/0140-7007(81)90053-0.

[91] Sundstrom DW, Lee Y-D. Thermal conductivity of polymers filled with particulate solids. J Appl Polym Sci 1972;16:3159-67. https://doi.org/10.1002/app.1972.070161210.

[92] Huang Y, Ellingford C, Bowen C, McNally T, Wu D, Wan C. Tailoring the electrical and thermal conductivity of multi-component and multi-phase polymer composites. Int Mater Rev 2019;65:129-63. https://doi.org/10.1080/09506608.2019.1582180.

[93] Hamilton RL, Crosser OK. Thermal conductivity of heterogeneous two-component systems. Ind Eng Chem Fundam 1962;1:187-91. https://doi.org/10.1021/i160003a005.

[94] Lewis T, Nielsen L. Dynamic mechanical properties of particulate-filled composites. J Appl Polym Sci 1970;14:1449-71. https://doi.org/10.1002/app.1970.070140604.

[95] Wu H, Kessler MR. Multifunctional cyanate ester nanocomposites reinforced by hexagonal boron nitride after noncovalent biomimetic functionalization. ACS Appl

Mater Interfaces 2015;7:5915-26. https://doi.org/10.1021/acsami.5b00147.

[96] Giri A, Hopkins PE, Wessel JG, Duda JC. Kapitza resistance and the thermal conductivity of amorphous superlattices. J Appl Phys 2015;118:165303. https://doi.org/10.1063/1.4934511.

[97] Burger N, Laachachi A, Ferriol M, Lutz M, Toniazzo V, Ruch D. Review of thermal conductivity in composites: Mechanisms, parameters and theory. Prog Polym Sci 2016;61:1-28. https://doi.org/10.1016/j.progpolymsci.2016.05.001.

[98] Hasselman D, Johnson LF. Effective thermal conductivity of composites with interfacial thermal barrier resistance. J Compos Mater 1987;21:508-15. https://doi.org/10.1177/002199838702100602.

[99] Hasselman D, Donaldson KY, Geiger AL. Effect of reinforcement particle size on the thermal conductivity of a particulate-silicon carbide-reinforced aluminum matrix composite. J Am Ceram Soc 1992;75:3137-40. https://doi.org/10.1111/j.1151-2916.1992.tb04400.x.

[100] Nan C-W, Birringer R, Clarke DR, Gleiter H. Effective thermal conductivity of particulate composites with interfacial thermal resistance. J Appl Phys 1997;81:6692-9. https://doi.org/10.1063/1.365209.

[101] Nan C-W, Liu G, Lin Y, Li M. Interface effect on thermal conductivity of carbon nanotube composites. Appl Phys Lett 2004;85:3549-51. https://doi.org/10.1063/1.1808874.

[102] Li Q, Guo Y, Li W, Qiu S, Zhu C, Wei X, et al. Ultrahigh thermal conductivity of assembled aligned multilayer graphene/epoxy composite. Chem Mater 2014;26:4459-65. https://doi.org/10.1021/cm501473t.

[103] Luo F, Wu K, Shi J, Du X, Li X, Yang L, et al. Green reduction of graphene oxide by polydopamine to a construct flexible film: superior flame retardancy and high thermal conductivity. J Mater Chem A 2017;5:18542-50. https://doi.org/10.1039/c7ta04740a.

[104] Pan C, Zhang J, Kou K, Zhang Y, Wu G. Investigation of the through-plane thermal conductivity of polymer composites with in-plane oriented hexagonal boron nitride. Int J Heat Mass Transfer 2018;120:1-8.

https://doi.org/10.1016/j.ijheatmasstransfer.2017.12.015.

[105] Qu Z, Wang K, Xu C-a, Li Y, Jiao E, Chen B, et al. Simultaneous enhancement in thermal conductivity and flame retardancy of flexible film by introducing covalent bond connection. Chem Eng J 2021;421:129729. https://doi.org/10.1016/j.cej.2021.129729.

[106] He X, Wang Y. Highly thermally conductive polyimide composite films with excellent thermal and electrical insulating properties. Ind Eng Chem Res 2020;59:1925-33. https://doi.org/10.1021/acs.iecr.9b05939.

[107] Yao Y, Zeng X, Wang F, Sun R, Xu J-~~b~~B, Wong C-P. Significant enhancement of thermal conductivity in bioinspired freestanding boron nitride papers filled with graphene oxide. Chem Mater 2016;28:1049-57. https://doi.org/10.1021/acs.chemmater.5b04187.

[108] Su Y, Li JJ, Weng GJ. Theory of thermal conductivity of graphene-polymer nanocomposites with interfacial Kapitza resistance and graphene-graphene contact resistance. Carbon 2018;137:222-33. https://doi.org/10.1016/j.carbon.2018.05.033.

[109] Agari Y, Uno T. Estimation on thermal conductivities of filled polymers. J Appl Polym Sci 1986;32:5705-12. https://doi.org/10.1002/app.1986.070320702.

[110] Agari Y, Ueda A, Nagai S. Thermal conductivities of composites in several types of dispersion systems. J Appl Polym Sci 1991;42:1665-9. https://doi.org/10.1002/app.1991.070420621.

[111] Foygel M, Morris RD, Anez D, French S, Sobolev VL. Theoretical and computational studies of carbon nanotube composites and suspensions: Electrical and thermal conductivity. Phys Rev B 2005;71:104201. https://doi.org/10.1103/PhysRevB.71.104201.

[112] Ryu SH, Cho H-B, Kwon Y-T, Song Y, Lee J, Lee S-B, et al. Quasi-isotropic thermal conduction in percolation networks: Using the pore-filling effect to enhance thermal conductivity in polymer nanocomposites. ACS Appl Polym Mater 2020;3:1293-305. https://doi.org/10.1021/acsapm.0c01061.

[113] Chu K, Li W-~~s~~S, Jia C-~~e~~C, Tang F-~~l~~L. Thermal conductivity of composites with hybrid carbon nanotubes and graphene nanoplatelets. Appl Phys Lett 2012;101:211903.

https://doi.org/10.1063/1.4767899.

[114] Wang Z-G, Gong F, Yu W-C, Huang Y-F, Zhu L, Lei J, et al. Synergetic enhancement of thermal conductivity by constructing hybrid conductive network in the segregated polymer composites. Compos Sci Technol 2018;162:7-13. https://doi.org/10.1016/j.compscitech.2018.03.016.

[115] Shen X, Wang Z, Wu Y, Liu X, He Y-B, Zheng Q, et al. A three-dimensional multilayer graphene web for polymer nanocomposites with exceptional transport properties and fracture resistance. Mater Horiz 2018;5:275-84. https://doi.org/10.1039/c7mh00984d.

[116] Yang J, Tang L-S, Bao R-Y, Bai L, Liu Z-Y, Yang W, et al. An ice-templated assembly strategy to construct graphene oxide/boron nitride hybrid porous scaffolds in phase change materials with enhanced thermal conductivity and shape stability for light–thermal–electric energy conversion. J Mater Chem A 2016;4:18841-51. https://doi.org/10.1039/c6ta08454k.

[117] Jia X, Li Q, Ao C, Hu R, Xia T, Xue Z, et al. High thermal conductive shape-stabilized phase change materials of polyethylene glycol/boron nitride@chitosan composites for thermal energy storage. Compos Part A Appl Sci Manuf 2020;129:105710. https://doi.org/10.1016/j.compositesa.2019.105710.

[118] Zhang X, Wu K, Liu Y, Yu B, Zhang Q, Chen F, et al. Preparation of highly thermally conductive but electrically insulating composites by constructing a segregated double network in polymer composites. Compos Sci Technol 2019;175:135-42. https://doi.org/10.1016/j.compscitech.2019.03.017.

[119] Wu B, Chen R, Fu R, Agathopoulos S, Su X, Liu H. Low thermal expansion coefficient and high thermal conductivity epoxy/Al_2O_3/T-ZnOw composites with dual-scale interpenetrating network structure. Compos Part A Appl Sci Manuf 2020;137:105993. https://doi.org/10.1016/j.compositesa.2020.105993.

[120] Xu C, Miao M, Jiang X, Wang X. Thermal conductive composites reinforced via advanced boron nitride nanomaterials. Compos Commun 2018;10:103-9. https://doi.org/10.1016/j.coco.2018.08.002.

[121] Fu Y-X, He Z-X, Mo D-C, Lu S-S. Thermal conductivity enhancement with

different fillers for epoxy resin adhesives. Appl Therm Eng 2014;66:493-8. https://doi.org/10.1016/j.applthermaleng.2014.02.044.

[122] Shen H, Cai C, Guo J, Qian Z, Zhao N, Xu J. Fabrication of oriented hBN scaffolds for thermal interface materials. RSC Adv 2016;6:16489-94. https://doi.org/10.1039/c6ra00980h.

[123] Choi S, Kim J. Thermal conductivity of epoxy composites with a binary-particle system of aluminum oxide and aluminum nitride fillers. Compos Part B Eng 2013;51:140-7. https://doi.org/10.1016/j.compositesb.2013.03.002.

[124] Yung KC, Liem H. Enhanced thermal conductivity of boron nitride epoxy-matrix composite through multi-modal particle size mixing. J Appl Polym Sci 2007;106:3587-91. https://doi.org/10.1002/app.27027.

[125] Wu Y, Ye K, Liu Z, Wang M, Chee KWA, Lin C-T, et al. Effective thermal transport highway construction within dielectric polymer composites via a vacuum-assisted infiltration method. J Mater Chem C 2018;6:6494-501. https://doi.org/10.1039/c8tc01464g.

[126] Wang S, Feng D, Guan H, Guo Y, Liu X, Yan C, et al. Highly efficient thermal conductivity of polydimethylsiloxane composites via introducing “Line-Plane”-like hetero-structured fillers. Compos Part A Appl Sci Manuf 2022;157:106911. https://doi.org/10.1016/j.compositesa.2022.106911.

[127] Shi X, Zhang R, Ruan K, Ma T, Guo Y, Gu J. Improvement of thermal conductivities and simulation model for glass fabrics reinforced epoxy laminated composites via introducing hetero-structured BNN-30@BNNS fillers. J Mater Sci Technol 2021;82:239-49. https://doi.org/10.1016/j.jmst.2021.01.018.

[128] Ruan K, Yan H, Zhang S, Shi X, Guo Y, Gu J. In-situ fabrication of hetero-structured fillers to significantly enhance thermal conductivities of silicone rubber composite films. Compos Sci Technol 2021;210:108799. https://doi.org/10.1016/j.compscitech.2021.108799.

[129] Zhang L, Keblinski P, Wang J-S, Li B. Interfacial thermal transport in atomic junctions. Phys Rev B 2011;83:064303. https://doi.org/10.1103/PhysRevB.83.064303.

[130] Ruan K, Guo Y, Lu C, Shi X, Ma T, Zhang Y, et al. Significant reduction of

interfacial thermal resistance and phonon scattering in graphene/polyimide thermally conductive composite films for thermal management. Research 2021;2021:8438614. https://doi.org/10.34133/2021/8438614.

[131] Song N, Cao D, Luo X, Wang Q, Ding P, Shi L. Highly thermally conductive polypropylene/graphene composites for thermal management. Compos Part A Appl Sci Manuf 2020;135:105912. https://doi.org/10.1016/j.compositesa.2020.105912.

[132] Fang H, Zhao Y, Zhang Y, Ren Y, Bai SL. Three-dimensional graphene foam-filled elastomer composites with high thermal and mechanical properties. ACS Appl Mater Interfaces 2017;9:26447-59. https://doi.org/10.1021/acsami.7b07650.

[133] Yao Y, Sun J, Zeng X, Sun R, Xu JB, Wong CP. Construction of 3D skeleton for polymer composites achieving a high thermal conductivity. Small 2018;14:1704044. https://doi.org/10.1002/smll.201704044.

[134] Fang H, Bai S-L, Wong CP. Thermal, mechanical and dielectric properties of flexible BN foam and BN nanosheets reinforced polymer composites for electronic packaging application. Compos Part A Appl Sci Manuf 2017;100:71-80. https://doi.org/10.1016/j.compositesa.2017.04.018.

[135] Malliaris A, Turner DT. Influence of particle size on the electrical resistivity of compacted mixtures of polymeric and metallic powders. J Appl Phys 1971;42:614-8. https://doi.org/10.1063/1.1660071.

[136] Pang H, Xu L, Yan D-X, Li Z-M. Conductive polymer composites with segregated structures. Prog Polym Sci 2014;39:1908-33. https://doi.org/10.1016/j.progpolymsci.2014.07.007.

[137] Yu S, Lee JW, Han TH, Park C, Kwon Y, Hong SM, et al. Copper shell networks in polymer composites for efficient thermal conduction. ACS Appl Mater Interfaces 2013;5:11618-22. https://doi.org/10.1021/am4030406.

[138] Liu C, Wu W, Wang Y, Wang Z, Chen Q. Silver-coated thermoplastic polyurethane hybrid granules for dual-functional elastomer composites with exceptional thermal conductive and electromagnetic interference shielding performances. Compos Commun 2021;25:100719. https://doi.org/10.1016/j.coco.2021.100719.

[139] Wang R, Cheng H, Gong Y, Wang F, Ding X, Hu R, et al. Highly thermally conductive polymer composite originated from assembly of boron nitride at an oil-water interface. ACS Appl Mater Interfaces 2019;11:42818-26. https://doi.org/10.1021/acsami.9b15259.

[140] Gao C, Lu H, Ni H, Chen J. Structure, thermal conductive, dielectric and electrical insulating properties of UHMWPE/BN composites with a segregated structure. J Polym Res 2017;25:6. https://doi.org/10.1007/s10965-017-1414-1.

[141] Wang X, Wu P. Preparation of highly thermally conductive polymer composite at low filler content via a self-assembly process between polystyrene microspheres and boron nitride nanosheets. ACS Appl Mater Interfaces 2017;9:19934-44. https://doi.org/10.1021/acsami.7b04768.

[142] Cao L, Wang J, Dong J, Zhao X, Li H-B, Zhang Q. Preparation of highly thermally conductive and electrically insulating PI/BNNSs nanocomposites by hot-pressing self-assembled PI/BNNSs microspheres. Compos Part B Eng 2020;188:107882. https://doi.org/10.1016/j.compositesb.2020.107882.

[143] Alam FE, Dai W, Yang M, Du S, Li X, Yu J, et al. In situ formation of a cellular graphene framework in thermoplastic composites leading to superior thermal conductivity. J Mater Chem A 2017;5:6164-9. https://doi.org/10.1039/c7ta00750g.

[144] Jiang Y, Liu Y, Min P, Sui G. BN@PPS core-shell structure particles and their 3D segregated architecture composites with high thermal conductivities. Compos Sci Technol 2017;144:63-9. https://doi.org/10.1016/j.compscitech.2017.03.023.

[145] Liu B, Li Y, Fei T, Han S, Xia C, Shan Z, et al. Highly thermally conductive polystyrene/polypropylene/boron nitride composites with 3D segregated structure prepared by solution-mixing and hot-pressing method. Chem Eng J 2020;385:123829. https://doi.org/10.1016/j.cej.2019.123829.

[146] Shen W, Wu W, Liu C, Wang Z, Huang Z. Achieving a high thermal conductivity for segregated BN/PLA composites via hydrogen bonding regulation through cellulose network. Polym Adv Technol 2020;31:1911-20. https://doi.org/10.1002/pat.4916.

[147] Yang S, Li W, Bai S, Wang Q. High-performance thermal and electrical conductive composites from multilayer plastic packaging waste and expanded graphite.

J Mater Chem C 2018;6:11209-18. https://doi.org/10.1039/c8tc02840k.

[148] Zhou H, Deng H, Zhang L, Fu Q. Significant enhancement of thermal conductivity in polymer composite via constructing macroscopic segregated filler networks. ACS Appl Mater Interfaces 2017;9:29071-81. https://doi.org/10.1021/acsami.7b07947.

[149] Ding J, Zheng R, Zhang Y, Zhang X, Liu G, Zheng K. The high thermal conductive and flexible boron nitride/silicone rubber composites with segregated structure. Mater Res Express 2021;8:035306. https://doi.org/10.1088/2053-1591/abed6b.

[150] Wang Y, Wu W, Drummer D, Liu C, Shen W, Tomiak F, et al. Highly thermally conductive polybenzoxazine composites based on boron nitride flakes deposited with copper particles. Mater Des 2020;191:108698. https://doi.org/10.1016/j.matdes.2020.108698.

[151] Wang Z-G, Huang Y-F, Zhang G-Q, Wang H-Q, Xu J-Z, Lei J, et al. Enhanced thermal conductivity of segregated poly(vinylidene fluoride) composites via forming hybrid conductive network of boron nitride and carbon nanotubes. Ind Eng Chem Res 2018;57:10391-7. https://doi.org/10.1021/acs.iecr.8b01764.

[152] Wu K, Lei C, Huang R, Yang W, Chai S, Geng C, et al. Design and preparation of a unique segregated double network with excellent thermal conductive property. ACS Appl Mater Interfaces 2017;9:7637-47. https://doi.org/10.1021/acsami.6b16586.

[153] Wu K, Li Y, Huang R, Chai S, Chen F, Fu Q. Constructing conductive multi-walled carbon nanotubes network inside hexagonal boron nitride network in polymer composites for significantly improved dielectric property and thermal conductivity. Compos Sci Technol 2017;151:193-201. https://doi.org/10.1016/j.compscitech.2017.07.014.

[154] Zhang P, Ding X, Wang Y, Gong Y, Zheng K, Chen L, et al. Segregated double network enabled effective electromagnetic shielding composites with extraordinary electrical insulation and thermal conductivity. Compos Part A Appl Sci Manuf 2019;117:56-64. https://doi.org/10.1016/j.compositesa.2018.11.007.

[155] Xue S, Lei C, Liu D, Wang K, Wu K, Fu Q. Thermo-conductive phase change

materials with binary fillers of core-shell-like distribution. Compos Part A Appl Sci Manuf 2021;144:106326. https://doi.org/10.1016/j.compositesa.2021.106326.

[156] Chen Y, Hou X, Liao M, Dai W, Wang Z, Yan C, et al. Constructing a "pea-pod-like" alumina-graphene binary architecture for enhancing thermal conductivity of epoxy composite. Chem Eng J 2020;381:122690. https://doi.org/10.1016/j.cej.2019.122690.

[157] Feng C-P, Chen L-B, Tian G-L, Bai L, Bao R-Y, Liu Z-Y, et al. Robust polymer-based paper-like thermal interface materials with a through-plane thermal conductivity over 9 W m^{-1} K^{-1}. Chem Eng J 2020;392:123784. https://doi.org/10.1016/j.cej.2019.123784.

[158] Lee W, Kim J. Enhanced through-plane thermal conductivity of paper-like cellulose film with treated hybrid fillers comprising boron nitride and aluminum nitride. Compos Sci Technol 2020;200:108424. https://doi.org/10.1016/j.compscitech.2020.108424.

[159] Zou D, Huang X, Zhu Y, Chen J, Jiang P. Boron nitride nanosheets endow the traditional dielectric polymer composites with advanced thermal management capability. Compos Sci Technol 2019;177:88-95. https://doi.org/10.1016/j.compscitech.2019.04.027.

[160] Li X, Li C, Zhang X, Jiang Y, Xia L, Wang J, et al. Simultaneously enhanced thermal conductivity and mechanical properties of PP/BN composites via constructing reinforced segregated structure with a trace amount of BN wrapped PP fiber. Chem Eng J 2020;390:124563. https://doi.org/10.1016/j.cej.2020.124563.

[161] Li T, Ma L-F, Bao R-Y, Qi G-Q, Yang W, Xie B-H, et al. A new approach to construct segregated structures in thermoplastic polyolefin elastomers towards improved conductive and mechanical properties. J Mater Chem A 2015;3:5482-90. https://doi.org/10.1039/c5ta00314h.

[162] Yu W-C, Zhang G-Q, Liu Y-H, Xu L, Yan D-X, Huang H-D, et al. Selective electromagnetic interference shielding performance and superior mechanical strength of conductive polymer composites with oriented segregated conductive networks. Chem Eng J 2019;373:556-64. https://doi.org/10.1016/j.cej.2019.05.074.

[163] Wang W-~~y~~Y, Ma X, Shao Y-~~w~~W, Qi X, Yang J, Wang Y. Flexible, multifunctional, and thermally conductive nylon/graphene nanoplatelet composite papers with excellent emi shielding performance, improved hydrophobicity and flame resistance. J Mater Chem A 2021;9:5033-44. https://doi.org/10.1039/d0ta11040j.

[164] Huang Q, Tang Z, Wang D, Wu S, Guo B. Engineering segregated structures in a cross-linked elastomeric network enabled by dynamic cross-link reshuffling. ACS Macro Lett 2021;10:231-6. https://doi.org/10.1021/acsmacrolett.0c00852.

[165] Li J, Zhao X, Zhang Z, Xian Y, Lin Y, Ji X, et al. Construction of interconnected Al_2O_3 doped rGO network in natural rubber nanocomposites to achieve significant thermal conductivity and mechanical strength enhancement. Compos Sci Technol 2020;186:107930. https://doi.org/10.1016/j.compscitech.2019.107930.

[166] Xiao C, Chen L, Tang Y, Zhang X, Zheng K, Tian X. Enhanced thermal conductivity of silicon carbide nanowires (SiCw)/epoxy resin composite with segregated structure. Compos Part A Appl Sci Manuf 2019;116:98-105. https://doi.org/10.1016/j.compositesa.2018.10.023.

[167] Sang Z, Ke K, Manas-Zloczower I. Design strategy for porous composites aimed at pressure sensor application. Small. 2019;15:1903487. https://doi.org/10.1002/smll.201903487.

[168] Fan YJ, Meng XS, Li HY, Kuang SY, Zhang L, Wu Y, et al. Stretchable porous carbon nanotube-elastomer hybrid nanocomposite for harvesting mechanical energy. Adv Mater 2017;29:1603115. https://doi.org/10.1002/adma.201603115.

[169] Chen F, Lu Y, Liu X, Song J, He G, Tiwari MK, et al. Table salt as a template to prepare reusable porous PVDF-MWCNT foam for separation of immiscible oils/organic solvents and corrosive aqueous solutions. Adv Funct Mater 2017;27:1702926. https://doi.org/10.1002/adfm.201702926.

[170] Xie Y, Lan X-R, Bao R-Y, Lei Y, Cao Z-Q, Yang M-B, et al. High-performance porous polylactide stereocomplex crystallite scaffolds prepared by solution blending and salt leaching. Mater Sci Eng C 2018;90:602-9. https://doi.org/10.1016/j.msec.2018.05.023.

[171] Xu X, Hu R, Chen M, Dong J, Xiao B, Wang Q, et al. 3D boron nitride foam

filled epoxy composites with significantly enhanced thermal conductivity by a facial and scalable approach. Chem Eng J 2020;397:125447. https://doi.org/10.1016/j.cej.2020.125447.

[172] Xiao C, Tang Y, Chen L, Zhang X, Zheng K, Tian X. Preparation of highly thermally conductive epoxy resin composites via hollow boron nitride microbeads with segregated structure. Compos Part A Appl Sci Manuf 2019;121:330-40. https://doi.org/10.1016/j.compositesa.2019.03.044.

[173] Wu Y, Ye K, Liu Z, Wang B, Yan C, Wang Z, et al. Cotton candy-templated fabrication of three-dimensional ceramic pathway within polymer composite for enhanced thermal conductivity. ACS Appl Mater Interfaces 2019;11:44700-7. https://doi.org/10.1021/acsami.9b15758.

[174] Liang S, Li Y, Chen Y, Yang J, Zhu T, Zhu D, et al. Liquid metal sponges for mechanically durable, all-soft, electrical conductors. J Mater Chem C 2017;5:1586-90. https://doi.org/10.1039/C6TC05358K.

[175] Wan Y, Qin N, Wang Y, Zhao Q, Wang Q, Yuan P, et al. Sugar-templated conductive polyurethane-polypyrrole sponges for wide-range force sensing. Chem Eng J 2020;383:123103. https://doi.org/10.1016/j.cej.2019.123103.

[176] Yao B, Xu X, Li H, Han Z, Hao J, Yang G, et al. Soft liquid-metal/elastomer foam with compression-adjustable thermal conductivity and electromagnetic interference shielding. Chem Eng J 2021;410:128288. https://doi.org/10.1016/j.cej.2020.128288.

[177] Choi SJ, Kwon TH, Im H, Moon DI, Baek DJ, Seol ML, et al. A polydimethylsiloxane (PDMS) sponge for the selective absorption of oil from water. ACS Appl Mater Interfaces 2011;3:4552-6. https://doi.org/10.1021/am201352w.

[178] Zhou W, Zhang Y, Wang J, Li H, Xu W, Li B, et al. Lightweight porous polystyrene with high thermal conductivity by constructing 3D interconnected network of boron nitride nanosheets. ACS Appl Mater Interfaces 2020;12:46767-78. https://doi.org/10.1021/acsami.0c11543.

[179] Li J, Li F, Zhao X, Zhang W, Li S, Lu Y, et al. Jelly-inspired construction of the three-dimensional interconnected BN network for lightweight, thermally conductive, and electrically insulating rubber composites. ACS Appl Electron Mater 2020;2:1661-

9. https://doi.org/10.1021/acsaelm.0c00227.

[180] Xiao C, Chen L, Tang Y, Zhang X, Zheng K, Tian X. Three dimensional porous alumina network for polymer composites with enhanced thermal conductivity. Compos Part A Appl Sci Manuf 2019;124:105511. https://doi.org/10.1016/j.compositesa.2019.105511.

[181] Zhang R, Hu R, Li X, Zhen Z, Xu Z, Li N, et al. A bubble-derived strategy to prepare multiple graphene-based porous materials. Adv Funct Mater 2018;28:1705879. https://doi.org/10.1002/adfm.201705879.

[182] Barg S, Perez FM, Ni N, do Vale Pereira P, Maher RC, Garcia-Tunon E, et al. Mesoscale assembly of chemically modified graphene into complex cellular networks. Nat Commun 2014;5:4328. https://doi.org/10.1038/ncomms5328.

[183] Li Y, Chen J, Huang L, Li C, Hong JD, Shi G. Highly compressible macroporous graphene monoliths via an improved hydrothermal process. Adv Mater 2014;26:4789-93. https://doi.org/10.1002/adma.201400657.

[184] Li Y, Li J, Deng Y, Guan W, Wang X, Qian T. Preparation of paraffin/porous TiO_2 foams with enhanced thermal conductivity as PCM, by covering the TiO_2 surface with a carbon layer. Appl Energy 2016;171:37-45. https://doi.org/10.1016/j.apenergy.2016.03.010.

[185] Li Y, Li J, Feng W, Wang X, Nian H. Design and preparation of the phase change materials paraffin/porous Al_2O_3@graphite foams with enhanced heat storage capacity and thermal conductivity. ACS Sustain Chem Eng 2017;5:7594-603. https://doi.org/10.1021/acssuschemeng.7b00889.

[186] Wu X, Han Y, Zhang X, Zhou Z, Lu C. Large-area compliant, low-cost, and versatile pressure-sensing platform based on microcrack-designed carbon black@polyurethane sponge for human-machine interfacing. Adv Funct Mater 2016;26:6246-56. https://doi.org/10.1002/adfm.201601995.

[187] Wu H-~~y~~Y, Li S-~~t~~T, Shao Y-~~w~~W, Jin X-~~z~~Z, Qi X-~~d~~D, Yang J-~~h~~H, et al. Melamine foam/reduced graphene oxide supported form-stable phase change materials with simultaneous shape memory property and light-to-thermal energy storage capability. Chem Eng J 2020;379:122373. https://doi.org/10.1016/j.cej.2019.122373.

[188] Kim E, Zhang H, Lee J-H, Chen H, Zhang H, Javed MH, et al. MXene/polyurethane auxetic composite foam for electromagnetic interference shielding and impact attenuation. Compos Part A Appl Sci Manuf 2021;147:106430. https://doi.org/10.1016/j.compositesa.2021.106430.

[189] Xue F, Lu Y, Qi X-~~d~~D, Yang J-~~h~~H, Wang Y. Melamine foam-templated graphene nanoplatelet framework toward phase change materials with multiple energy conversion abilities. Chem Eng J 2019;365:20-9. https://doi.org/10.1016/j.cej.2019.02.023.

[190] Xiao Y-~~y~~Y, Bai D-~~y~~Y, Xie Z-~~p~~P, Yang Z-~~y~~Y, Yang J-~~h~~H, Qi X-~~d~~D, et al. Flexible copper foam-based phase change materials with good stiffness-toughness balance, electro-to-thermal conversion ability and shape memory function for intelligent thermal management. Compos Part A Appl Sci Manuf 2021;146:106420. https://doi.org/10.1016/j.compositesa.2021.106420.

[191] Wu H, Deng S, Shao Y, Yang J, Qi X, Wang Y. Multiresponsive shape-adaptable phase change materials with cellulose nanofiber/graphene nanoplatelet hybrid-coated melamine foam for light/electro-to-thermal energy storage and utilization. acs applied materials & interfaces. 2019;11:46851-63. https://doi.org/10.1021/acsami.9b16612.

[192] Tao W, Zeng S, Xu Y, Nie W, Zhou Y, Qin P, et al. 3D graphene - sponge skeleton reinforced polysulfide rubber nanocomposites with improved electrical and thermal conductivity. Compos Part A Appl Sci Manuf 2021;143:106293. https://doi.org/10.1016/j.compositesa.2021.106293.

[193] Wu B, Lao D, Fu R, Su X, Liu H, Jin X. Novel PEG/EP form-stable phase change materials with high thermal conductivity enhanced by 3D ceramics network. Ceram Int 2020;46:25285-92. https://doi.org/10.1016/j.ceramint.2020.06.321.

[194] Lee S, Kim J. Thermally conductive 3D binetwork structured aggregated boron nitride/Cu-foam/polymer composites. Synth Met 2020;270:116587. https://doi.org/10.1016/j.synthmet.2020.116587.

[195] Wang H, Li L, Wei X, Hou X, Li M, Wu X, et al. Combining alumina particles with three-dimensional alumina foam for high thermally conductive epoxy composites. ACS Appl Polym Mater 2021;3:216-25. https://doi.org/10.1021/acsapm.0c01055.

[196] Yang T, Jiang Z, Han H, Cai X, Liu Y, Zhang X, et al. Welding dopamine modified graphene nanosheets onto graphene foam for high thermal conductive composites. Compos Part B Eng 2021;205:108509. https://doi.org/10.1016/j.compositesb.2020.108509.

[197] Dai W, Lv L, Ma T, Wang X, Ying J, Yan Q, et al. Multiscale structural modulation of anisotropic graphene framework for polymer composites achieving highly efficient thermal energy management. Adv Sci 2021;8:2003734. https://doi.org/10.1002/advs.202003734.

[198] Xue F, Jin XZ, Xie X, Qi XD, Yang JH, Wang Y. Constructing reduced graphene oxide/boron nitride frameworks in melamine foam towards synthesizing phase change materials applied in thermal management of microelectronic devices. Nanoscale 2019;11:18691-701. https://doi.org/10.1039/c9nr07273j.

[199] Liu Z, Shen D, Yu J, Dai W, Li C, Du S, et al. Exceptionally high thermal and electrical conductivity of three-dimensional graphene-foam-based polymer composites. RSC Adv 2016;6:22364-9. https://doi.org/10.1039/c5ra27223h.

[200] Liu Z, Chen Y, Li Y, Dai W, Yan Q, Alam FE, et al. Graphene foam-embedded epoxy composites with significant thermal conductivity enhancement. Nanoscale 2019;11:17600-6. https://doi.org/10.1039/c9nr03968f.

[201] Jiang F, Zhou S, Xu T, Song N, Ding P. Enhanced thermal conductive and mechanical properties of thermoresponsive polymeric composites: Influence of 3D interconnected boron nitride network supported by polyurethane@polydopamine skeleton. Compos Sci Technol 2021;208:108779. https://doi.org/10.1016/j.compscitech.2021.108779.

[202] Tan X, Liu T-H, Zhou W, Yuan Q, Ying J, Yan Q, et al. Enhanced electromagnetic shielding and thermal conductive properties of polyolefin composites with a $Ti_3C_2T_x$ MXene/graphene framework connected by a hydrogen-bonded interface. ACS Nano 2022;16:9254-66. https://doi.org/10.1021/acsnano.2c01716.

[203] Deville S. Freezing colloids: observations, principles, control, and use: Applications in materials science, life science, earth science, food science, and engineering. Springer 2017; pp:1-598. https://doi.org/10.1007/978-3-319-50515-2.

[204] Li WL, Lu K, Walz JY. Freeze casting of porous materials: Review of critical factors in microstructure evolution. Int Mater Rev 2013;57:37-60. https://doi.org/10.1179/1743280411y.0000000011.

[205] Scotti KL, Dunand DC. Freeze casting–a review of processing, microstructure and properties via the open data repository, FreezeCasting. net. Prog Mater Sci 2018;94:243-305. https://doi.org/10.1016/j.pmatsci.2018.01.001.

[206] Deville S. Ice-templating, freeze casting: Beyond materials processing. J Mater Res 2013;28:2202-19. https://doi.org/10.1557/jmr.2013.105.

[207] Deville S. Freeze-casting of porous ceramics: A review of current achievements and issues. Adv Eng Mater 2008;10:155-69. https://doi.org/10.1002/adem.200700270.

[208] Deville S, Meille S, Seuba J. A meta-analysis of the mechanical properties of ice-templated ceramics and metals. Sci Technol Adv Mater 2016;16:043501. https://doi.org/10.1088/1468-6996/16/4/043501.

[209] Shao G, Hanaor DAH, Shen X, Gurlo A. Freeze casting: From low-dimensional building blocks to aligned porous structures-a review of novel materials, methods, and applications. Adv Mater 2020;32:1907176. https://doi.org/10.1002/adma.201907176.

[210] Xie X, Zhou Y, Bi H, Yin K, Wan S, Sun L. Large-range control of the microstructures and properties of three-dimensional porous graphene. Sci Rep 2013;3:2117. https://doi.org/10.1038/srep02117.

[211] Jo H, Kim MJ, Choi H, Sung Y-E, Choe H, Dunand DC. Morphological study of directionally freeze-cast nickel foams. Metall Mater Trans E 2016;3:46-54. https://doi.org/10.1007/s40553-016-0068-y.

[212] White MA, Conrad J, Chen R, Romao C, Pereira A, Hill I. Applications of ice-templated ceramics. Int J Appl Ceram Technol 2018;15:1075-83. https://doi.org/10.1111/ijac.12896.

[213] Li X-H, Li X, Liao K-N, Min P, Liu T, Dasari A, et al. Thermally annealed anisotropic graphene aerogels and their electrically conductive epoxy composites with excellent electromagnetic interference shielding efficiencies. ACS Appl Mater Interfaces. 2016;8:33230-9. https://doi.org/10.1021/acsami.6b12295.

[214] Gao W, Zhao N, Yu T, Xi J, Mao A, Yuan M, et al. High-efficiency

electromagnetic interference shielding realized in nacre-mimetic graphene/polymer composite with extremely low graphene loading. Carbon 2020;157:570-7. https://doi.org/10.1016/j.carbon.2019.10.051.

[215] Xie C, He L, Shi Y, Guo ZX, Qiu T, Tuo X. From monomers to a lasagna-like aerogel monolith: An assembling strategy for aramid nanofibers. ACS Nano 2019;13:7811-24. https://doi.org/10.1021/acsnano.9b01955.

[216] Wicklein B, Kocjan A, Salazar-Alvarez G, Carosio F, Camino G, Antonietti M, et al. Thermally insulating and fire-retardant lightweight anisotropic foams based on nanocellulose and graphene oxide. Nat Nanotechnol 2014;10:277-83. https://doi.org/10.1038/nnano.2014.248.

[217] Yu Z-L, Yang N, Zhou L-C, Ma Z-Y, Zhu Y-B, Lu Y-Y, et al. Bioinspired polymeric woods. Sci Adv 2018;4:eaat7223. https://doi.org/10.1126/sciadv.aat7223.

[218] Zeng Z, Jin H, Chen M, Li W, Zhou L, Zhang Z. Lightweight and anisotropic porous MWCNT/WPU composites for ultrahigh performance electromagnetic interference shielding. Adv Funct Mater 2016;26:303-10. https://doi.org/10.1002/adfm.201503579.

[219] Cheng Q, Huang C, Tomsia AP. Freeze casting for assembling bioinspired structural materials. Adv Mater 2017;29:1703155. https://doi.org/10.1002/adma.201703155.

[220] Ouyang A, Gong Q, Liang J. Carbon nanotube–chitosan composite beads with radially aligned channels and nanotube-exposed walls for bilirubin adsorption. Adv Eng Mater 2015;17:460-6. https://doi.org/10.1002/adem.201400250.

[221] Yu R, Shi Y, Yang D, Liu Y, Qu J, Yu Z-Z. Graphene oxide/chitosan aerogel microspheres with honeycomb-cobweb and radially oriented microchannel structures for broad-spectrum and rapid adsorption of water contaminants. ACS Appl Mater Interfaces 2017;9:21809-19. https://doi.org/10.1021/acsami.7b04655.

[222] Yao Y, Li Y, Zeng X, Sun N, Sun R, Xu J-B, et al. Liquid nitrogen driven assembly of nanomaterials into spongy millispheres for various applications. J Mater Chem A 2018;6:5984-92. https://doi.org/10.1039/c8ta00310f.

[223] Cui Y, Gong H, Wang Y, Li D, Bai H. A Thermally insulating textile inspired by

polar bear hair. Adv Mater 2018;30:1706807. https://doi.org/10.1002/adma.201706807.

[224] Gaudillere C, Garcia-Fayos J, Balaguer M, Serra JM. Enhanced oxygen separation through robust freeze-cast bilayered dual-phase membranes. ChemSusChem 2014;7:2554-61. https://doi.org/10.1002/cssc.201402324.

[225] Kim BS, Lee J. Macroporous PVDF/TiO_2 membranes with three-dimensionally interconnected pore structures produced by directional melt crystallization. Chem Eng J 2016;301:158-65. https://doi.org/10.1016/j.cej.2016.05.003.

[226] Cativa NM, Alvarez Cerimedo MS, Puig J, Arenas GF, Trabadelo F, Ayude MA, et al. PEG-based cross-linked films with aligned channels: Combining cryogenic processing and photopolymerization for the design of micro-patterned oriented platforms. Mol Syst Des Eng 2019;4:133-43. https://doi.org/10.1039/C8ME00085A.

[227] Gao H-L, Lu Y, Mao L-B, An D, Xu L, Gu J-T, et al. A shape-memory scaffold for macroscale assembly of functional nanoscale building blocks. Mater Horiz 2014;1:69-73. https://doi.org/10.1039/C3MH00040K.

[228] Riblett BW, Francis NL, Wheatley MA, Wegst UGK. Ice-templated scaffolds with microridged pores direct DRG neurite growth. Adv Funct Mater 2012;22:4920-3. https://doi.org/10.1002/adfm.201201323.

[229] Wegst UG, Schecter M, Donius AE, Hunger PM. Biomaterials by freeze casting. Phil Trans R Soc A 2010;368:2099-121. https://doi.org/10.1098/rsta.2010.0014.

[230] Wegst UG, Bai H, Saiz E, Tomsia AP, Ritchie RO. Bioinspired structural materials. Nat Mater 2015;14:23-36. https://doi.org/10.1038/nmat4089.

[231] Deville S, Saiz E, Nalla RK, Tomsia AP. Freezing as a Path to Build Complex Composites. Science 2006;311:515-8. https://doi.org/10.1126/science.1120937.

[232] Gawryla MD. Low density materials through freeze-drying: Clay aerogels and beyond. Case Western Reserve University 2009. http://rave.ohiolink.edu/etdc/view?acc_num=case1247013426.

[233] Zhou X, Yin L, Yang B, Chen C, Chen W, Xie Y, et al. Programmable local orientation of micropores by mold - assisted ice templating. Small Methods 2021 ;5:2000963. https://doi.org/10.1002/smtd.202000963.

[234] Yang M, Wu J, Bai H, Xie T, Zhao Q, Wong T-W. Controlling three-dimensional ice template via two-dimensional surface wetting. AIChE J 2016;62:4186-92. https://doi.org/10.1002/aic.15509.

[235] Zhao N, Li M, Gong H, Bai H. Controlling ice formation on gradient wettability surface for high-performance bioinspired materials. Sci Adv 2020;6:eabb4712. https://doi.org/10.1126/sciadv.abb4712.

[236] Gao H-L, Xu L, Long F, Pan Z, Du Y-X, Lu Y, et al. Macroscopic free-standing hierarchical 3D architectures assembled from silver nanowires by ice templating. Angew Chem Int Ed 2014;53:4561-6. https://doi.org/10.1002/anie.201400457.

[237] Pot MW, Faraj KA, Adawy A, van Enckevort WJ, van Moerkerk HT, Vlieg E, et al. Versatile wedge-based system for the construction of unidirectional collagen scaffolds by directional freezing: practical and theoretical considerations. ACS Appl Mater Interfaces 2015;7:8495-505. https://doi.org/10.1021/acsami.5b00169.

[238] Porter MM, Imperio R, Wen M, Meyers MA, McKittrick J. Bioinspired scaffolds with varying pore architectures and mechanical properties. Adv Funct Mater 2014;24:1978-87. https://doi.org/10.1002/adfm.201302958.

[239] Zhang H, Shen X, Kim E, Wang M, Lee J-H, Chen H, et al. Integrated water and thermal managements in bioinspired hierarchical MXene aerogels for highly efficient solar-powered water evaporation. Adv Funct Mater 2022;32:2111794. https://doi.org/10.1002/adfm.202111794.

[240] Zeng Z, Jin H, Chen M, Li W, Zhou L, Xue X, et al. Microstructure design of lightweight, flexible, and high electromagnetic shielding porous multiwalled carbon nanotube/polymer composites. Small 2017;13:1701388. https://doi.org/10.1002/smll.201701388.

[241] Liang C, Song P, Qiu H, Zhang Y, Ma X, Qi F, et al. Constructing interconnected spherical hollow conductive networks in silver platelets/reduced graphene oxide foam/epoxy nanocomposites for superior electromagnetic interference shielding effectiveness. Nanoscale 2019;11:22590-8. https://doi.org/10.1039/C9NR06022G.

[242] Qiu L, Liu JZ, Chang SL, Wu Y, Li D. Biomimetic superelastic graphene-based cellular monoliths. Nat Commun 2012;3:1241. https://doi.org/10.1038/ncomms2251.

[243] Si Y, Wang X, Dou L, Yu J, Ding B. Ultralight and fire-resistant ceramic nanofibrous aerogels with temperature-invariant superelasticity. Sci Adv 2018;4:eaas8925. https://doi.org/10.1126/sciadv.aas8925.

[244] Yang M, Zhao N, Cui Y, Gao W, Zhao Q, Gao C, et al. Biomimetic architectured graphene aerogel with exceptional strength and resilience. ACS Nano 2017;11:6817-24. https://doi.org/10.1021/acsnano.7b01815.

[245] Zhao N, Yang M, Zhao Q, Gao W, Xie T, Bai H. Superstretchable nacre-mimetic graphene/poly(vinyl alcohol) composite film based on interfacial architectural engineering. ACS Nano 2017;11:4777-84. https://doi.org/10.1021/acsnano.7b01089.

[246] Bai H, Chen Y, Delattre B, Tomsia AP, Ritchie RO. Bioinspired large-scale aligned porous materials assembled with dual temperature gradients. Sci Adv 2015;1:e1500849. https://doi.org/10.1126/sciadv.1500849.

[247] Bai H, Walsh F, Gludovatz B, Delattre B, Huang C, Chen Y, et al. Bioinspired hydroxyapatite/poly(methyl methacrylate) composite with a nacre-mimetic architecture by a bidirectional freezing method. Adv Mater 2016;28:50-6. https://doi.org/10.1002/adma.201504313.

[248] Wu Y, Wang Z, Shen X, Liu X, Han NM, Zheng Q, et al. Graphene/boron nitride–polyurethane microlaminates for exceptional dielectric properties and high energy densities. ACS Appl Mater Interfaces 2018;10:26641-52. https://doi.org/10.1021/acsami.8b08031.

[249] Kim J, Han NM, Kim J, Lee J, Kim JK, Jeon S. Highly conductive and fracture-resistant epoxy composite based on non-oxidized graphene flake aerogel. ACS Appl Mater Interfaces 2018;10:37507-16. https://doi.org/10.1021/acsami.8b13415.

[250] Guo F, Shen X, Zhou J, Liu D, Zheng Q, Yang J, et al. Highly thermally conductive dielectric nanocomposites with synergistic alignments of graphene and boron nitride nanosheets. Adv Funct Mater 2020;30:1910826. https://doi.org/10.1002/adfm.201910826.

[251] Xu W, Xing Y, Liu J, Wu H, Cui Y, Li D, et al. Efficient water transport and solar steam generation via radially, hierarchically structured aerogels. ACS Nano

2019;13:7930-8. https://doi.org/10.1021/acsnano.9b02331.

[252] Wang C, Chen X, Wang B, Huang M, Wang B, Jiang Y, et al. Freeze-casting produces a graphene oxide aerogel with a radial and centrosymmetric structure. ACS Nano 2018;12:5816-25. https://doi.org/10.1021/acsnano.8b01747.

[253] Bai H, Wang D, Delattre B, Gao W, De Coninck J, Li S, et al. Biomimetic gradient scaffold from ice-templating for self-seeding of cells with capillary effect. Acta Biomater 2015;20:113-9. https://doi.org/10.1016/j.actbio.2015.04.007.

[254] Su F, Mok J, McKittrick J. Radial-concentric freeze casting inspired by porcupine fish spines. Ceramics 2019;2:161-79. https://doi.org/10.3390/ceramics2010015.

[255] Liao W, Zhao H-B, Liu Z, Xu S, Wang Y-Z. On controlling aerogel microstructure by freeze casting. Compos Part B Eng 2019;173:107036. https://doi.org/10.1016/j.compositesb.2019.107036.

[256] Tang Y, Qiu S, Miao Q, Wu C. Fabrication of lamellar porous alumina with axisymmetric structure by directional solidification with applied electric and magnetic fields. J Eur Ceram Soc 2016;36:1233-40. https://doi.org/10.1016/j.jeurceramsoc.2015.12.012.

[257] Nelson I, Gardner L, Carlson K, Naleway SE. Freeze casting of iron oxide subject to a tri-axial nested Helmholtz-coils driven uniform magnetic field for tailored porous scaffolds. Acta Mater 2019;173:106-16. https://doi.org/10.1016/j.actamat.2019.05.003.

[258] Ogden TA, Prisbrey M, Nelson I, Raeymaekers B, Naleway SE. Ultrasound freeze casting: Fabricating bioinspired porous scaffolds through combining freeze casting and ultrasound directed self-assembly. Mater Des 2019;164:107561. https://doi.org/10.1016/j.matdes.2018.107561.

[259] Niksiar P, Su F, Frank M, Ogden T, Naleway S, Meyers M, et al. External field assisted freeze casting. Ceramics 2019;2:208-34. https://doi.org/10.3390/ceramics2010018.

[260] Yang J, Yang W, Chen W, Tao X. An elegant coupling: Freeze-casting and versatile polymer composites. Prog Polym Sci 2020;109:101289. https://doi.org/10.1016/j.progpolymsci.2020.101289.

[261] Chen H, Jing Y, Lee J-H, Liu D, Kim J, Chen S, et al. Human skin-inspired

integrated multidimensional sensors based on highly anisotropic structures. Mater Horiz 2020;7:2378-89. https://doi.org/10.1039/D0MH00922A.

[262] Ma J, Shang T, Ren L, Yao Y, Zhang T, Xie J, et al. Through-plane assembly of carbon fibers into 3D skeleton achieving enhanced thermal conductivity of a thermal interface material. Chem Eng J 2020;380:122550. https://doi.org/10.1016/j.cej.2019.122550.

[263] Hou X, Chen Y, Dai W, Wang Z, Li H, Lin C-T, et al. Highly thermal conductive polymer composites via constructing micro-phragmites communis structured carbon fibers. Chem Eng J 2019;375:121921. https://doi.org/10.1016/j.cej.2019.121921.

[264] Guo L, Zhang Z, Li M, Kang R, Chen Y, Song G, et al. Extremely high thermal conductivity of carbon fiber/epoxy with synergistic effect of MXenes by freeze-drying. Compos Commun 2020;19:134-41. https://doi.org/10.1016/j.coco.2020.03.009.

[265] Wang J, Ren P, Ren F, Zhu G, Sun A, You C. Preparation of highly thermally conductive epoxy composites via constructing a vertically aligned foam of cetyltrimethylammonium bromide–graphene@polydopamine–multi-walled carbon nanotubes. J Mater Sci 2021;56:7951-65. https://doi.org/10.1007/s10853-021-05795-4.

[266] Lian G, Tuan C-C, Li L, Jiao S, Wang Q, Moon K-S, et al. Vertically aligned and interconnected graphene networks for high thermal conductivity of epoxy composites with ultralow loading. Chem Mater 2016;28:6096-104. https://doi.org/10.1021/acs.chemmater.6b01595.

[267] Li X-H, Liu P, Li X, An F, Min P, Liao K-N, et al. Vertically aligned, ultralight and highly compressive all-graphitized graphene aerogels for highly thermally conductive polymer composites. Carbon 2018;140:624-33. https://doi.org/10.1016/j.carbon.2018.09.016.

[268] Wang Y, Zhang Z, Li T, Ma P, Zhang X, Xia B, et al. Artificial nacre epoxy nanomaterials based on janus graphene oxide for thermal management applications. ACS Appl Mater Interfaces 2020;12:44273-80. https://doi.org/10.1021/acsami.0c11062.

[269] Liu P, Li X, Min P, Chang X, Shu C, Ding Y, et al. 3D lamellar-structured graphene aerogels for thermal interface composites with high through-plane thermal

conductivity and fracture toughness. Nano-Micro Lett 2021;13:22. https://doi.org/10.1007/s40820-020-00548-5.

[270] Thieu NAT, Vu MC, Kim DH, Choi WK, Kim SR. Effect of aspect ratio of vertically aligned copper nanowires in the presence of cellulose nanofibers on the thermal conductivity of epoxy composites. Polym Adv Technol 2020;31:2351-9. https://doi.org/10.1002/pat.4954.

[271] Zhang L, Liu X, Deb A, Feng G. Ice-templating synthesis of hierarchical and anisotropic silver-nanowire-fabric aerogel and its application for enhancing thermal energy storage composites. ACS Sustain Chem Eng 2019;7:19910-7. https://doi.org/10.1021/acssuschemeng.9b05413.

[272] Dong J, Cao L, Li Y, Wu Z, Teng C. Largely improved thermal conductivity of PI/BNNS nanocomposites obtained by constructing a 3D BNNS network and filling it with AgNW as the thermally conductive bridges. Compos Sci Technol 2020;196:108242. https://doi.org/10.1016/j.compscitech.2020.108242.

[273] Li H, Fu C, Chen N, Zhang T, Liu J, Du G, et al. Ice-templated assembly strategy to construct three-dimensional thermally conductive networks of BN nanosheets and silver nanowires in polymer composites. Compos Commun 2021;25:100601. https://doi.org/10.1016/j.coco.2020.100601.

[274] Wang D, Lin Y, Hu D, Jiang P, Huang X. Multifunctional 3D-MXene/PDMS nanocomposites for electrical, thermal and triboelectric applications. Compos Part A Appl Sci Manuf 2020;130:105754. https://doi.org/10.1016/j.compositesa.2019.105754.

[275] Ji C, Wang Y, Ye Z, Tan L, Mao D, Zhao W, et al. Ice-templated MXene/Ag-epoxy nanocomposites as high-performance thermal management materials. ACS Appl Mater Interfaces 2020;12:24298-307. https://doi.org/10.1021/acsami.9b22744.

[276] An D, Duan X, Cheng S, Zhang Z, Yang B, Lian Q, et al. Enhanced thermal conductivity of natural rubber based thermal interfacial materials by constructing covalent bonds and three-dimensional networks. Compos Part A Appl Sci Manuf 2020;135:105928. https://doi.org/10.1016/j.compositesa.2020.105928.

[277] An D, Cheng S, Zhang Z, Jiang C, Fang H, Li J, et al. A polymer-based thermal management material with enhanced thermal conductivity by introducing three-

dimensional networks and covalent bond connections. Carbon 2019;155:258-67. https://doi.org/10.1016/j.carbon.2019.08.072.

[278] Hu J, Huang Y, Yao Y, Pan G, Sun J, Zeng X, et al. Polymer composite with improved thermal conductivity by constructing a hierarchically ordered three-dimensional interconnected network of BN. ACS Appl Mater Interfaces 2017;9:13544-53. https://doi.org/10.1021/acsami.7b02410.

[279] Yang J, Yu P, Tang LS, Bao RY, Liu ZY, Yang MB, et al. Hierarchically interconnected porous scaffolds for phase change materials with improved thermal conductivity and efficient solar-to-electric energy conversion. Nanoscale 2017;9:17704-9. https://doi.org/10.1039/c7nr05449a.

[280] Yang J, Tang L-S, Bai L, Bao R-Y, Liu Z, Xie B-H, et al. Photodriven shape-stabilized phase change materials with optimized thermal conductivity by tailoring the microstructure of hierarchically ordered hybrid porous scaffolds. ACS Sustain Chem Eng 2018;6:6761-70. https://doi.org/10.1021/acssuschemeng.8b00565.

[281] Wu F, Chen S, Tang X, Fang H, Tian H, Li D, et al. Thermal conductivity of polycaprolactone/three-dimensional hexagonal boron nitride composites and multi-orientation model investigation. Compos Sci Technol 2020;197:108245. https://doi.org/10.1016/j.compscitech.2020.108245.

[282] Ghosh B, Xu F, Grant DM, Giangrande P, Gerada C, George MW, et al. Highly Ordered $BN_{\perp}$–$BN_{\perp}$ Stacking Structure for Improved Thermally Conductive Polymer Composites. Adv Electron Mater 2020;6:2000627. https://doi.org/10.1002/aelm.202000627.

[283] Yao Y, Ye Z, Huang F, Zeng X, Zhang T, Shang T, et al. Achieving significant thermal conductivity enhancement via an ice-templated and sintered BN-SiC skeleton. ACS Appl Mater Interfaces 2020;12:2892-902. https://doi.org/10.1021/acsami.9b19280.

[284] Wu F, Chen A, Pan H, Li D, Zhang L, Fang H, et al. Synergistic enhancement of thermal conductivity by addition of graphene nanoplatelets to three-dimensional boron nitride scaffolds for polyamide 6 composites. Polym Eng Sci 2021;61:1415-26.

https://doi.org/10.1002/pen.25658.

[285] Jiang F, Song N, Ouyang R, Ding P. Wall density-controlled thermal conductive and mechanical properties of three-dimensional vertically aligned boron nitride network-based polymeric composites. ACS Appl Mater Interfaces 2021;13:7556-66. https://doi.org/10.1021/acsami.0c22702.

[286] Wang X, Wu P. 3D vertically aligned BNNS network with long-range continuous channels for achieving a highly thermally conductive composite. ACS Appl Mater Interfaces 2019;11:28943-52. https://doi.org/10.1021/acsami.9b09398.

[287] Huang T, Li Y, Chen M, Wu L. Bi-directional high thermal conductive epoxy composites with radially aligned boron nitride nanosheets lamellae. Compos Sci Technol 2020;198:108322. https://doi.org/10.1016/j.compscitech.2020.108322.

[288] He S, Zhang Y-~~s~~S, Zhang N, Huang T, Qi X-~~d~~D, Yang J-~~h~~H, et al. Multi-directionally thermal conductive epoxy/boron nitride composites based on circinate vane type network. Compos Commun 2021;25:100744. https://doi.org/10.1016/j.coco.2021.100744.

[289] Wei Z, Xie W, Ge B, Zhang Z, Yang W, Xia H, et al. Enhanced thermal conductivity of epoxy composites by constructing aluminum nitride honeycomb reinforcements. Compos Sci Technol 2020;199:108304. https://doi.org/10.1016/j.compscitech.2020.108304.

[290] Shen Z, Feng J. Achieving vertically aligned SiC microwires networks in a uniform cold environment for polymer composites with high through-plane thermal conductivity enhancement. Compos Sci Technol 2019;170:135-40. https://doi.org/10.1016/j.compscitech.2018.11.036.

[291] Song J, Zhang Y. Vertically aligned silicon carbide nanowires/reduced graphene oxide networks for enhancing the thermal conductivity of silicone rubber composites. Compos Part A Appl Sci Manuf 2020;133:105873. https://doi.org/10.1016/j.compositesa.2020.105873.

[292] Yao Y, Zhu X, Zeng X, Sun R, Xu J-B, Wong C-P. Vertically aligned and interconnected SiC nanowire networks leading to significantly enhanced thermal conductivity of polymer composites. ACS Appl Mater Interfaces 2018;10:9669-78.

https://doi.org/10.1021/acsami.8b00328.

[293] Huang C, Peng J, Wan S, Du Y, Dou S, Wagner HD, et al. Ultra-tough inverse artificial nacre based on epoxy-graphene by freeze-casting. Angew Chem Int Ed 2019;58:7636-40. https://doi.org/10.1002/anie.201902410.

[294] Han NM, Wang Z, Shen X, Wu Y, Liu X, Zheng Q, et al. Graphene size-dependent multifunctional properties of unidirectional graphene aerogel/epoxy nanocomposites. ACS Appl Mater Interfaces 2018;10:6580-92. https://doi.org/10.1021/acsami.7b19069.

[295] An F, Li X, Min P, Li H, Dai Z, Yu Z-Z. Highly anisotropic graphene/boron nitride hybrid aerogels with long-range ordered architecture and moderate density for highly thermally conductive composites. Carbon 2018;126:119-27. https://doi.org/10.1016/j.carbon.2017.10.011.

[296] Chen J, Huang X, Zhu Y, Jiang P. Cellulose nanofiber supported 3D interconnected BN nanosheets for epoxy nanocomposites with ultrahigh thermal management capability. Adv Funct Mater 2017;27:1604754. https://doi.org/10.1002/adfm.201604754.

[297] Yang J, Chan K-Y, Venkatesan H, Kim E, Adegun MH, Lee J-H, et al. Superinsulating BNNS/PVA composite aerogels with high solar reflectance for energy-efficient buildings. Nano-Micro Lett 2022;14:54. https://doi.org/10.1007/s40820-022-00797-6.

[298] Chan KY, Shen X, Yang J, Lin KT, Venkatesan H, Kim E, et al. Scalable anisotropic cooling aerogels by additive freeze-casting. Nature Commun 2022;13:5553. https://doi.org/10.1038/s41467-022-33234-8.

[299] Chen Z, Ren W, Gao L, Liu B, Pei S, Cheng HM. Three-dimensional flexible and conductive interconnected graphene networks grown by chemical vapour deposition. Nat Mater 2011;10:424-8. https://doi.org/10.1038/nmat3001.

[300] Cao X, Shi Y, Shi W, Lu G, Huang X, Yan Q, et al. Preparation of novel 3D graphene networks for supercapacitor applications. Small 2011;7:3163-8. https://doi.org/10.1002/smll.201100990.

[301] Mi Z, Tianquan L, Fuqiang H, Yajuan Z, Zhou W, Yufeng T, et al. Highly

conductive porous graphene/ceramic composites for heat transfer and thermal energy storage. Adv Funct Mater 2013;23:2263-9. https://doi.org/doi:10.1002/adfm.201202638.

[302] Huang H, Bi H, Zhou M, Xu F, Lin T, Liu F, et al. A three-dimensional elastic macroscopic graphene network for thermal management application. J Mater Chem A 2014;2:18215-8. https://doi.org/10.1039/C4TA03801K.

[303] Bi H, Lin T, Xu F, Tang Y, Liu Z, Huang F. New graphene form of nanoporous monolith for excellent energy storage. Nano Lett 2016;16:349-54. https://doi.org/10.1021/acs.nanolett.5b03923.

[304] Jia J, Sun X, Lin X, Shen X, Mai Y-W, Kim J-K. Exceptional electrical conductivity and fracture resistance of 3D interconnected graphene foam/epoxy composites. ACS Nano 2014;8:5774-83. https://doi.org/10.1021/nn500590g.

[305] Garakani MA, Abouali S, Xu Z-L, Huang J, Huang J-Q, Kim J-K. Heterogeneous, mesoporous $NiCo_2O_4$–MnO_2/graphene foam for asymmetric supercapacitors with ultrahigh specific energies. J Mater Chem A 2017;5:3547-57. https://doi.org/10.1039/c6ta08929a.

[306] Hu G, Xu C, Sun Z, Wang S, Cheng HM, Li F, et al. 3D Graphene-foam-reduced-graphene-oxide hybrid nested hierarchical networks for high-performance Li-S batteries. Adv Mater 2016;28:1603-9. https://doi.org/10.1002/adma.201504765.

[307] Ren H, Tang M, Guan B, Wang K, Yang J, Wang F, et al. Hierarchical graphene foam for efficient omnidirectional solar-thermal energy conversion. Adv Mater 2017;29:1702590. https://doi.org/10.1002/adma.201702590.

[308] Zheng Q, Liu X, Xu H, Cheung MS, Choi YW, Huang HC, et al. Sliced graphene foam films for dual-functional wearable strain sensors and switches. Nanoscale Horiz 2018;3:35-44. https://doi.org/10.1039/c7nh00147a.

[309] Sun X, Liu X, Shen X, Wu Y, Wang Z, Kim J-K. Graphene foam/carbon nanotube/poly(dimethyl siloxane) composites for exceptional microwave shielding. Compos Part A Appl Sci Manuf 2016;85:199-206. https://doi.org/10.1016/j.compositesa.2016.03.009.

[310] Wu Y, Wang Z, Liu X, Shen X, Zheng Q, Xue Q, et al. Ultralight graphene

foam/conductive polymer composites for exceptional electromagnetic interference shielding. ACS Appl Mater Interfaces 2017;9:9059-69. https://doi.org/10.1021/acsami.7b01017.

[311] Fang H, Zhang X, Zhao Y, Bai S-L. Dense graphene foam and hexagonal boron nitride filled PDMS composites with high thermal conductivity and breakdown strength. Compos Sci Technol 2017;152:243-53. https://doi.org/10.1016/j.compscitech.2017.09.032.

[312] Zhao Y-H, Zhang Y-F, Bai S-L. High thermal conductivity of flexible polymer composites due to synergistic effect of multilayer graphene flakes and graphene foam. Compos Part A Appl Sci Manuf 2016;85:148-55. https://doi.org/10.1016/j.compositesa.2016.03.021.

[313] Zhao Y-H, Zhang Y-F, Wu Z-K, Bai S-L. Synergic enhancement of thermal properties of polymer composites by graphene foam and carbon black. Compos Part B Eng 2016;84:52-8. https://doi.org/10.1016/j.compositesb.2015.08.074.

[314] Vu MC, Choi W-K, Lee SG, Park PJ, Kim DH, Islam MA, et al. High thermal conductivity enhancement of polymer composites with vertically aligned silicon carbide sheet scaffolds. ACS Appl Mater Interfaces 2020;12:23388-98. https://doi.org/10.1021/acsami.0c02421.

[315] Vu MC, Thieu NAT, Choi WK, Islam MA, Kim S-R. Ultralight covalently interconnected silicon carbide aerofoam for high performance thermally conductive epoxy composites. Compos Part A Appl Sci Manuf 2020;138:106028. https://doi.org/10.1016/j.compositesa.2020.106028.

[316] Kholmanov I, Kim J, Ou E, Ruoff RS, Shi L. Continuous carbon nanotube–ultrathin graphite hybrid foams for increased thermal conductivity and suppressed subcooling in composite phase change materials. ACS Nano 2015;9:11699-707. https://doi.org/10.1021/acsnano.5b02917.

[317] Hu N, Li H, Wei Q, Zhou K, Zhu W, Zhang L, et al. Continuous diamond-carbon nanotube foams as rapid heat conduction channels in composite phase change materials based on the stable hierarchical structure. Compos Part B Eng 2020;200:108293. https://doi.org/10.1016/j.compositesb.2020.108293.

[318] Uetani K, Ata S, Tomonoh S, Yamada T, Yumura M, Hata K. Elastomeric thermal interface materials with high through-plane thermal conductivity from carbon fiber fillers vertically aligned by electrostatic flocking. Adv Mater 2014;26:5857-62. https://doi.org/10.1002/adma.201401736.

[319] Fujihara T, Cho H-B, Nakayama T, Suzuki T, Jiang W, Suematsu H, et al. Field-induced orientation of hexagonal boron nitride nanosheets using microscopic mold for thermal interface materials. J Am Ceram Soc 2012;95:369-73. https://doi.org/10.1111/j.1551-2916.2011.04942.x.

[320] Wu S, Ladani RB, Zhang J, Bafekrpour E, Ghorbani K, Mouritz AP, et al. Aligning multilayer graphene flakes with an external electric field to improve multifunctional properties of epoxy nanocomposites. Carbon 2015;94:607-18. https://doi.org/10.1016/j.carbon.2015.07.026.

[321] Yuan C, Duan B, Li L, Xie B, Huang M, Luo X. Thermal conductivity of polymer-based composites with magnetic aligned hexagonal boron nitride platelets. ACS Appl Mater Interfaces 2015;7:13000-6. https://doi.org/10.1021/acsami.5b03007.

[322] Yuan C, Xie B, Huang M, Wu R, Luo X. Thermal conductivity enhancement of platelets aligned composites with volume fraction from 10% to 20%. Int J Heat Mass Transfer 2016;94:20-8. https://doi.org/10.1016/j.ijheatmasstransfer.2015.11.045.

[323] He J, Wang H, Qu Q, Su Z, Qin T, Tian X. Three-dimensional network constructed by vertically oriented multilayer graphene and SiC nanowires for improving thermal conductivity and operating safety of epoxy composites with ultralow loading. Compos Part A Appl Sci Manuf 2020;139:106062. https://doi.org/10.1016/j.compositesa.2020.106062.

[324] An F, Li X, Min P, Liu P, Jiang ZG, Yu ZZ. Vertically aligned high-quality graphene foams for anisotropically conductive polymer composites with ultrahigh through-plane thermal conductivities. ACS Appl Mater Interfaces 2018;10:17383-92. https://doi.org/10.1021/acsami.8b04230.

[325] Chen J, Huang X, Sun B, Wang Y, Zhu Y, Jiang P. Vertically aligned and interconnected boron nitride nanosheets for advanced flexible nanocomposite thermal interface materials. ACS Appl Mater Interfaces 2017;9:30909-17.

https://doi.org/10.1021/acsami.7b08061.

[326] Jung H, Yu S, Bae NS, Cho SM, Kim RH, Cho SH, et al. High through-plane thermal conduction of graphene nanoflake filled polymer composites melt-processed in an L-shape kinked tube. ACS Appl Mater Interfaces 2015;7:15256-62. https://doi.org/10.1021/acsami.5b02681.

[327] Feng C-P, Bai L, Shao Y, Bao R-Y, Liu Z-Y, Yang M-B, et al. A facile route to fabricate highly anisotropic thermally conductive elastomeric POE/NG composites for thermal management. Adv Mater Interfaces 2018;5:1700946. https://doi.org/10.1002/admi.201700946.

[328] Xue Y, Li X, Wang H, Zhao F, Zhang D, Chen Y. Improvement in thermal conductivity of through-plane aligned boron nitride/silicone rubber composites. Mater Des 2019;165:107580. https://doi.org/10.1016/j.matdes.2018.107580.

[329] Wu X, Tang B, Chen J, Shan L, Gao Y, Yang K, et al. Epoxy composites with high cross-plane thermal conductivity by constructing all-carbon multidimensional carbon fiber/graphite networks. Compos Sci Technol 2021;203:108610. https://doi.org/10.1016/j.compscitech.2020.108610.

[330] Geng Y, He H, Jia Y, Peng X, Li Y. Enhanced through-plane thermal conductivity of polyamide 6 composites with vertical alignment of boron nitride achieved by fused deposition modeling. Polym Compos 2019;40:3375-82. https://doi.org/10.1002/pc.25198.

[331] Guo H, Zhao H, Niu H, Ren Y, Fang H, Fang X, et al. Highly thermally conductive 3D printed graphene filled polymer composites for scalable thermal management applications. ACS Nano 2021;15:6917-28. https://doi.org/10.1021/acsnano.0c10768.

[332] Zhao Y-H, Wu Z-K, Bai S-L. Study on thermal properties of graphene foam/graphene sheets filled polymer composites. Compos Part A Appl Sci Manuf 2015;72:200-6. https://doi.org/10.1016/j.compositesa.2015.02.011.

[333] Cardarelli F. Materials handbook. Springer 2018. https://doi.org/10.1007/978-3-319-38925-7.

[334] Yang W, Zhao Z, Wu K, Huang R, Liu T, Jiang H, et al. Ultrathin flexible reduced graphene oxide/cellulose nanofiber composite films with strongly anisotropic thermal

conductivity and efficient electromagnetic interference shielding. J Mater Chem C 2017;5:3748-56. https://doi.org/10.1039/c7tc00400a.

[335] Song N, Jiao D, Cui S, Hou X, Ding P, Shi L. Highly anisotropic thermal conductivity of layer-by-layer assembled nanofibrillated cellulose/graphene nanosheets hybrid films for thermal management. ACS Appl Mater Interfaces 2017;9:2924-32. https://doi.org/10.1021/acsami.6b11979.

[336] Shen Z, Feng J. Highly thermally conductive composite films based on nanofibrillated cellulose in situ coated with a small amount of silver nanoparticles. ACS Appl Mater Interfaces 2018;10:24193-200. https://doi.org/10.1021/acsami.8b07249.

[337] Wang X, Wu P. Fluorinated carbon nanotube/nanofibrillated cellulose composite film with enhanced toughness, superior thermal conductivity, and electrical insulation. ACS Appl Mater Interfaces 2018;10:34311-21. https://doi.org/10.1021/acsami.8b12565.

[338] Zeng X, Sun J, Yao Y, Sun R, Xu JB, Wong CP. A combination of boron nitride nanotubes and cellulose nanofibers for the preparation of a nanocomposite with high thermal conductivity. ACS Nano 2017;11:5167-78. https://doi.org/10.1021/acsnano.7b02359.

[339] Wu K, Fang J, Ma J, Huang R, Chai S, Chen F, et al. Achieving a collapsible, strong, and highly thermally conductive film based on oriented functionalized boron nitride nanosheets and cellulose nanofiber. ACS Appl Mater Interfaces 2017;9:30035-45. https://doi.org/10.1021/acsami.7b08214.

[340] Hu Z, Wang S, Chen G, zhang Q, Wu K, Shi J, et al. An aqueous-only, green route to exfoliate boron nitride for preparation of high thermal conductive boron nitride nanosheet/cellulose nanofiber flexible film. Compos Sci Technol 2018;168:287-95. https://doi.org/10.1016/j.compscitech.2018.09.020.

[341] Yu C, Zhang Q, Zhang J, Geng R, Tian W, Fan X, et al. One-step in situ ball milling synthesis of polymer-functionalized few-layered boron nitride and its application in high thermally conductive cellulose composites. ACS Appl Nano Mater 2018;1:4875-83. https://doi.org/10.1021/acsanm.8b01047.

[342] Wang J, Wu Y, Xue Y, Liu D, Wang X, Hu X, et al. Super-compatible functional

boron nitride nanosheets/polymer films with excellent mechanical properties and ultra-high thermal conductivity for thermal management. J Mater Chem C 2018;6:1363-9. https://doi.org/10.1039/C7TC04860B.

[343] Wang X, Wu P. Highly thermally conductive fluorinated graphene films with superior electrical insulation and mechanical flexibility. ACS Appl Mater Interfaces 2019;11:21946-54. https://doi.org/10.1021/acsami.9b07377.

[344] Wu Y, Xue Y, Qin S, Liu D, Wang X, Hu X, et al. BN nanosheet/polymer films with highly anisotropic thermal conductivity for thermal management applications. ACS Appl Mater Interfaces 2017;9:43163-70. https://doi.org/10.1021/acsami.7b15264.

[345] Wu K, Wang J, Liu D, Lei C, Liu D, Lei W, et al. Highly thermoconductive, thermostable, and super-flexible film by engineering 1D rigid rod-like aramid nanofiber/2D boron nitride nanosheets. Adv Mater 2020;32:1906939. https://doi.org/10.1002/adma.201906939.

[346] Ma T, Zhao Y, Ruan K, Liu X, Zhang J, Guo Y, et al. Highly thermal conductivities, excellent mechanical robustness and flexibility, and outstanding thermal stabilities of aramid nanofiber composite papers with nacre-mimetic layered structures. ACS Appl Mater Interfaces 2020;12:1677-86. https://doi.org/10.1021/acsami.9b19844.

[347] Chen J, Huang X, Sun B, Jiang P. Highly thermally conductive yet electrically insulating polymer/boron nitride nanosheets nanocomposite films for improved thermal management capability. ACS Nano 2019;13:337-45. https://doi.org/10.1021/acsnano.8b06290.

[348] Chen J, Wei H, Bao H, Jiang P, Huang X. Millefeuille-inspired thermally conductive polymer nanocomposites with overlapping BN nanosheets for thermal management applications. ACS Appl Mater Interfaces 2019;11:31402-10. https://doi.org/10.1021/acsami.9b10810.

[349] Yang G, Zhang X, Shang Y, Xu P, Pan D, Su F, et al. Highly thermally conductive polyvinyl alcohol/boron nitride nanocomposites with interconnection oriented boron nitride nanoplatelets. Compos Sci Technol 2021;201:108521. https://doi.org/10.1016/j.compscitech.2020.108521.

[350] Guo Y, Pan L, Yang X, Ruan K, Han Y, Kong J, et al. Simultaneous improvement

of thermal conductivities and electromagnetic interference shielding performances in polystyrene composites via constructing interconnection oriented networks based on electrospinning technology. Compos Part A Appl Sci Manuf 2019;124:105484. https://doi.org/10.1016/j.compositesa.2019.105484.

[351] Fan L, Zhang S, Zhao G, Fu Q. Constructing Fibrillated Skeleton with Highly Aligned Boron Nitride Nanosheets Confined in Alumina Fiber via Electrospinning and Sintering for Thermally Conductive Composite. Compos Part A Appl Sci Manuf 2021;143:106282. https://doi.org/10.1016/j.compositesa.2021.106282.

[352] Yu C, Gong W, Tian W, Zhang Q, Xu Y, Lin Z, et al. Hot-pressing induced alignment of boron nitride in polyurethane for composite films with thermal conductivity over 50 W $m^{-1} K^{-1}$. Compos Sci Technol 2018;160:199-207. https://doi.org/10.1016/j.compscitech.2018.03.028.

[353] Gao Y, Zhang M, Chen X, Zhu Y, Wang H, Yuan S, et al. A high-performance thermal conductive and outstanding electrical insulating composite based on robust neuron-like microstructure. Chem Eng J 2021;426:131280. https://doi.org/10.1016/j.cej.2021.131280.

[354] Shen H, Guo J, Wang H, Zhao N, Xu J. Bioinspired modification of h-BN for high thermal conductive composite films with aligned structure. ACS Appl Mater Interfaces 2015;7:5701-8. https://doi.org/10.1021/am507416y.

[355] Ou X, Chen S, Lu X, Lu Q. Enhancement of thermal conductivity and dimensional stability of polyimide/boron nitride films through mechanochemistry. Compos Commun 2021;23:100549. https://doi.org/10.1016/j.coco.2020.100549.

[356] Feng CP, Chen LB, Tian GL, Wan SS, Bai L, Bao RY, et al. Multifunctional thermal management materials with excellent heat dissipation and generation capability for future electronics. ACS Appl Mater Interfaces 2019;11:18739-45. https://doi.org/10.1021/acsami.9b03885.

[357] Pan X, Debije MG, Schenning A, Bastiaansen CWM. Enhanced thermal conductivity in oriented polyvinyl alcohol/graphene oxide composites. ACS Appl Mater Interfaces 2021;13:28864-9. https://doi.org/10.1021/acsami.1c06415.

[358] Song N, Yang J, Ding P, Tang S, Shi L. Effect of polymer modifier chain length

on thermal conductive property of polyamide 6/graphene nanocomposites. Compos Part A Appl Sci Manuf 2015;73:232-41. https://doi.org/10.1016/j.compositesa.2015.03.018.

[359] He Q, chen R, Li S, Wang Z, Wen F, Wang B, et al. Excellent thermally conducting modified graphite nanoplatelets and MWCNTs/poly(phenylene sulfone) composites for high-performance electromagnetic interference shielding effectiveness. Compos Part A Appl Sci Manuf 2021;143:106280. https://doi.org/10.1016/j.compositesa.2021.106280.

[360] Wu K, Liu D, Lei C, Xue S, Fu Q. Is filler orientation always good for thermal management performance: A visualized study from experimental results to simulative analysis. Chem Eng J 2020;394:124929. https://doi.org/10.1016/j.cej.2020.124929.

[361] Rondelez F, Urbach W, Hervet H. Origin of thermal conductivity anisotropy in liquid crystalline phases. Phys Rev Lett 1978;41:1058-62. https://doi.org/10.1103/PhysRevLett.41.1058.

[362] Zhu X, Yang C, Wu P, Ma Z, Shang Y, Bai G, et al. Precise control of versatile microstructure and properties of graphene aerogel via freezing manipulation. Nanoscale 2020;12:4882-94. https://doi.org/10.1039/c9nr07861d.

[363] Zhang Y-P, Zhou C-G, Sun W-J, Wang T, Jia L-C, Yan D-X, et al. Injection molding of segregated carbon nanotube/polypropylene composite with enhanced electromagnetic interference shielding and mechanical performance. Compos Sci Technol 2020;197:108253. https://doi.org/10.1016/j.compscitech.2020.108253.

[364] Li D, Bu X, Xu Z, Luo Y, Bai H. Bioinspired multifunctional cellular plastics with a negative Poisson's ratio for high energy dissipation. Adv Mater 2020;32:2001222. https://doi.org/10.1002/adma.202001222.

[365] Deng B, Liu Z, Peng H. Toward mass production of CVD graphene films. Adv Mater 2019;31:1800996. https://doi.org/10.1002/adma.201800996.

[366] Zheng Q, Li Z, Yang J, Kim J-K. Graphene oxide-based transparent conductive films. Prog Mater Sci 2014;64:200-47. https://doi.org/10.1016/j.pmatsci.2014.03.004.

[367] Xu S, Wang S, Chen Z, Sun Y, Gao Z, Zhang H, et al. Electric-field-assisted growth of vertical graphene arrays and the application in thermal interface materials. Adv Funct Mater 2020;30:2003302. https://doi.org/10.1002/adfm.202003302.

[368] Shahil KM, Balandin AA. Graphene-multilayer graphene nanocomposites as highly efficient thermal interface materials. Nano Lett 2012;12:861-7. https://doi.org/10.1021/nl203906r.

[369] Yang J, Tang L-S, Bai L, Bao R-Y, Liu Z-Y, Xie B-H, et al. High-performance composite phase change materials for energy conversion based on macroscopically three-dimensional structural materials. Mater Horiz 2019;6:250-73. https://doi.org/10.1039/c8mh01219a.

[370] Yang L, Yang J, Tang L-S, Feng C-P, Bai L, Bao R-Y, et al. Hierarchically porous pva aerogel for leakage-proof phase change materials with superior energy storage capacity. Energy Fuels 2020;34:2471-9. https://doi.org/10.1021/acs.energyfuels.9b04212.

[371] Zhang X, Chao X, Lou L, Fan J, Chen Q, Li B, et al. Personal thermal management by thermally conductive composites: A review. Compos Commun 2021;23:100595. https://doi.org/10.1016/j.coco.2020.100595.

[372] Arivazhagan R, Geetha NB, Sivasamy P, Kumaran P, Kumara Gnanamithra M, Sankar S, et al. Review on performance assessment of phase change materials in buildings for thermal management through passive approach. Mater Today Proceed 2020;22:419-31. https://doi.org/10.1016/j.matpr.2019.07.616.

[373] Yang J, Qi G-Q, Liu Y, Bao R-Y, Liu Z-Y, Yang W, et al. Hybrid graphene aerogels/phase change material composites: Thermal conductivity, shape-stabilization and light-to-thermal energy storage. Carbon 2016;100:693-702. https://doi.org/10.1016/j.carbon.2016.01.063.

[374] Tang L, Zhao X, Feng C, Bai L, Yang J, Bao R, et al. Bacterial cellulose/MXene hybrid aerogels for photodriven shape-stabilized composite phase change materials. Sol Energy Mater Sol Cells 2019;203:110174. https://doi.org/10.1016/j.solmat.2019.110174.

[375] Yang J, Qi G-Q, Tang L-S, Bao R-Y, Bai L, Liu Z-Y, et al. Novel photodriven composite phase change materials with bioinspired modification of BN for solar-thermal energy conversion and storage. J Mater Chem A 2016;4:9625-34. https://doi.org/10.1039/c6ta03733j.

[376] Jiang Y, Wang Z, Shang M, Zhang Z, Zhang S. Heat collection and supply of interconnected netlike graphene/polyethyleneglycol composites for thermoelectric devices. Nanoscale 2015;7:10950-3. https://doi.org/10.1039/c5nr02051d.

[377] Chen G, Li Y, Bick M, Chen J. Smart textiles for electricity generation. Chem Rev 2020;120:3668-720. https://doi.org/10.1021/acs.chemrev.9b00821.

[378] Kim H-J, Sim K, Thukral A, Yu C. Rubbery electronics and sensors from intrinsically stretchable elastomeric composites of semiconductors and conductors. Sci Adv 2017;3:e1701114. https://doi.org/10.1126/sciadv.1701114.

[379] Ren L, Zeng X, Sun R, Xu J-B, Wong C-P. Spray-assisted assembled spherical boron nitride as fillers for polymers with enhanced thermally conductivity. Chem Eng J 2019;370:166-75. https://doi.org/10.1016/j.cej.2019.03.217.

[380] Kusunose T, Uno Y, Tanaka Y, Sekino T. Isotropic enhancement of the thermal conductivity of polymer composites by dispersion of equiaxed polyhedral boron nitride fillers. Compos Sci Technol 2021;208:108770. https://doi.org/10.1016/j.compscitech.2021.108770.

[381] Park KH, Kim BH, Song SH, Kwon J, Kong BS, Kang K, et al. Exfoliation of non-oxidized graphene flakes for scalable conductive film. Nano Lett 2012;12:2871-6. https://doi.org/10.1021/nl3004732.

[382] Dai W, Ma T, Yan Q, Gao J, Tan X, Lv L, et al. Metal-level thermally conductive yet soft graphene thermal interface materials. ACS Nano 2019;13:11561-71. https://doi.org/10.1021/acsnano.9b05163.

[383] Huang L, Xiao G, Wang Y, Li H, Zhou Y, Jiang L, et al. Self-exfoliation of flake graphite for bioinspired compositing with aramid nanofiber toward integration of mechanical and thermoconductive properties. Nano-Micro Lett 2022;14:168. https://doi.org/10.1007/s40820-022-00919-0.

[384] Wu S, Li T, Tong Z, Chao J, Zhai T, Xu J, et al. High-performance thermally

conductive phase change composites by large-size oriented graphite sheets for scalable thermal energy harvesting. Adv Mater 2019;31:1905099. https://doi.org/10.1002/adma.201905099.

[385] Yan Q, Dai W, Gao J, Tan X, Lv L, Ying J, et al. Ultrahigh-aspect-ratio boron nitride nanosheets leading to superhigh in-plane thermal conductivity of foldable heat spreader. ACS Nano 2021;15:6489-98.https://doi.org/10.1021/acsnano.0c09229.

[386] Zhang Y, Lei C, Wu K, Fu Q. Fully organic bulk polymer with metallic thermal conductivity and tunable thermal pathways. Adv Sci 2021;8:2004821. https://doi.org/10.1002/advs.202004821.

[387] Zhang Y, Wu K, Fu Q. A structured phase change material with controllable thermoconductive highways enables unparalleled electricity via solar-thermal-electric conversion. Adv Funct Mater 2022;32:2109255. https://doi.org/10.1002/adfm.202109255.

[388] Chen X, Wu K, Zhang Y, Liu D, Li R, Fu Q. Tropocollagen-inspired hierarchical spiral structure of organic fibers in epoxy bulk for 3D high thermal conductivity. Adv Mater 2022;34:2206088. https://doi.org/10.1002/adma.202206088.

[389] Lin Y, Huang X, Chen J, Jiang P. Epoxy thermoset resins with high pristine thermal conductivity. High Volt 2017;2:139-46. https://doi.org/10.1049/hve.2017.0120.

[390] Ruan K, Guo Y, Gu J. Liquid crystalline polyimide films with high intrinsic thermal conductivities and robust toughness. Macromolecules 2021;54:4934-44. https://doi.org/10.1021/acs.macromol.1c00686.

[391] Gu J, Ruan K. Breaking through bottlenecks for thermally conductive polymer composites: A perspective for intrinsic thermal conductivity, interfacial thermal resistance and theoretics. Nano-Micro Lett 2021;13:110. https://doi.org/10.1007/s40820-021-00640-4.

[392] Ruan K, Gu J. Ordered alignment of liquid crystalline graphene fluoride for significantly enhancing thermal conductivities of liquid crystalline polyimide composite films. Macromolecules 2022;55:4134-45. https://doi.org/10.1021/acs.macromol.2c00491.

[393] Ruan K, Zhong X, Shi X, Dang J, Gu J. Liquid crystal epoxy resins with high

intrinsic thermal conductivities and their composites: A mini-review. Mater Today Phys 2021;20:100456. https://doi.org/10.1016/j.mtphys.2021.100456.

[394] Ma T-B, Ma H, Ruan K-P, Shi X-T, Qiu H, Gao S-Y, et al. Thermally conductive poly(lactic acid) composites with superior electromagnetic shielding performances via 3D printing technology. Chinese J Polym Sci 2022;40:248-55. https://doi.org/10.1007/s10118-022-2673-9.

[395] Guo Y, Qiu H, Ruan K, Wang S, Zhang Y, Gu J. Flexible and insulating silicone rubber composites with sandwich structure for thermal management and electromagnetic interference shielding. Compos Sci Technol 2022;219:109253. https://doi.org/10.1016/j.compscitech.2021.109253.

[396] Guo Y, Qiu H, Ruan K, Zhang Y, Gu J. Hierarchically multifunctional polyimide composite films with strongly enhanced thermal conductivity. Nano-Micro Lett 2021;14:26. https://doi.org/10.1007/s40820-021-00767-4.

[397] Han Y, Ruan K, Gu J. Janus (BNNS/ANF)-(AgNWs/ANF) thermal conductivity composite films with superior electromagnetic interference shielding and Joule heating performances. Nano Res 2022;15:4747-55. https://doi.org/10.1007/s12274-022-4159-z.

[398] Ma Z, Kang S, Ma J, Shao L, Zhang Y, Liu C, et al. Ultraflexible and mechanically strong double-layered aramid nanofiber-$Ti_3C_2T_x$ MXene/silver nanowire nanocomposite papers for high-performance electromagnetic interference shielding. ACS Nano 2020;14:8368-82. https://doi.org/10.1021/acsnano.0c02401.

[399] Yu H, Chen C, Sun J, Zhang H, Feng Y, Qin M, et al. Highly thermally conductive polymer/graphene composites with rapid room-temperature self-healing capacity. Nano-Micro Lett 2022;14:135. https://doi.org/10.1007/s40820-022-00882-w.

[400] Yu H, Feng Y, Gao L, Chen C, Zhang Z, Feng W. Self-healing high strength and thermal conductivity of 3D graphene/pdms composites by the optimization of multiple molecular interactions. Macromolecules 2020;53:7161-70. https://doi.org/10.1021/acs.macromol.9b02544.

[401] Wang D, Liu D, Xu J, Fu J, Wu K. Highly thermoconductive yet ultraflexible polymer composites with superior mechanical properties and autonomous self-healing

functionality via a binary filler strategy. Mater Horiz 2022;9:640-52. https://doi.org/10.1039/d1mh01746b.

[402] Chen Y, Zhang H, Chen J, Guo Y, Jiang P, Gao F, et al. Thermally conductive but electrically insulating polybenzazole nanofiber/boron nitride nanosheets nanocomposite paper for heat dissipation of 5G base stations and transformers. ACS Nano 2022;16:14323-33. https://doi.org/10.1021/acsnano.2c04534.

[403] Su L, Ma X, Zhou J, Liu X, Du F, Teng C. Large-scale preparation of high-performance boron nitride/aramid nanofiber dielectric composites. Nano Res 2022;15:8648-55. https://doi.org/10.1007/s12274-022-4456-6.

[404] Ma R, Zhang H, Luo T. Exploring high thermal conductivity amorphous polymers using reinforcement learning. ACS Appl Mater Interfaces 2022;14:15587-98. https://doi.org/10.1021/acsami.1c23610.

[405] Wu K, Zhang Y, Gong F, Liu D, Lei C, Fu Q. Highly thermo-conductive but electrically insulating filament via a volume-confinement self-assembled strategy for thermoelectric wearables. Chem Eng J 2021;421:127764. https://doi.org/10.1016/j.cej.2020.127764.

[406] Gao J, Yan Q, Lv L, Tan X, Ying J, Yang K, et al. Lightweight thermal interface materials based on hierarchically strucntured graphene paper with superior through-plane thermal conductivity. Chem Eng J 2021;419:129609. https://doi.org/10.1016/j.cej.2021.129609.

[407] Pang K, Song X, Xu Z, Liu X, Liu Y, Zhong L, et al. Hydroplastic foaming of graphene aerogels and artificially intelligent tactile sensors. Sci Adv 2020;6:eabd4045. https://doi.org/10.1126/sciadv.abd4045.